Master's thesis

NTNU
Norwegian University of Science and Technology
Faculty of Natural Sciences
Department of Chemical Engineering

Eirik Søreide Hansen

Safety aspects of maritime hydrogen fuel from local sorption-enhanced ethanol steam reforming

Master's thesis in Chemical Engineering and Biotechnology
Supervisor: De Chen & Edd Anders Blekkan
August 2020

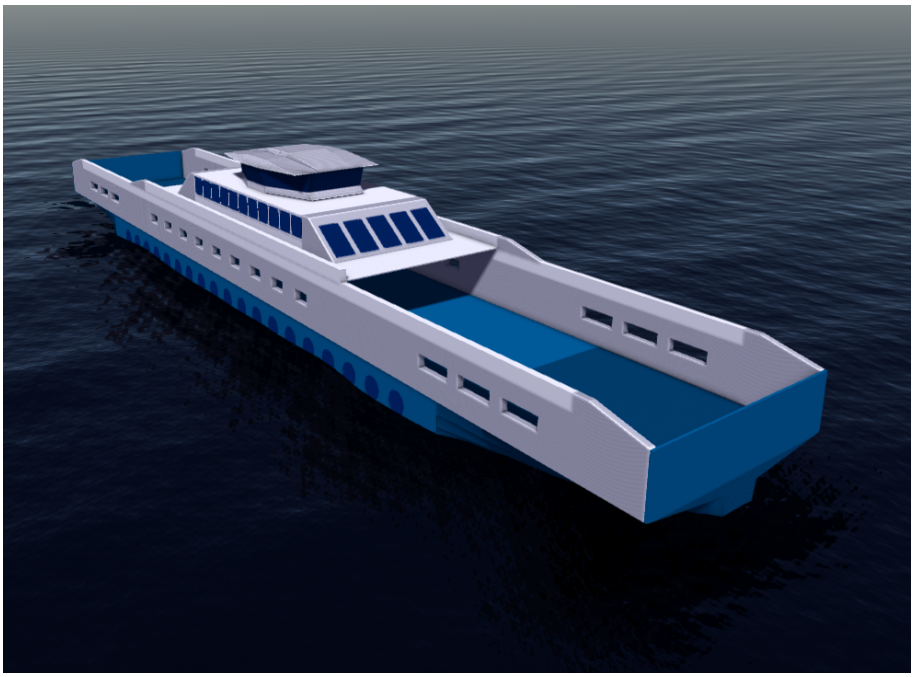

NTNU
Norwegian University of
Science and Technology

Eirik Søreide Hansen

Safety aspects of maritime hydrogen fuel from local sorption-enhanced ethanol steam reforming

Master's thesis in Chemical Engineering and Biotechnology
Supervisor: De Chen & Edd Anders Blekkan
August 2020

Norwegian University of Science and Technology
Faculty of Natural Sciences
Department of Chemical Engineering

NTNU
Norwegian University of
Science and Technology

Abstract

Sorption-enhanced ethanol steam reforming (SEESR) has potential as an efficient conversion process of ethanol to hydrogen. The present thesis considers safety aspects of a conceptualised local SEESR system. A concept double-ended ferry was considered with IMO alternative design procedure in mind. In the concept, solid-oxide fuel cells were used to generate power. FLACS, a CFD code, was used to estimate consequences and risk from loss of containment scenarios. As part of the work, ethanol properties were gathered and used to define ethanol as a substance that could be modelled in FLACS. The SEESR system was demonstrated to at least be equally safe for use in maritime vessels as conventional fuels. The low amount of hydrogen that can potentially leak during operation of a SEESR system was emphasised as an important factor in arriving at this conclusion. If the ethanol is stored below its flash point at 13 °C, the risk of fire or explosion in the storage holding space should be negligible.

Sammendrag

Damp reformering av etanol med integrert CO_2-fangst, såkalt sorption-enhanced ethanol steam reforming (SEESR), har potensiale til å effektivt konvertere etanol til hydrogen. I denne masteroppgaven vurderes sikkerhetsaspekter tilknyttet et lokalt, maritimt SEESR system. Sikkerheten ved et fergekonsept ble vurdert i tråd med IMO sine regler for alternativ design. I konseptet ble solid-oxide fuel cell (SOFC) brenselceller brukt til å generere strøm fra hydrogenet produsert. FLACS, en CFD programvare, ble benyttet til å kvantifisere konsekvenser og risiko knyttet til utslipp av gasser i forbindelse med lekkasjer eller brudd på rør eller utstyr. Som del av arbeidet ble termodynamiske egenskaper ved etanol samlet og brukt til å definere etanol som en gass i FLACS, slik at den kan modelleres. Det SEESR-baserte systemet ble demonstrert til å være minst like trygt som systemer basert på konvensjonelle drivstoff. Systemet har små mengder av hydrogen som potensielt kan lekke, og dette ble vektlagt som en styrke ved SEESR-systemet med tanke på sikkerhet. Dersom etanol oppbevares kjølig ved temperatur under flammepunkt på 13 °C, vil fare for eksplosjon og brann i lagerrommet være svært begrenset.

Acknowledgements

This thesis was written for the Institute of Chemical Process Engineering at the Norwegian University of Science and Technology (NTNU). It was completed under supervision from the project group of De Chen and Edd A. Blekkan, part of the wider catalysis research group.

The thesis marks the end of my five years at NTNU. Chemistry was my favourite subject at high school, and I felt privileged when moving to Trondheim to become an NTNU student. The combination of research-based high-quality teaching with a school -and city environment that allows for multiple forms of personal development have made this period truly inspiring and enriching. Despite the heavy workload and many mandatory sessions, I could be active in sports and sports administration – and even combine studies with the role as President of Norway's largest sports association, NTNUI.

Thanks to the many clever lecturers and the extremely service-minded administration at the Department of Chemical Engineering, I have enjoyed my academic life in Trondheim, and feel confident that my study track is tailored to a professional and academic career.

During the last part of the study, I became especially interested in the emerging hydrogen economy and relevant technology. I was fortunate to be included in the project group of De Chen and Edd A. Blekkan, where I received excellent feedback and support throughout the year. Initially, I started on a different thesis, which centred on the production and application of hydrotalcite catalysts for ethanol steam reforming. Due to the emergence of the Covid-19 pandemic, the lab was closed, and that thesis became impossible to complete. Two months into the thesis period, I had to change theme, and turned the work into a more theoretical study. Thanks to the project group, and especially to Mario E. Casalegno, for all support throughout the last year.

I am convinced that the thesis and engagement with the project group will be highly relevant for my future professional work.

I am deeply grateful to Remi Martini at Lloyd's Register Consulting in Bergen for cooperation and for allowing me access to their FLACS software license for use in this thesis. Lloyd's Register, by Liam Blackmore at the Global Technology Centre in Southampton, generously provided information and access to draft rules and regulations related to the maritime application of ethanol.

Thank you.

Declaration of compliance

I hereby declare that this thesis is an independent work in agreement with the exam rules and regulations of the Norwegian University of Science and Technology.

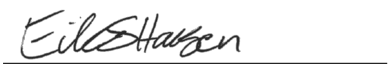

Eirik Søreide Hansen
August 25, 2020
Trondheim, Norway

Table of Contents

List of Tables

List of Figures

Abbreviations

ACH	=	Air Changes per Hour
AIP	=	Approval in Principle
ALARP	=	As Low As Reasonably Practicable
ATR	=	Auto-Thermal Reforming
BTL	=	Biomass To Liquid
CAD	=	Computer Aided Design
CAPEX	=	Capital Expenditure
CASD	=	Computer Aided Scenario Design
CFD	=	Computational Fluid Dynamics
C-NS	=	Compressible Navier-Stokes
ECHA	=	European Chemicals Agency
EMSA	=	European Maritime Safety Agency
EOS	=	Equation Of State
ESR	=	Ethanol Steam Reforming
EU	=	European Union
FANS	=	Favre-Averaged Compressible Navier-Stokes
FAR	=	Fatal Accident Rate
FCEV	=	Fuel Cell Electric Vehicle
FCHS	=	Fuel Cell Holding Space
FLACS	=	Flame Acceleration Simulator
FSA	=	Formal Safety Assessment
GTL	=	Gas To Liquid
HAZID	=	Hazard Identification
HSE	=	Health and Safety Executive
HyRAM	=	Hydrogen Risk Assessment Model (Sandia)
ICE	=	Internal Combustion Engine
IEA	=	International Energy Agency
IGF Code	=	International Code of Safety for Ship Using Gases or Other Low-flashpoint Fuels
IMO	=	International Maritime Organization
IPCC	=	Intergovernmental Panel on Climate Change
IRENA	=	International Renewable Energy Agency
LCEE	=	Linearised Compressible Euler Equations
LFL/LEL	=	Lower Flammability Limit/Lower Explosion Limit
LNG	=	Liquefied Natural Gas
LR	=	Lloyd's Register
MGO	=	Marine Gas Oil

NMA	=	National Maritime Authority
OGP	=	International Association of Oil & Gas Producers
PEMFC	=	Proton Exchange Membrane Fuel Cell
PLOFAM	=	Process Leaks for Offshore installations Frequency Assessment Model
POX	=	Partial OXidation
RANS	=	Reynolds-Averaged Navier-Stokes
RBD	=	Risk-Based Design
RIVM	=	National Institute for Public Health and the Environment of Netherlands
SCR	=	Selective Catalytic Reduction
SEESR	=	Sorption-enhanced ethanol steam reforming
SER	=	Sorption-Enhanced Reforming
SMR	=	Steam Methane Reforming
SOFC	=	Solid-Oxide Fuel Cell
SOLAS	=	International Convention for the Safety of Life at Sea
SRK	=	Soave-Redlich-Kwong
TCS	=	Tank Connection Space
UFL/UEL	=	Upper Flammability Limit/Upper Explosion Limit
WGS	=	Water-Gas Shift

Chapter 1

Introduction

In the years after the turn of the millennium, increasing emphasis has been placed on the emission of greenhouse gases following increasing industrialisation and economic growth. According to the Intergovernmental Panel on Climate Change (IPCC), these gases and especially CO_2, contribute to a higher average temperature on Earth, with potentially adverse consequences especially for people living near the equator and in coastal areas. There exist multiple international initiatives with the aim of countering this trend. Countries and companies set ambitious climate targets. For example, the new European Commission of 2019 labelled the situation a crisis and decreed few weeks after inauguration that all new EU policy must align with their climate targets (EC 2019*a*). However, to enable the European Union (EU), governments and other actors to reach the targets set by the Paris Agreement of 2015, viable solutions for carbon neutral energy carriers to replace petroleum must be developed.

Facing a shift towards more environmentally friendly sources of energy, hydrogen is predicted to become more important as a carrier of energy in the coming years. The gas was placed at the heart of the EU's long-term climate strategy (EC 2019*b*). In theory, hydrogen has a comparable energy density to fossil fuels, lower per unit of volume and higher per unit of mass, with only water as the end product. In practise, the volumetric energy density is of most economic importance. The storage methods used to counter the low density, e.g. metal hydrides, high-pressure or cryogenic tanks, add a significant weight and negate the high gravimetric energy density of hydrogen. Although there are multiple challenges in shifting from fossil fuels to hydrogen-based energy – e.g. the lack of hydrogen infrastructure, the price of production, safety concerns and the low volumetric energy density discussed – hydrogen is still considered as a viable alternative for the future (Gül et al. 2019, Reigstad et al. 2019, Tomasgard et al. 2019).

To improve the terms of hydrogen storage, the gas can be converted from hydrogen-dense substances such as methane or ammonia. These are easier to handle and have a higher volumetric energy density than pure hydrogen. Liquefied natural gas has a high energy

density, but will still emit CO_2 and requires cryogenic storage. Ammonia is perhaps a more promising candidate, with no CO_2 emissions and a global supply chain accustomed to handling the chemical. But on the other hand, ammonia is tough to ignite, in addition to being toxic and has a repelling odour. Its low volumetric and gravimetric energy densities make storing and transporting the fuel costly. Hydrogen Europe, a hydrogen and fuel cell umbrella association, still considers ammonia as the best renewable alternative for long-haul shipping (Pawelec 2020). This is due to a lack of better alternatives.

Demand for modern biofuels is rapidly growing, at 7% per year. Ethanol is the biofuel produced in highest quantities, and many countries are set to increase production of the fuel. In 2018 Brazil, already among the largest producers globally, saw a 15% increase in ethanol production capacity, while China saw a 25% increase and India saw a 70% increase (Zervos & Adib 2019, WBA 2019, Teter 2020). In 2019, the International Energy Agency (IEA) predicted demand for biofuels to increase further by 25% by 2024 (Bahar et al. 2019). In a transition to a hydrogen economy, biofuels seem to become a large source of renewable hydrocarbons, which can be converted to hydrogen. Ethanol can be converted through ethanol steam reforming, a process in which ethanol and steam reacts to become hydrogen and CO_2. This process is paramount for ethanol to take part in a potential hydrogen economy.

The International Maritime Organization (IMO) is an example of an organisation setting high targets for cutting emissions. By 2050, the IMO's members have pledged to cut greenhouse gas emissions by 50%, from 2008 levels (IMO 2018*a*). As the estimated lifespan of a ship is often set to 30 years, the industry needs to adapt now. As a consequence, there are many pilot projects and innovation initiatives in the maritime sector, focused both on establishing new fuels and on more efficient fuel use, due to the lower energy densities of the alternative fuels. Double-ended ferries are well suited for such projects, with a limited range requirement and fixed bunkering location (Pratt & Klebanoff 2016, Verbruggen 2018, Stocker 2018).

There are several operational aspects to examine before determining the viability of ethanol as a maritime fuel. These are emissions, safety, cost and practicality. Practicality refers to logistics, storage and handling of the fuel. While emissions and practicalities are discussed, this thesis mainly considers the safety of a double-ended ferry powered by hydrogen from ethanol steam reforming.

Chapter 2

Scope of study

The aim of this study was to illustrate a double-ended ferry powered by hydrogen reformed from bioethanol and study the safety aspects of such a concept. The bioethanol was to be processed by a local sorption-enhanced steam reformer to produce hydrogen, which would be sent directly to a connected fuel cell. To achieve this, a model ferry was constructed based on examples from the Norwegian west coast. A risk assessment was performed with regard to the power system. FLACS, a CFD software specialised on gas explosion and dispersion studies, was used to quantify the consequences from potential hazards. Ethanol was not among the fuels pre-defined in FLACS and had to be defined and to some degree validated before the simulations could proceed.

Chapter 3

Background

3.1 Power generation systems

This section aims to briefly encompass different systems for power generation on-board vessels. The systems discussed are the internal combustion engine, batteries and fuel cells. Efficiency, emissions and risk are the main topics when discussing the different systems.

3.1.1 Internal combustion engines

The first internal combustion engines (ICE) were developed in the late 18th century and the engines have through the last two centuries played an important part in revolutionising transportation. This holds especially true for land-based personal transportation. The engine itself generates energy by combustion of fuel in a combustion chamber. The force from the reaction can be applied to pistons or turbines which movement is used to generate momentum. The ICE is typically fed with fossil fuels like natural gas, distillate fuels or gasoline, but any combustible fuel can be applied. There are many different sorts of ICEs. The piston ICE, either with two- or four-stroke cycles are the most common. The cycles define how the ICE takes in new fuel, ignites the fuel and removes the exhaust gas. The gas turbine and the jet engine are other notable ICEs.

According to Caton, the internal combustion engine can theoretically reach efficiencies of 67% (Caton 2017). Due to high exergy destruction, for example by loss of heat to the environment, the theoretical efficiency is not higher. In practise, ICEs using gasoline have a low efficiency, in the range 20-35% (Baglione 2007). The engine efficiency vary between the different types of ICEs. The diesel engine used in large vehicles can reach an efficiency up to 45% (Takaishi et al. 2008). Gas turbines can reach above 60% (PEI 2010). Reducing pollution from ICEs has been a pressing research topic in recent decades. In the late 1900s, the development of the selective catalytic reduction (SCR) technology contributed to reduced NO_x and particulate matter emissions by up to 95% (Stultz & Kitto

2015). CO_2-emissions remain inevitable given the nature of the fuels.

The main risk of the ICE is its potential to ignite a flammable atmosphere. The fuel is in the ICE ignited, and the applied fuels are highly flammable. The US Occupational Safety and Health Administration (OSHA) highlighted the ICE's ignition capabilities and cited several incidents where an ICE ignited a flammable release. The ICE requires a specific ratio of fuel to air to function properly. If there are flammable gases present in the atmosphere surrounding the ICE, these will disturb this ratio and provide more fuel than the engine is designed to handle, causing extensive wear and ultimate failure. Unignited fuel may cause backfire, where such fuels ignite in the exhaust channel (OSHA 2012). To handle the challenges, ICEs must be situated away from areas with potentially flammable atmospheres. Shut-down systems with sensors monitoring the air intake should prevent potential accidents.

3.1.2 Batteries

A battery is defined as an instrument containing at least one electrochemical cell connected to an external circuit. A battery is a device for storing energy. When connected to a circuit, a redox reaction converts high-energy reactants to low-energy products and electrons are sent through the external circuit, in the process delivering the free-energy difference of the reaction. Battery technology is currently developed at pace, powered by the rise in popularity of electric vehicles and portable electric devices.

A wide range of batteries are in the market. Primary batteries provide power only until they run out, while secondary batteries can be recharged. The most popular secondary batteries are as of now based on Li, while Ni-based batteries too have large shares of the market. The Pb-acid battery, which was developed as early as the 1800s, has traditionally been the dominant type of battery used for vessels and vehicles, but Li-ion batteries are now the most widely applied (Munuera 2020). According to the IEA, the price of batteries has fallen dramatically in recent years, from 1100 USD/kWh in 2010 to only 160 USD/kWh in 2019. Most battery-powered personal cars now have batteries containing 50-70 kWh, with selected pick-up trucks in 2020 containing up to 200 kWh (Gül et al. 2020, EVD 2020).

For batteries to globally reduce the impact of fossil fuels with regard to emissions, their life-cycle emissions must be analysed. Presented in their 2020 EV Outlook, the IEA found that most of the emissions from batteries were dependent on the electricity mix. Based on the average global electric mixture, the emissions of hybrid, battery and fuel cell vehicles were roughly equal and all had, on average, to a small degree lower emissions over their lifetime than ICE vehicles. The difference decreased further as the battery sizes increased. The emissions from ICE vehicles would for a similar case be three times more CO_2 intensive than electric vehicles if the electric mixture was renewable (Gül et al. 2020).

With regard to safety, battery incidents are rare relative to the number of products in use. For Li-ion batteries, incidents are by design supposed to happen at a rate below 10^{-6} per year. Such are often caused because of errors during manufacture. Microscopic metal par-

ticles are not kept out to a satisfactory degree. These may cause a weak current between the electrodes, which in turn causes heat to build up until the battery fails through a fire or explosion. Producers often prevent such failures by use of X-ray scanning to monitor every single part of the battery before releasing them to the market. Batteries should be perfectly safe if used correctly. Vibrations or heat exposure are examples of situations that may provoke a failure.

Batteries still cause incidents, due to highly flammable electrolytes (Wang et al. 2005). These are expelled during short-circuits and heat buildup. In October 2019 in Norway, a ferry caught fire in the battery department and released electrolytes from the batteries (Josdal 2019). Firemen had to be treated for exposure to hydroflouric acid in the aftermath. In that case, the escaped electrolyte was trapped in the ferry and caused an explosion the next morning. The incident was caused by a failure in the battery cooling system, causing a fire. Salt water was distributed by the sprinkler system to stop the fire, but the salt also caused short-circuits in the other batteries, and more electrolyte escaped.

According to the Society of Fire Protection Engineers (SFPE), lead-acid batteries produce large amounts of hydrogen when failing and produces smaller amounts when charging normally (Brzezinska 2018). If not able to escape, explosive atmospheres can develop. The batteries have caused many accidents in the 21st century, especially in mines (BQ 2015).

Battery systems must be designed so that a single failure is unable affect other cells. Escalation must be prevented. From the incident of the Norwegian ferry, the cooling system based on water was at fault. Air ventilation was in the aftermath concluded to be a better option.

.

3.1.3 Fuel cells

A fuel cell is a device through which a set of redox reactions convert the chemical energy of a fuel and an oxidising agent into electrical energy. In the same way as batteries, the fuel cells supply the free energy of the reactions to an external circuit. Fuel cells are an old technology, developed in the early 1800s. The first hydrogen fuel cell was developed in 1932. Fuel cells are used widely as a source of back-up power in remote locations. There are great expectations to fuel cells in the field of transportation, although fuel cells are applied in few vessels or vehicles as of 2020 (Tronstad et al. 2017).

There are several different types of fuel cells. For the European Maritime Safety Agency (EMSA), DNV GL produced a thorough roadmap for maritime fuel cell technologies and rated these after applicability for the industry (Tronstad et al. 2017). The three most highly rated fuel cell types were the proton exchange membrane fuel cell (PEMFC), the high-temperature PEM fuel cell (HT-PEMFC) and the solid oxide fuel cell (SOFC). Some of the other types of fuel cells included in the comparison were the alkaline, direct methanol and molten carbonate fuel cells. Figure 3.1 illustrates the general concept of a fuel cell, in

this case for a SOFC. The most highly rated cells in the report, the SOFC and the PEMFC, will be discussed on the following paragraphs. The HT-PEMFC is similar to the PEMFC in most ways except for the higher operating temperature and higher tolerance for impurities in the reactant stream.

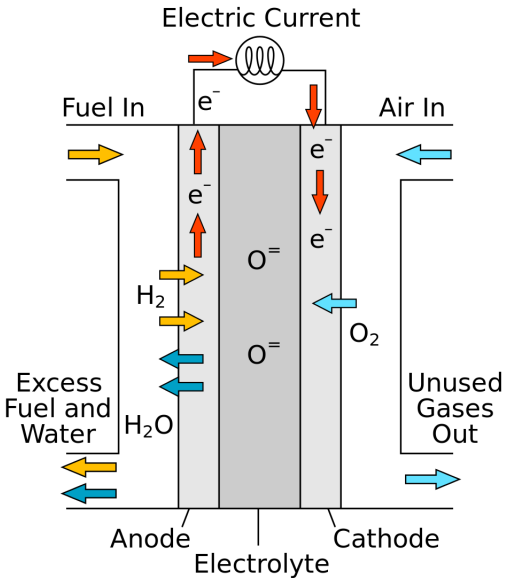

Figure 3.1: The general concept of a solid-oxide fuel cell. Illustration publicly available from Wikimedia Commons.

The PEMFC is currently one of the most mature fuel cell types and is used for many applications. This fuel cell employs platinum-based electrodes and a humidified polymer membrane as electrolyte. The electrolyte works as an electric insulator and allows only hydrogen cations through. The operating temperature of the PEMFCs is usually in the range of 50-100 °C. As the membrane must be kept wet, 100°C is the upper limit for operation. PEMFCs convert hydrogen and oxygen to water and electricity. The PEMFCs are sensitive with regard to hydrogen purity. Other fuels must be converted to hydrogen prior to entering the fuel cell. In the EMSA study on fuel cells in shipping, the PEMFC scored the highest among the fuel cell technologies. The strengths mentioned were its high power density, low operating temperature, flexibility with regard to load, small size and mature technology. Among the weaknesses discussed were the expensive catalysts, lower thermal efficiency and fuel sensitivity (Tronstad et al. 2017). When adapted to a reforming system, the PEMFC would require further purification of the reformation products. This is usually achieved by adding an extra water-gas shift unit.

The SOFC is a high-temperature fuel cell. Temperatures vary between 500-1000°C. The SOFCs are often used for large-scale power production, with capacities ranging up to 10

MW. SOFCs have been applied in several research projects for maritime use (Stensvold & Jensen 2020, Klingner 2005, Barrett 2008). The SOFCs are flexible with regard to fuel, able to receive LNG, methanol and diesel, to name some. Fossil fuels are converted to hydrogen and CO_2 in the fuel cell. The high temperature allows for efficient utilisation of the outlet steam flow. The electrical efficiencies of the SOFCs generally lie between 50-70%. If a heat recovery system is applied, the thermal efficiency of a SOFC can reach higher than 85%. In the comparison by DNV GL for EMSA, the SOFC received the second highest score. The strengths noted were the following: Fuel flexibility and handling of impurities, mature technology (though not to the same degree as with PEMFC) and a high efficiency. Its weaknesses were a low tolerance for cycling, relative cost compared to other fuel cells and its high operating temperature. The operating temperature allows for a high thermal efficiency, as mentioned, although poses a potential safety hazard. The report states that the weakness to cycling is not an issue when combined with a battery (Tronstad et al. 2017).

According to the IEA, the life-cycle emissions of fuel cell electric vehicles (FCEV) depend mostly on the fuel applied. If using green hydrogen, the FCEVs may have lower emission-levels than those of battery electric vehicles running on renewable electricity (Gül et al. 2020). The emissions from components and production of the fuel cells are low and similar to those of electric batteries.

With regard to safety, no combustion takes place and hydrogen and oxygen remain separated. Small amounts of gas are handled by the individual modules. The greatest potential risk is the leakage of hydrogen into the local atmosphere, in particular to confined volumes (Lanz et al. 2001).

3.2 Steam reforming

Steam reforming is the most widespread method of producing hydrogen today, accounting for three quarters of all production. Coal gasification is the second most widespread production process and accounts for 23% (Gül et al. 2019). In this section, steam reforming of both methane and ethanol are discussed.

3.2.1 Steam methane reforming

Steam methane reforming (SMR) is the most common reforming process, where methane and water are mixed and heated, yielding syngas after reaction with a catalyst. Hydrogen production through SMR is a mature process and a central part of the production of ammonia and refinement of petroleum. The IEA estimates that these two processes respectively used 43% and 52% of the global hydrogen supply in 2018. The general reaction for SMR is represented by Equation 3.1. The reaction is strongly endothermic and requires external heating (Blackman & Gahan 2013).

$$CH_4 + H_2O \rightleftharpoons CO + 3H_2 \quad \Delta H^{\circ}_{r298} = 206kJ/mol \tag{3.1}$$

The SMR reaction takes place in a reactor where a pressurised mixture of methane and steam enters and comes into contact with a catalyst. Nickel catalysts are most popular for the reforming process due to availability and price, although noble metals to some extent can offer better performance. The shape of the catalysts is used as an asset to minimise pressure drop in the reactor. After the SMR reaction, the carbon monoxide is converted to CO_2 by the mildly exothermic water-gas shift (WGS) reaction, given in Equation 3.2. According to the New York State Energy Research and Development Authority, hydrogen production from steam reforming of methane is about 65-75% efficient, though not stated in the report, the number was probably defined by the hydrogen lower heating value (NYSERDA 2005). Although this statement originated in 2005, it probably still holds true, due to the maturity of the process.

$$CO + H_2O \rightleftharpoons CO_2 + H_2 \quad \Delta H^{\circ}_{r298} = -41kJ/mol \tag{3.2}$$

Partial oxidation

Partial oxidation (POX) is an alternative to steam reforming which has received attention in recent years. Sengodan et al. produced in 2018 an extensive review on the technology, which has formed the basis for the present paragraph (Sengodan et al. 2018). The essence of the POX process is to partially combust a sub-stoichiometric mixture of fuel and air and produce a syngas, rich in hydrogen. The process has the advantages of being quicker than SMR, exothermic, less fuel sensitive and uses more compact equipment. However, a lower hydrogen yield than that of steam reforming along with soot formation problems and the necessary air separation have until now hindered extensive adaptation of the method.

The combination of POX and solid-oxide fuel cells (SOFC) are currently studied for its potential in a future hydrogen economy, possibly allowing for cheaper modules and higher energy densities (Sengodan et al. 2018).

Auto-thermal reforming

Steam reforming and POX can be combined in a process called auto-thermal reforming (ATR). This process capitalises on the capabilities of POX as an exothermic process, as it provides heat for the endothermic reforming process. It is most commonly used for small-scale hydrogen production and has quicker start-up and response rates than those of SMR, and ATR produces hydrogen at higher yields than POX. Due to encompassing two different reaction schemes, ATR cannot use specialised catalysts for SMR or POX, as these oftentimes are less compatible with the unfamiliar reaction. For ATR of shorter hydrocarbons, copper catalysts are frequently applied (Kilner et al. 2012).

Chemical looping reforming

Chemical looping reforming (CLR) is a more novel technique for reforming methane to hydrogen. Chemical looping is based on the principle of circulating an oxygen carrier, often a metal oxide, between two reactors in a loop of sorts. In an air reactor, the carrier receives oxygen which it delivers to the fuel reactor. By this way, the oxygen is easily extracted from the air and nitrogen is excluded from the fuel reactor. The technique combines POX and SMR and uses a metal carrier to deliver the oxygen for the combustion process. By these means, CLR reaches auto-thermal conditions and additionally has a high hydrogen yield. The exclusion of nitrogen prompts NO_X-free combustion. In addition, less catalyst is required per unit of fuel than with SMR (Luo et al. 2018, Tang et al. 2015). The CLR process is still developed with regard to catalysts.

Sorption-enhanced reforming

Sorption-enhanced reforming (SER) is another alternative, in which the CO_2 produced is captured during the reaction. As CO_2 and hydrogen are on the same side of the WGS reaction, the capture of CO_2 will shift the reaction to produce more hydrogen. A dolomite is a popular option as the CO_2 adsorbent, while catalysts are usually based on Ni (Giuliano & Gallucci 2018). The method has several advantages. The CO_2-capture allows for potential carbon capture and storage as part of the hydrogen production, by which the hydrogen would be categorised as zero-emission fuel. The swing of the WGS reaction gives high hydrogen yields compared to other methods and reduces the necessity of a secondary WGS unit, and a CO_2 and hydrogen separation unit. The gases are usually separated by pressure-swing adsorption. This is an expensive process in which adsorbents preferentially capture the components of a gas mixture (Ogo & Sekine 2020).

The main challenges relate to the regeneration of the adsorbent, a separate process. The reformer unit will have to cycle between production and regeneration, instead of operating at steady-state. For a steady-state solution, at least two reformers will be required. CO_2 capture and storage is not currently economically feasible, and the advantage is therefore of limited degree. SER has still not been applied at industrial scale, but ZEG Power and CCB Energy Park in Norway are now building a 1 MW unit. The carbon will in this case be captured and then stored below the seabed (Meyer et al. 2014, Njøsen 23/01/2020).

Risks of steam methane reforming

As steam reforming has been widely used for many decades, the potential hazards of the process are familiar. When discussing recent SMR accidents in Iran, Jafari et al. describes the process as high-risk. According to them, the most frequent accidents accompanied handling of hydrogen. With regard to a worst-case scenario, they stated that a rupture of the desulfurisation reactor can produce fatal over-pressures of 0.83 bar at a distance of 45 m, while a burst of the large reformer studied would produce similar pressures at 25 m (Jafari et al. 2014). In 1985 in Norway, a leak from a reformer unit caused a powerful explosion and demolished an ammonia plant operated by Norsk Hydro (TU 2000). In 2010 in the US, the burst of a heat exchanger at the Tesoro Anacortes Refinery released large amounts of hot hydrogen which ignited and caused a large explosion, killing 7 employees (CSB 2010).

3.2.2 Ethanol steam reforming

Ethanol steam reforming (ESR) is a type of steam reforming, similar to SMR, but with ethanol replacing methane on the reactant side. Much of the information given here is gathered from the recent review on ethanol steam reforming by Ogo et al. (Ogo & Sekine 2020). The general reaction for ESR is given by Equation 3.3. The reaction mechanism is described in more detail by Equations 3.4-3.6. Some of the prominent side reactions are given in Equations 3.7-3.11 and the coke reactions are given in Equations 3.12-3.14.

$$C_2H_5OH + 3H_2O \rightleftharpoons 2CO_2 + 6H_2 \tag{3.3}$$

(Main reaction path)
Ethanol dehydrogenation

$$C_2 2H_5OH(g) \rightleftharpoons CH_3CHO(g) + H_2(g) \quad \Delta H^{\circ}_{r298} = 68.9kJ/mol \tag{3.4}$$

Acetaldehyde steam reforming

$$CH_3CHO(g) + H_2O(g) \rightleftharpoons 2CO(g) + 3H_2(g) \quad \Delta H^{\circ}_{r298} = 186.8kJ/mol \tag{3.5}$$

Water-gas shift

$$CO(g) + H_2O(g) \rightleftharpoons CO_2(g) + H_2(g) \quad \Delta H^\circ_{r298} = -41.4kJ/mol \tag{3.6}$$

(Side reactions)
Ethanol dehydration

$$C_2H_5OH(g) \rightleftharpoons C_2H_4(g) + H_2O(g) \quad \Delta H^\circ_{r298} = 45.5kJ/mol \tag{3.7}$$

Acetaldehyde decomposition

$$CH_3CHO(g) \rightleftharpoons CH_4(g) + CO(g) \quad \Delta H^\circ_{r298} = -19.3kJ/mol \tag{3.8}$$

Acetone formation

$$2CH_3CHO(g) \rightleftharpoons CH_3COCH_3(g) + CO(g) + H_2(g) \quad \Delta H^\circ_{r298} = 4.1kJ/mol \tag{3.9}$$

Methanation

$$CO(g) + 3H_2(g) \rightleftharpoons CH_4(g) + H_2O(g) \quad \Delta H^\circ_{r298} = -206.1kJ/mol \tag{3.10}$$

$$CO_2(g) + 4H_2(g) \rightleftharpoons CH_4(g) + 2H_2O(g) \quad \Delta H^\circ_{r298} = -164.8kJ/mol \tag{3.11}$$

(Coke formation reactions) Ethylene decomposition

$$C_2H_4(g) \rightleftharpoons 2C(s) + 2H_2(g) \quad \Delta H^\circ_{r298} = -52.3kJ/mol \tag{3.12}$$

Methane decomposition

$$CH_4(g) \rightleftharpoons C(s) + 2H_2(g) \quad \Delta H^\circ_{r298} = 74.9kJ/mol \tag{3.13}$$

CO disproportionation (Boudouard reaction)

$$2CO(g) \rightleftharpoons C(s) + CO_2(g) \quad \Delta H^\circ_{r298} = -172.6kJ/mol \tag{3.14}$$

The main pathway for ESR includes the ethanol dehydrogenation (Eq. 3.4), acetaldehyde steam reforming (Eq. 3.5) and WGS-reactions (Eq. 3.6). Among the many side reactions given above, the acetaldehyde decomposition (Eq. 3.8) is especially problematic, as much methane forms through this path, ultimately lowering hydrogen selectivity. The methanation reactions (Eq. 3.10, Eq. 3.11) also reduces selectivity as hydrogen is consumed. The coke formations reactions present the most notable challenge for viable ESR, as these reactions quickly can deactivate the catalyst. The mechanism is illustrated in Figure 3.2.

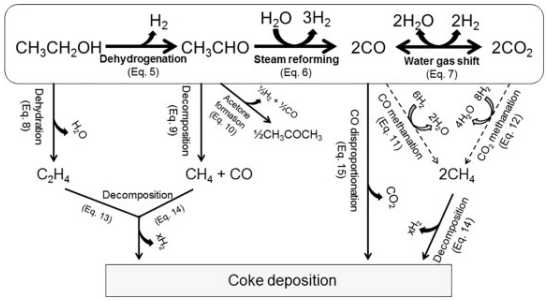

Figure 3.2: The reaction pathway for ethanol steam reforming (Ogo & Sekine 2020). Used with approval by Elsevier.

Noble metals, such as Pt, Ru, Rh, Pd and Ir, exhibit excellent catalytic properties for ESR, namely high levels of activity, high degrees of stability and low levels of coke formation (Haryanto et al. 2005, Contreras et al. 2014, Zanchet et al. 2015). Among the noble metals, Rh catalysts reaches the highest levels of activity (Ogo & Sekine 2020). Even so, noble metals are too expensive to be suitable for industrial hydrogen production. Several non-noble metals have also been shown to reach high levels of activity for ESR. Ni, Co and Cu are the most commonly used such metals (Vaidy & Rodrigues 2006, Ogo & Sekine 2020). For non-noble catalysts, deactivation by coke-formation and extensive methane production pose major difficulties. Combining different metals have been viewed as a solution to these problems, along with adjusting the support material.

Multiple studies have indicated that a basic support will suppress both coke and by-product production. Ethylene, a dominant coke precursor, is formed by ethanol dehydration and relies on acid sites (Han et al. 2017, Cerdá-Moreno et al. 2019, Ogo et al. 2015). Hydrotalcite and hydroxyapatite are two natural minerals popular as basic supports for ESR. With regard to combining metals, Ni and Co can together produce bimetallic catalysts with higher performance than those of the monometallic catalysts (Sharma et al. 2015, Rodriguez-Gomez & Caballero 2015). Ni is a particularly good cleaver of C-C bonds, while Co provides better stability with regard to coke formation and reduces the impact of methanation (Ogo et al. 2015). As Ni has such high C-C cleaving capabilities, an alternative mechanism has been proposed for ESR, where the ethanol is cleaved to methane and CO, which in turn react by the water-gas shift (Eq. 3.6) and methane steam reforming

(Eq. 3.1) reactions to form CO_2 and hydrogen (Contreras et al. 2014, Mattos et al. 2012, Zanchet et al. 2015, Sharma et al. 2015). This alternative pathway is illustrated in Figure 3.3.

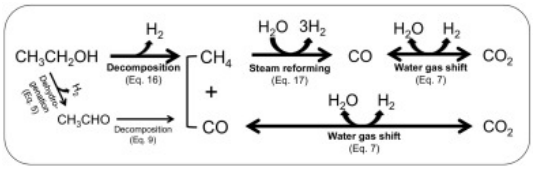

Figure 3.3: An alternative reaction pathway for ethanol steam reforming using nickel catalysts (Ogo & Sekine 2020). Used with approval by Elsevier.

The ESR reaction is usually performed in a fixed-bed reactor at temperatures around 450-600 °C (Ogo & Sekine 2020, Alonso et al. 2009). Gibbs free energy for the reaction becomes negative at 205 °C, but a higher temperature positively affects conversion and lowers levels of coke formation. The steam to carbon ratio and catalyst particle size are other variables used to minimise coke formation. Özkan et al. conclude that a steam to ethanol ratio of more than 3 can prevent formation of coke (Mattos et al. 2012, Ozkan et al. 2019). The catalyst particle size must be as small as possible to limit coke formation, which happens in acid sites. Larger catalyst particles bring the reaction further from the support and this ultimately weakens the effect of choosing a basic material (Mattos et al. 2012, Zanchet et al. 2015, Sharma et al. 2015, da Silva et al. 2009). By integrating the catalyst particles with the support material through the synthesis method, e.g. through co-precipitation, a strong influence from the support can be secured.

Sorption-enhanced ethanol steam reforming

Sorption-enhanced ethanol steam reforming (SEESR) is in principle similar to SER of methane. By removing the CO_2 in situ, hydrogen yield from ESR can be increased further. CO_2 and hydrogen are both products of the WGS reaction, and when CO_2 is removed, this reaction is shifted to produce more hydrogen. The procedure eliminates the need for separation of CO_2 and hydrogen downstream of the ESR. In conventional SMR, the WGS reaction requires its own reactor, as this process is exothermic, while the reforming is endothermic. This expense is also avoided in the sorption-enhanced process, as the removal of CO_2 shifts the WGS reaction towards hydrogen production.

CaO, dolomites, hydrotalcites and alkali metal ceramics are some of the alternatives as CO_2 sorbents. These are rated on the ability to capture and store CO_2 efficiently, while later releasing CO_2 at higher temperatures (Memon et al. 2017). The CO_2 adsorption is exothermic and makes the overall reaction in the reformer close to auto-thermal (Iruretagoyena et al. 2018, Fermoso et al. 2018). According to Dou et al., the ratio of sorbent to catalyst should rest between 2 and 3, S/C = 3 and T = 600 °C (Dou et al. 2018). The results indicate that the levels of sorbent in the reactor should exceed the levels of catalyst.

Rawadieh et al. published results expressing that a well-mixed bed performs better than a catalyst-sorbent layered arrangement (Rawadieh & Gomes 2009, Menendez et al. 2018). Using the sorption-enhanced technique, a number of studies have managed to reach hydrogen yields up to 99% (Menendez et al. 2018, Johnsen et al. 2006, Essaki et al. 2008, He et al. 2010). Sintering of the CO_2 adsorbent is a major challenge to be overcome for the sorption-enhanced method to be viable. He et al. was one of the groups managing to reach 99% hydrogen yield. After 110 minutes on stream, the adsorbent had to be regenerated for 30 minutes. Each cycle was shorter than the previous one, with the eight cycle lasting 20 minutes, shorter than the regeneration period (He et al. 2010). During the regeneration, heat was increased to release the CO_2 for the adsorbent. For this process, He et al. used Ar to sweep the reactor of CO_2 and hydrogen to make sure the catalysts were reduced before a new cycle (He et al. 2010).

3.3 Fuel alternatives

Numerous fuels are available for use in ferries. While distillate fuel traditionally has been the conventional fuel for the vessels, the search for less CO_2-, sulphur- and NO_X-emitting technologies has contributed to the development of multiple alternatives, of various stages of commercial maturity (Cottrell 2011). Liquefied natural gas (LNG) has since the first implementation in a Norwegian ferry in 2000 proven technically viable and is now a favoured option by most shipowners and crew who have converted from marine gas oil (MGO), a distillate fuel (Blikom 2012). The transition to gas has enabled the sector to greatly reduce carbon, NO_x, SO_x and particulate emissions. In 2015, 9 out of the 10 most environmentally friendly vessels were Norwegian and running on LNG, according to a rating by the Environmental Ship Index (Andersen 2015). HSC Francisco, which is operated by Buquebus of Argentina and currently the fastest ferry in the world, is also using LNG as fuel (Le & Phillips 2015).

New fuel options investigated for maritime vessels include hydrogen and ammonia systems, in addition to purely electric alternatives. While Norway in 2015 had 15 LNG ferries in operation, the country has in later years invested more in electrifying the fleet (Stensvold 2015*b*, 2018*a*). MF Ampere, the world's first electric ferry, was built in 2014. In April of 2020, 60 fully electric ferries were under production in Norway (Stensvold 2015*a*, Tomasgard 2020). In this chapter, the different fuels are evaluated for use in ferries. Purely electric systems are not viable for larger distances due to a disproportional increase in battery size with capacity, along with long charging times for large systems (Thomas 2012). The fully electric alternative is not included in this comparison, but batteries are further discussed under Chapter 3.1. The fuels included in this section are distillate fuel (MGO), LNG, hydrogen, ammonia and biofuel. The section presents simple parameters for evaluation of the fuels. The fuels will be compared on energy density and potential risk of handling, along with price.

3.3.1 Distillate fuel

Diesel fuel is broadly defined as any liquid fuel applied in diesel engines, where the fuel is ignited without a spark, but through injection of the fuel into compressed air. The diesel engine itself is discussed in more detail under Section 3.1.1. Diesel fuel has been adapted to a wide range of applications due to a higher thermal efficiency and thereby a higher fuel efficiency, than that of the petrol engine (Reif 2017).

The most common form of diesel is derived from petrol through fractional distillation, which is practised industrially using large columns to separate crude oil into different fractions based on volatility. Other types of diesel are currently being developed, such as biodiesel, biomass to liquid (BTL) diesel and gas to liquid (GTL) diesel. Biodiesel and BTL diesel have much lower CO_2-emissions throughout the value chain, while GTL diesel has somewhat lower CO_2-emission and much lower emissions of sulphur, particulate matter and carbon monoxide (Knottenbelt 2002). Biodiesel is discussed further in Chapter 3.3.5. For marine use, the IEA predicts marine gas oil (MGO) to be in highest demand in

each of the years 2020-2023 (IEA 2019). MGO are lighter distillates for marine use, popular in the shipping industry. The rest of this section will focus mainly on MGO. From the beginning of 2020, new regulation by the IMO entered into force. The limit for maximum sulphur content of fuels was lowered from 3.5% to 0.5%. MGO previously contained up to 1.5%, but suppliers lowered the content to 0.5% to be compliant with the new rules (Meyertons 2020).

Properties and risks

MGO is a petrol fuel, made of carbon chains averaging at 12 carbon atoms in length. While mostly saturated hydrocarbons, 25% of MGO is usually composed of aromatic hydrocarbons and brand specific additives may also be part of the blends (Date 2011, Chilcott 2006, Whall et al. 2002). The fuel is clear in colour with a viscosity slightly greater than that of water and has a characteristic "aromatic" smell. Some of the relevant properties of MGO are specified in Table 3.1 below. As MGO is a blend of components rather than a pure substance, the values of Table 3.1 are rough estimates and not accurate for MGO in general. Much of the information in the table is gathered from safety data sheets for MGO or related distillates.

Table 3.1: Selected thermophysical properties of MGO at 1 bar and 25 °C.

Property	Unit	MGO value	Reference
Lower heating value	MJ/kg	43	(Martinez 2020) (Ellis & Tanneberger 2015)
Density	kg/m^3	860	(Ellis & Tanneberger 2015)
Vapour pressure	kPa	$<$0.5	(Chevron 2010)
Viscosity	mPa·s	2.7	(Lapuerta et al. 2010)
Boiling point	K	450-920	(Ellis & Tanneberger 2015)
Flash point	°C	$>$60	(GP 2016) (Chevron 2010)
Minimum ignition energy	mJ	1.15	(Huang et al. 2015)
Auto-ignition temperature	K	520-570	(Ellis & Tanneberger 2015) (Zabetakis 1965)
LFL	%	1.0	(Ellis & Tanneberger 2015) (Chevron 2010)
UFL	%	6.0	(Ellis & Tanneberger 2015) (Chevron 2010)
Maximum laminar burning velocity	cm/s	40	(Zabetakis 1965)

MGO as a substance proves a minor health hazard, and fumes can irritate eyes, respiratory system and skin. Inhalation of strong fumes may cause serious lung damage, and MGO might have carcinogenic capabilities as well. Short exposure is not considered dangerous (Chilcott 2006). From the vapour pressure, it is evident that MGO does not produce con-

centrated fumes.

With regard to the fuel's explosive characteristics, MGO seems mostly unproblematic to use. If ignited, MGO clouds may cause serious explosions. The laminar burning velocity is a measure of how quickly the flame moves through a gas cloud, releasing energy. Higher velocities cause higher blast waves. According to Chong et al., the laminar burning velocity at 100 °C of diesel is 80 cm/s (Chong & Hochgreb 2011). No value for the burning velocity of distillates at room temperature was found in literature. In a major 1965 study for the US Bureau of Mines, Michael George Zabetakis published data on flammability limits, burning velocities, auto-ignition temperatures and burning rate of more than 200 combustible gases (Zabetakis 1965). The study has for decades been considered a standard reference in the field. While not specifically discussing the properties of distillates, he compared values of several hydrocarbons. At room temperature, the burning velocities seemed to remain constant at about 40-45 cm/s as the number of carbon atoms in the chain increased. The value of 40 cm/s is therefore included in Table 3.1.

For MGO, the most obvious safety measure is to prevent development of flammable gas concentrations. A substance's flash point is the temperature at which its vapours can ignite if provided with an ignition source. According to IMO rules, MGO has a lower limit for the flash point at 60 °C (IMO 2015). Ships using fuels with flash points below 60 °C will be subject to the more strict IGF code regarding low flash point fuels. With a flash point at 60 °C, flammable atmospheres will not develop if kept away from hot areas.

3.3.2 Liquefied natural gas

Natural gas is composed mostly of methane(85-90%), with the rest made up of ethane and nitrogen (EB 2020). There may also be traces of heavier hydrocarbons in the mixture. LNG is produced by cooling natural gas to exist in liquid state. Cryogenic storage solutions were developed in the late 19th century Munich and refers to handling of gases liquefied at temperatures at around 120 K or lower. Liquefying natural gas became popular in the US as a peak-shaving process. Liquefying excess natural gas allowed for companies to meet peak demand by re-gasifying stored LNG. During the 20th century, the liquefaction process has developed to become much more efficient, and the demand for LNG has ultimately increased (Chiu 2008, Williams et al. 2015).

In the 21st century, the world energy consumption is rapidly increasing. The IEA announced in 2008 that natural gas was expected to meet much of the increased demand and predicted the gas to account for about a quarter of the global demand by 2030 (Birol et al. 2008). According to the Shell LNG Outlooks of 2016-2020, the demand has been exceeding expectations. In 2018, natural gas already accounted for 25% of the global energy consumption. Since then, LNG demand increased further by 12.5% to 359 Mt produced in 2019 (Shell 2016*a*,*b*,*c*,*d*, Ritchie & Roser 2014). The outlooks assume the growth is driven by the lower CO_2 emission rates of LNG compared to coal, which is rapidly being replaced by gas (Shell 2016*e*, Williams et al. 2015). LNG is still a fossil fuel and a net emitter of CO_2, although at a lower rate than those of MGO and other petrol fuels. Ac-

cording to Navingo BV, an international media company, 600 vessels were currently either in operation or under production in 2018, with a rapid growth in demand (NBV 2018). However, due to quickly emerging carbon-neutral technologies, LNG may by many be viewed as a transition fuel. As mentioned earlier, Norway is already moving away from LNG as a fuel in ferries, not considering the reduced emissions compared to conventional petrol fuels good enough.

Properties and risks

Natural gas consists of mostly methane. In its pure state, the gas is colourless and odourless. LNG is combustible and releases large amounts of energy when ignited. As it would be gaseous at room temperature, LNG is stored at low temperatures, just above its atmospheric boiling point but pressurised to remain in liquid form (Faramawy et al. 2016). Some relevant properties of LNG are summarised in Table 3.2.

Similar to distillates, natural gas is not a pure substance, but a mixture of different components at varying concentrations. Some of the properties, for example density and the flammability limits are dependent on composition, temperature and pressure. The minimum ignition energy and the flammability limits of the table describe the vapour behaviour of the gas. The values of Table 3.2 are therefore estimates rather than accurate values.

Table 3.2: Selected thermophysical properties of natural gas (NG) at 1 bar and 25 °C.

Property	Unit	NG value	Reference
Lower heating value	MJ/kg	47	(Kumar et al. 2016) (Ellis & Tanneberger 2015)
Liquid density	kg/m^3	420-450	(Fjeldheim 2012)
Boiling point	K	112	(Kumar et al. 2016) (Ellis & Tanneberger 2015)
Minimum ignition energy	mJ	0.28	(Cui et al. 2016)
Flash-point	K	85	(HSDB 2020*b*)
Auto-ignition temperature	K	810	(Ellis & Tanneberger 2015)
LFL	%	5.0	(Liao et al. 2005) (Zabetakis 1965)
UFL	%	15	(Fjeldheim 2012) (Zabetakis 1965)
Maximum laminar burning velocity	cm/s	45	(Zabetakis 1965)
Speed of sound	m/s	450	(Zuckerwar 2002)

Natural gas is a highly flammable substance with a flammability range between 5.0 and 15%. The values for UFL and LFL seem to remain fairly constant with changes in ethane content, according to Liao et al. (Liao et al. 2005). Zabatakis found the LFL for methane and ethane to be 5.0% and 3.0%, respectively (Zabetakis 1965). The values suggest that

the LFL would be close to 4.0% when the natural gas is composed of equal amounts of ethane and methane. As methane is the most abundant in the mixture, the LFL rests close to 5.0%.

According to Kumar et al., the lower heating value of natural gas is about 46.7 MJ/kg (Kumar et al. 2016). This is higher than that of diesel. Because of the higher density of diesel, however, the energy content of diesel per litre is much higher than that of LNG, at about 36 MJ/l versus 21 MJ/l. With regard to most applications of the fuel, the volumetric energy density is of most importance.

The risk of explosion is higher with substances that are gaseous at room temperature compared to liquids with high flash points. A substance's speed of sound sets the limit for the leak velocity when driven by pressure differences. Methane carries sound at higher velocities than air and therefore leaks and mixes with air more quickly than denser gases would manage (Zuckerwar 2002).

Due to the boiling point of natural gas being well below room temperature, LNG only exists as a gas at room temperature. When stored cryogenically, the temperature will slowly rise due to heat leaks. The leak causes some of the LNG to evaporate, producing so called boil-off gas. This gas will steadily increase the pressure in the tanks and must be handled before the stress on the tanks becomes too great. It can either be re-liquefied, torched or used as fuel. Re-liquefaction requires large and expensive equipment, and is primarily an option for LNG carriers or spacious ships travelling longer distances. Burning the fuel may wastes valuable energy. Use as fuel is not always ideal either, as the more volatile parts of the LNG mixture evaporates first and gas turbines can be highly sensitive to the composition of the fuel. LNG therefore presents a challenge for long-haul vessels with variable travel distances and docking frequency.

According to the safety data sheet of Gasnor, an LNG producer and distributor, LNG is not poisonous or harmful to inhale. If large amounts evaporate, LNG may harm by lowering the oxygen content locally, and an ignition may cause flames and powerful explosions. Apart from these considerations, LNG is cold and may cause frostbite upon contact (Fjeldheim 2012). Evaporated LNG is lighter than air, but due to the cold temperature the gas will cool the surrounding atmosphere and fall downwards in ambient environments. This event may generate flammable clouds close to the ground.

3.3.3 Hydrogen

Hydrogen and energy have a long, shared history. Hydrogen powers the stars of the universe, and although the chemical does not naturally exist in its pure form on Earth, humans have managed to produce and use it for centuries. Hydrogen was the fuel of the first internal combustion engines more than 200 years ago, and in the 20th century it powered spaceflights. During the mid-20th century, hydrogen became an important part of the oil refining industry. Thus, the demand increased, and it has continued to rise in the 21st century. Hydrogen is today almost exclusively produced from fossil fuels. As a consequence,

hydrogen producers were in 2019 according to the IEA responsible for emitting a similar amount of CO_2 as the UK and Indonesia combined, at 830 Mt (Gül et al. 2019). Hydrogen has, however, the potential to supply energy without any greenhouse gas emissions. Hydrogen is today produced synthetically at industrial scale, but the gas can be produced renewably from electricity, biomass and fossil fuels with carbon capture.

According to the IEA, the annual production of pure hydrogen was in 2019 estimated to have reached 73.7 Mt by 2018. 94.3% of the hydrogen is used by the refining (42.7%) and ammonia production (51.6%) industries (Gül et al. 2019). The data indicates a lack of initiatives globally to implement hydrogen as a fuel. The demand for hydrogen for other uses has risen since 2010, at an annual rate of 4%. The level will still have to increase at an even quicker pace for hydrogen to become a major energy carrier during the next decades. The EU aims to achieve this, with hydrogen produced by electrolysis a key part of their climate strategy (EC 2019*a*). In Norway, there are several initiatives ongoing. Norled, a shipowner, has planned for two hydrogen ferries in operation by 2021 (Stensvold 2018*b*, 2019*a*). The Hellesylt Hydrogen Hub, an interest group, is facilitating for large-scale hydrogen electrolysis to supply cruises and ferries in the Geieranger fjord, and a liquid hydrogen production facility is planned at the Mongstad refinery (Brunborg 2019, Skarsgård 11/05/2020).

Properties and risks

In contrast to the previously discussed fuels, hydrogen is a pure substance with better defined thermophysical properties. The gas itself is colourless and odourless. Some of the properties of hydrogen are presented in Table 3.3.

Table 3.3: Selected thermophysical properties of hydrogen at 1 bar and 25 °C.

Property	Unit	Hydrogen value	Reference
Molar mass	g/mol	2.0	(Blackman & Gahan 2013)
Lower heating value	MJ/kg	120	(Linstrom & Mallard 2020)
Density	kg/m^3	0.081	(ET 2018)
Boiling point	K	20	(Haynes 2015)
Minimum ignition energy	mJ	0.017	(Ono et al. 2007)
Auto-ignition temperature	K	830	(Colonna 2010)
LFL	%	4.0	(Liu & Zhang 2014) (Zabetakis 1965)
UFL	%	75	(Zabetakis 1965)
Maximum laminar burning velocity	cm/s	300	(Dahoe 2005) (Dong et al. 2010)
Speed of sound	m/s	1300	(Zuckerwar 2002)

Hydrogen is a special gas, as reflected by some of the properties in Table 3.3. It has an extensive flammability interval, boils at extremely low temperatures, ignites much more

easily than other fuels and it is the lightest of all gases. One conclusion of the table is the very different nature of hydrogen, compared to the previously discussed MGO and LNG.

Looking at the lower heating value, hydrogen is unrivalled by fuels in its gravimetric energy density, with 120 MJ/kg. On the other hand, when combined with the density of hydrogen the gas displays a poor volumetric energy density, at 0.011 MJ/l. This compares to 36 MJ/l for diesel, for example. If in liquid state, the mass density is 71 kg/m^3 and the energy density 8.5 MJ/l (Linstrom & Mallard 2020). This reflects a major obstacle for effective hydrogen application as a fuel. As previously discussed, the volumetric density is usually of most importance. The references for the the mass, density and the calorific value are the NIST Chemistry WebBook and SI Chemical Data, both considered to be the most reliable sources of information.

The combination of the wide flammability range and the insignificant ignition energy required for combustion to occur, designates hydrogen as a more challenging fuel to handle than those previously discussed. In addition, according to two separate studies, hydrogen has several times been reported to ignite spontaneously, without any apparent source of the ignition (Astbury & Hawksworth 2007, Bragin & Molkov 2011). Regarding the flammability limits, ignition at concentrations below 8% are unlikely to reach any strong reactions, and flames will only manage to propagate upwards through buoyancy, according to Zabetakis (Zabetakis 1965).

At ambient conditions, the speed of sound travels through hydrogen at about 1300 m/s, much faster than for the other fuels discussed. As a consequence, pressurised hydrogen leaks quickly, and smaller leaks may contribute to large amounts of hydrogen escaping, relative to other gases. The laminar burning velocity of hydrogen at reactive concentrations is also much higher than for the other fuels discussed. The value is high enough to develop blast waves unconfined situations, heightening the potential damage explosions can cause. The maximum burning velocity of 300 cm/s is verified by several studies (Dahoe 2005, Dong et al. 2010). Hydrogen burns faster in fuel rich mixtures, and the maximum value is reached at equivalence ratio $\phi = 1.7$. The equivalence ratio represents the amount of fuel in the mixture compared to the stoichiometric relation.

The *CRC Handbook of Chemistry and Physics* is used as a reference on the boiling point of hydrogen. The value of 20 K implies that large amounts of energy, along with specialised storage tanks will be required to store liquid hydrogen, as the storage temperature must be kept at 20-30 K and 1-10 bar. The alternative to storing hydrogen in liquid form, is to compress the gas to several hundred bar, also requiring energy.

Relative to other substances, hydrogen is among the molecules with the weakest attractive forces, as indicated by the corresponding van der Waals constant of the gas, at only 0.25 L^{2}bar/mol^2(Weast 1972). This attribute contributes to more resistance to compression relative to other gases, as modelled by Tietze et al. The results indicate a substantial difference in energy requirement for compressing hydrogen relative to methane. On a compression ratio of 5, the energy required was 20-25% higher for hydrogen for both

isenthalpic and isentropic compression (Tietze & Stolten 2015). Methane has a higher calorific value than hydrogen. The results are therefore worse for hydrogen when considering the measure of energy required to compress each unit of energy.

3.3.4 Ammonia

The development of the Haber-Bosch process in the early 1900s opened the door for ammonia production on industrial scale. In recent years, the annual demand for ammonia has been around 170 Mt. Traditionally, ammonia production has been driven by fertiliser demand. In later years, demand for ammonia has risen also in other sectors, and the chemical is widely used in refrigeration, pharmaceuticals and textiles (MI 2019). According to the Food and Agriculture Organization of the UN, the fertiliser industry is expected to consume 50-60% of ammonia supply in the years 2020-2022, as has been done in 2016-2019 (FAO 2019). According to the IEA, the production capacity is expected to increase somewhat in the coming years, due to increased production in Southeast Asia (Levi et al. 2019).

As a carbon-free carrier of hydrogen, ammonia has recently received attention for its potential to store energy chemically. There are now multiple initiatives for producing ammonia from electrolysed hydrogen. Saudi Arabia is building world's largest production plant for ammonia from electrolysed hydrogen, and the project is due to finish by 2025 (Sampson 2020). Siemens has recently announced a 5 GW electrolyser plant in Australia, and considers ammonia as a potential carrier for the hydrogen produced (Brown 2019*b*). In Norway, Yara International, a fertiliser and chemicals producer, are also currently preparing for "green" ammonia production from electrolysis of hydrogen (Stensvold 2019*c*, 2020).

Properties and risks

Ammonia is as hydrogen a pure substance. The gas is colourless and has a characteristic and repelling odour in addition to being highly toxic. Some of the properties of ammonia are presented in Table 3.4.

Table 3.4: Selected thermophysical properties of ammonia at 1 bar and 25 °C.

Property	Unit	Ammonia value	Reference
Molar mass	g/mol	17	(Blackman & Gahan 2013)
Lower heating value	MJ/kg	19	(Linstrom & Mallard 2020)
Density	kg/m^3	0.69	(Blackman & Gahan 2013)
Boiling point	K	240	(O'Neil 2013)
Minimum ignition energy	mJ	680	(Buschman 1980)
Auto-ignition temperature	K	920	(Colonna 2010)
LFL	%	15	(Colonna 2010)
UFL	%	28	(Colonna 2010)
Maximum laminar burning velocity	cm/s	6.5	(Hayakawa et al. 2015)
Speed of sound	m/s	440	(ET 2008)

By combining the density and lower heating value of Table 3.4, ammonia has a higher volumetric energy density to that of hydrogen, at around 12 MJ/m^3 versus 10 MJ/m^3. However, the liquid density of ammonia is 680 kg/m^3, and to reach high energy densities, ammonia is therefore often stored and transported below its boiling point or pressurised at ambient temperature. Wang et al. argues that even though ammonia can be applied in internal combustion engines, it is more effective as a hydrogen carrier (Wang et al. 2013). This is due to a high auto-ignition temperature and minimum ignition energy, as presented in Table 3.4 (Gill et al. 2012). The difficulty combusting heightens the risk of ammonia slip, and operating temperatures must be high for all of the fuel to react. To avoid ammonia slip, the gas is often burned together with another, more combustible gas, e.g. hydrogen or diesel. As indicated, ammonia is an efficient carrier of hydrogen, storing up to 136 kg/m^3.

The flammability range of ammonia begins at a concentration of 15%. As ammonia has a strong odour, the gas can easily be detected before significant concentrations manage to build. According to Smeets et al., whose team empirically tested many subjects, humans can usually notice ammonia concentrations lower than 5 ppm (Smeets et al. 2007). Ammonia can become severely irritable at concentrations above 100 ppm for more than an hour. At around 1000 ppm (0.1%), people exposed are incapacitated from coughing and eye irritation, and above 5,000 ppm (0.5%) short exposure can be fatal (TFI 2010). As ammonia exposure will be fatal well below its lower flammability limit, toxicity is of most concern. Ammonia requires a strong ignition source to ignite and burns at a slow pace. According to Hayakawa et al., ammonia burns slowly enough for buoyancy to disrupt the flammable cloud, as heated gases rise more quickly than the flame front (Hayakawa et al. 2015). The explosion risk is thus negligible, compared to the toxic properties of the gas.

3.3.5 Biofuels

A biofuel is a fuel produced from biomass through modern processes, in contrast to the natural and more gradual production of fossil fuels. Biofuels can be produced either from food crops or from energy crops, which are inexpensive crops with a low maintenance

requirement and solely produced for biofuel production. Biofuels can alternatively be produced from biological waste, available in large amounts industrially and domestically. The supply of biomass from waste more than doubled from the year 2000 to 2016, yet constitutes less than 5% of total biomass available for use in fuel production, highlighting the important contributions from food and energy crops (WBA 2019). Biofuels are mainly used as additives to gasoline blends, and the IEA predicts ethanol to replace 10% of fossil fuels used in such blends by 2030 (Teter 2020). The demand for biofuels is increasing, and the annual production of ethanol has in return increased more than eight-fold from 2000 to 2019, to around 90 Mt (EIA 2016, RFA 2020).

There exists multiple types of biofuels, though the two most common types of biofuels are bioethanol and biodiesel, with respective shares of 62% and 26% of global biofuel production in 2017 (WBA 2019). Bioethanol can be produced by fermentation of carbohydrates, while biodiesel is produced through transesterification of vegetable and waste oils. The reactants for the biofuel production may derive from a variety of crops, resulting in an ethical dilemma about whether to use arable land for biofuels production. This places fuel production in direct competition with food production and raises food prices.

First generation biofuels are produced from food crops grown on arable land, typically starch and sugars, along with vegetable oil. Second generation biofuels has a wider definition, with the main difference being that the production does not hinder food production. Second generation biofuel feedstocks comprises biological waste and lignocellulosic biomass, woody crops and energy crops grown on land unsuitable for food production. Third generation biofuels are produced from algae, which in theory is a more efficient alternative with regard to area and would not compete with food production. This production route requires further development before becoming commercially viable, yet it seems an interesting prospect for the future (Raheem et al. 2018, Hossain et al. 2019).

With global population increasing fast, second generation biofuels have the advantage of not competing with food production. On the other hand, the fuel is usually harder to extract from second generation feedstocks, requiring more expensive and complex production pathways (Miret et al. 2016, Sanches & Cardona 2007, Taylor et al. 2009, Rastogi & Shrivastava 2017). Even so, production of second generation biofuels is on the rise, with multiple new facilities planned for the coming years (Zervos & Adib 2019). In this section, only bioethanol will be considered further.

Properties and risks

Ethanol has uses ranging from functions as a disinfectant, a chemical solvent and a food and drinks ingredient, to that of a fuel. The substance is clear and colourless, with a characteristic vinous odour. Some of the relevant properties of ethanol are given in Table 3.5.

Table 3.5: Selected thermophysical properties of ethanol at 1 bar and 25 °C.

Property	Unit	Ethanol value	Reference
Molar mass	g/mol	46	(Blackman & Gahan 2013)
Lower heating value	MJ/kg	27	(Haynes 2015) (Medina & Roberts 2013)
Density	kg/m^3	790	(Blackman & Gahan 2013) (Ellis & Tanneberger 2015)
Vapour pressure	kPa	8.1	(ILO 2017)
Viscosity	mPa·s	1.1	(Haynes 2015)
Boiling point	K	350	(Haynes 2015) (Medina & Roberts 2013)
Flash point	°C	13	(HSDB 2020*a*)
Minimum ignition energy	mJ	0.23	(Benedetti & Benedetti 2003)
Auto-ignition temperature	K	640	(Ellis & Tanneberger 2015) (Colonna 2010)
LFL	%	3.3	(Coronado et al. 2012) (Brooks & Crowl 2007)
UFL	%	19	(Coronado et al. 2012) (Brooks & Crowl 2007)
Maximum laminar burning velocity	cm/s	47	(Gulder 1982)

From Table 3.5, ethanol has a higher lower heating value than that of ammonia, yet lower than that of diesel. The volumetric energy density is at 21 MJ/m^3, the highest of all the fuels discussed except for diesel. Ethanol has a low boiling point, and may produce explosive vapours at room temperature, as indicated by the flash point. If allowed to reach its vapour pressure at 20 °C (6.0%) and ignited, ethanol can combust stoichiometrically (ILO 2017). The alcohol is an effective hydrogen carrier as well, but while hydrogen makes up 18% of the molar mass of ammonia, only 13% of the molar mass of ethanol derives from hydrogen. In total, the hydrogen content of ethanol can reach 103 kg/m^3, lower than ammonia but higher than for pure hydrogen in liquid phase.

Controlling the temperature below 287 K can be an effective safety measure for ethanol, as leaks will not be able to produce explosive vapours. A combination of temperature control and ventilation may be a good option to control ethanol safety. Ethanol is not considered harmful. Strong vapours may mildly irritate skin, eyes and throat.

3.3.6 Summary

Diesel, LNG, hydrogen, ammonia and ethanol have been presented as some of the fuels available for use in ferries. Diesel and LNG have been used in ferries for years, hydrogen ferries are expected in operation during the next years and a larger ammonia-fuelled vessel is currently being built. In Norway, a pioneer in new energy solutions for the maritime sector, hydrogen and ammonia ferries and offshore vessels are under production (Stensvold

2018*b*, Stensvold & Jensen 2020, Stensvold 2019*b*). Ethanol, however, is novel for use in vessels. Ethanol has been widely used for cars in fuel blends, but the fuel has not been applied to marine vessels.

Table 3.6: Price per unit of energy for the fuels discussed in this section.

Fuel	Price [USD/GJ]	Reference
MGO	14	(S&B 2020)
LNG	7.6	(DNV GL 2020)
Hydrogen - SMR	6.7	(Brown 2019*a*)
Hydrogen - Electrolysis	50	(HC 2020)
Ammonia - SMR	32	(Etienne et al. 2016)
Ammonia - Electrolysis	64	(Brown 2020*a*)
Ethanol	56	(GPP 2020*b*)
Bioethanol	56	(PDA 2020)

The prices of the different fuels are estimated in Table 3.6. The table is to give an impression of the relative costs for the fuels, as the prices are volatile and the values are gathered from different regions. The MGO price is given by the low sulphur Rotterdam price at the end of 2019. The prices for carbon-based fuels are usually high in Norway when compared to international prices. For example, in the summer of 2020, Norway had the highest road-diesel prices globally (GPP 2020*a*).

The LNG price is gathered from a report by DNV GL on the current price development for oil and gas. The gas price presented in Table 3.6 is based on a price of 4.0 USD/mmBTU for European gas, a rough estimate for the last two years. Liquefaction adds a cost of 4.0 USD/mmBTU, with the report estimating this expense to add 3-5 USD/mmBTU to the price.

The SMR hydrogen price is for the Netherlands (Brown 2019*a*). For hydrogen especially, added costs may be expected due to the lack of infrastructure. The electrolysis hydrogen price is, as the table indicates, at the moment far from cost competitive. The electrolysis hydrogen price is given as about 6.0 USD/kg in a recent report by the Hydrogen Council (HC 2020). Though stating that the price depended heavily on region, no further details about the assumed price of electricity were provided.

The ammonia price is presented in a paper by Etienne et al., presenting data from the World Bank on the ammonia price (Etienne et al. 2016). The value given in Table 3.6 is a rough estimate of the average value in the US for the last ten years, at 600 USD/ton. The green ammonia price is based on an article by the Ammonia Energy Association, which in the summer of 2020 estimated the price of green ammonia to be about double the price of conventional ammonia (Brown 2020*a*). The price of green ammonia should be slightly higher than the price for green hydrogen.

The price for ethanol is also gathered from the GlobalPetrolPrices.com database, and the

value is the based on Swedish ethanol (GPP 2020*b*). The bioethanol price is on the other hand based on standard Philippine prices, due to lack of other sources (PDA 2020). The similarity between the two ethanol prices is in this case a coincidence. Sweden, as with Norway, seems to have relatively high fuel prices, while the Philippines seem to have diesel prices at less than half of those in Norway and Sweden (GPP 2020*a*). There is reason to believe that the prices would be different in a similar setting. From the values gathered in Table 3.6, ethanol has the highest price per unit of energy of the fuels in this section. Price is therefore at the moment a significant barrier for widespread ethanol application.

In the Markets Insider database, US bioethanol prices can be compared to those of natural gas and gasoline (MI 2020). For the last three years, the average prices for ethanol, natural gas and gasoline were about \$17/GJ, \$2.6/GJ and \$13/GJ, respectively. The US prices are low, relative to European prices. Ethanol production is also subsidised in the US (TCS 2015). The US prices likewise indicate a relatively high ethanol price. The US ethanol prices from Market Insider correlate to those from GlobalPetrolPrices.com. Swedish prices are roughly three times higher than those of the US. The example demonstrates the inaccuracy in comparing prices across regions and fuels.

Even though SMR hydrogen has the lowest value of Table 3.6, the added costs following the lack of infrastructure and an increase of CAPEX due to safety and the required extra storage volume will affect the factual value positively. The International Renewable Energy Agency (IRENA) estimated in 2018 that with low prices and renewable electricity like in Denmark and Norway, green hydrogen can be sold at the price of 41 USD/GJ, lower than the 2020 road-diesel price of Norway, at about 45 USD/GJ (Taibi et al. 2018, GPP 2020*a*). IRENA's estimates were criticised by the International Council on Clean Transportation for being overly optimistic with regard to power prices (Bellini 2020).

The discussion on fuel prices in this section is simplified, as the aim is not to give a thorough economic analysis but only ballpark estimates. The production costs, life-cycle efficiencies and other factors affecting the fuel prices are not discussed. For example are the prices of green hydrogen and ammonia almost solely dependent on the price of renewable electricity.

In the subsections on the different fuels, properties for each have been presented. Some of these properties are presented in Table 3.7. The references are presented in the subsections. The densities of this table are based on the storage conditions of the individual fuel. For hydrogen, the liquid density is provided in the table.

Table 3.7: Comparison of selected thermophysical properties of the different fuels discussed.

Property	Unit	MGO	LNG	Hydrogen	Ammonia	Ethanol
Lower heating value	MJ/kg	43	47	120	19	27
Density	kg/m^3	860	430	71	680	790
Boiling point	K	450-920	110	20	240	350
Flash point	°C	60	-	-	-	13
Minimum ignition energy	mJ	1.15	0.28	0.017	680	0.23
Auto-ignition temperature	K	520-570	810	770	920	640
Flammability interval	%	1.0-6.0	4.0-15	4.0-77	15-28	3.3-19
Maximum laminar burning velocity	cm/s	40	45	300	6.5	47

From the properties of the fuels as presented in Table 3.7, hydrogen is by a margin the most reactive fuel, requiring most attention. While MGO and LNG currently have IMO frameworks for fuel application in vessels, application of hydrogen, ammonia and ethanol demands an alternative design procedure, a thorough and expensive process described in Chapter 3.5. In this section, ethanol was concluded to be relatively safe to handle. The IMO is in 2020 also developing rules for ethanol, an indication that the hazards posed are manageable by standardised solutions (IMO 2019). Insight into the proposed rules is provided in Chapter 3.5.

3.4 Computational fluid dynamics

3.4.1 Introduction to CFD

The aim of computational fluid dynamics (CFD) is solving problems involving fluid flows and heat transfer, using numerical analysis and data structures. Codes designed to solve such problems are applied in a wide range of fields. These allow users to easily observe how fluids interact with surroundings, without performing an experiment. In this section, CFD software specialised in gas dispersion and explosion studies for safety purposes is discussed.

CFD codes across disciplines are fundamentally structured in a similar fashion, differing only in which assumptions form the basis of the calculations. In the ensuing paragraph, the basic equations for CFD codes are described briefly. The FLACS software, which is most relevant for this thesis, will be described in more detail later in this chapter (Stultz & Kitto 2002).

The foundation for the codes are conservation laws. For single phase, single specie and compressible flow, the mass, linear momentum and energy are conserved locally and can only be transferred by a continuous flow. This system of equations must then be coupled with the following sets of equations:

- Fundamental relationships for the viscous stress tensor, governing the transfer of momentum across the fluid.
- Fundamental relationships for the diffusive heat flux, governing the transfer of heat across the fluid.
- A thermodynamic equation of state (EOS), relating state variables and describing the state of matter under a given set of physical conditions.
- A caloric equation of state, relating temperature and internal energy and heat capacity.

Given the sets of equations above, the compressible Navier-Stokes (C-NS) equations can describe the flow of a viscous fluid on a Cartesian grid when solved for the three dimensions, in addition to the time dimension. The C-NS equations are derived by applying Newton's law of motion to a fluid element. The equations mathematically express the conservation of momentum, energy and mass and generate a velocity vector for every point in the fluid at every moment in a time interval. The equation for the x-value of the vector is given in Equation 3.15 (Stultz & Kitto 2002, CFDO 2020*c*).

$$\rho\Big(\frac{\partial u_x}{\partial t} + u_x\frac{\partial u_x}{\partial x} + u_y\frac{\partial u_x}{\partial y} + u_z\frac{\partial u_x}{\partial z}\Big) = -\frac{\partial \rho}{\partial x} + \mu\Big(\frac{\partial^2 u_x}{\partial x^2} + \frac{\partial^2 u_x}{\partial y^2} + \frac{\partial^2 u_x}{\partial z^2}\Big) + \frac{1}{3}\mu\frac{\partial}{\partial x}\Big(\frac{\partial u_x}{\partial x} + \frac{\partial u_y}{\partial y} + \frac{\partial u_z}{\partial z}\Big) \tag{3.15}$$

From this point, the CFD code can be specialised for its purpose. To observe sound waves, for example, one begins by deriving the compressible Euler equations from the C-NS by assuming a frictionless flow and no diffusive heat flux. Then the linearised compressible Euler equations (LCEE) can be derived by assuming that all flow variables, e.g. velocity and density, can be explained by the equation $f = f_0 + f'$, where f_0 is the value at at reference state and f' the change from this state. The LCEE have many variations in the field for aeroacoustics (Bailly & Juvé 2000).

In all approaches, the same elemental procedure is inherent. In the first step, pre-processing, the geometry is built and physical boundaries defined, usually with help of computer aided design (CAD). From the geometry, the fluid domain is set. The volume of the domain is arranged into discrete cells, to simplify the equations to a limited volume. Together, these cells form the grid of the simulation. The scenario is set up, specifying which models to use for the simulation, and the boundary conditions are set, including the initial conditions for transient simulations. In the second step, the simulations are initiated and the sets of equations are solved iteratively. In the third step, a post-processor prepares the results for visualisation.

3.4.2 Different codes

According to Plasmans et al., a major challenge with CFD software in the risk management field is the difference in results obtained from different codes (Plasmans et al. 2013). The article lacks a good discussion of the strengths and weaknesses of different codes. A base case is given and the results obtained using different codes are presented without the reader understanding of which tool each result was produced from. The results are presented as different, as they are, but the results are exaggerated by one extreme value in each case presented. Either way, the paper presents the valid point that results vary greatly, both between codes but also between users of the same code. Experience built by using software to recreate empirical data is of high value when setting up the geometries and scenarios. Knowing the limits and validity of the code and how to size the spatial resolution with regard to the scenario and geometry studied may lead to exponential differences in time-consumption, and not least, major differences in prediction for otherwise similar simulations.

CFD codes are difficult to compare and there are few published studies where different codes are applied to the same task. However, during the European HySafe programme developers of different CFD codes and other users were invited to estimate the outcome of hydrogen release and dispersion in a container. The study was a blind test, where the programmers were unaware of the observed results (Venetsanos et al. 2009). This is likely to be the largest comparison of different CFD codes with regard to dispersion prediction. The codes included in the benchmark study were PHOENIX, FLACS, KFX, CFX, Cast3M, ADREA-HF, GASFLOW, Fluent and FDS. FLACS obtained good predictions at all gas sensor locations by two independent modelling teams. The highly diverse results between the different codes and the different users support the statement of Plasmans et al. For example, CFX and Fluent were used by 3-4 different teams. For both, a large scatter

in results among the different users were observed. The results can only to a small degree be used to compare the codes, as they are heavily user dependent and may specialise on different scenarios. This study only observed hydrogen, a substance with many extreme properties to various degrees covered by the different codes.

3.4.3 FLACS

FLACS was chosen as the CFD consequence model for this thesis. The FLACS software was developed by Gexcon (Earlier CMI/CMR) in Bergen. The development was sponsored by the Gas Explosion Safety programme, funded by the oil companies BP, Elf Aquitaine, Esso, Mobil, Norsk Hydro and Statoil. The first version of the code was released in 1986 (Gexcon 2019).

In the pre-processor, CASD, the geometry is built or imported from CAD, models and boundary conditions are chosen, the initial conditions are specified and the grid is defined. Porcalc, a program, then reads the grid and the geometry files and assigns volume and area porosities to each cell, allowing sub-grid objects to influence the simulations. The simulations can be initiated either from the command line or from RunManager, a software supplied by Gexcon. Flowvis, the post-processor, prepares the results for analyses and visualisations.

Fundamental equations

From the C-NS, the FLACS code assumes any flow variable f defined by the representation $f = F + f''$, where F is the classical ensemble-average, i.e. expectancy value, of the flow variable and f'' represents the deviation from this average. By these assumptions, the Reynolds-averaged Navier-Stokes (RANS) equations are derived. The RANS equations allow for simpler solutions to the C-NS for fluid flow and facilitates for greatly reduced computation times than by solving the complete C-NS. By averaging the variables, some information is lost, and the size of the ensembles becomes a question of accuracy versus computing time. The RANS model required additional modelling to close non-linear terms, and multiple turbulence models have been designed for this purpose (Panton 2013).

The k-epsilon (k-ϵ) turbulence model is one of the most common and validated forms of generating mean flow characteristics from turbulent conditions for CFD codes (CFDO 2020*b*,*a*). The model is based on the RANS equations and predicts turbulence based on two partial differential equations defining turbulence kinetic energy (k) and dissipation of turbulent kinetic energy (ϵ). The model is tailored for planar shear layers and recirculating flows. It should not be used for flows containing large pressure gradients, such as inlets or compressors. For FLACS' part, the model is the simplest turbulence model for which only initial- and boundary conditions needs to be specified. Together with the ideal gas equation of state, the two extra equation sets allow for closure of the RANS equations (Launder & Spalding 1974). In the code, the FLACS manual informs that the k-ϵ model is coupled with other sub-grid models, to account for influence from objects not resolved

on the computational grid. Examples of such sub-grid models can be initial flame propagation, point-leaks, flames and fluid flow around small geometries and the effect of water spray on an explosion (Gexcon 2019, Hisken 2018).

To simulate gas explosions, the numerical model of FLACS solves Favre-averaged C-NS (FANS) equations for mass, momentum, heat, turbulent kinetic energy, rate of dissipation of turbulent kinetic energy, mass fraction of fuel and mixture fraction on a structured Cartesian grid (Gexcon 2019). While RANS equations average over time, FANS equations average over density and are more complicated than the RANS. For explosions, where significant fluctuations in density can occur, FANS equations will provide more accurate results than those of RANS equations (CFDO 2020*a*).

Equation of state

FLACS applies the ideal gas EOS. An EOS relates temperature, volume and pressure. The generic formula for an EOS can therefore be written on the form of Equation 3.16. The ideal gas EOS is represented by Equation 3.17, where R is the ideal gas constant and n represents the amount of substance in mol.

$$f(T, p, V) = 0 \tag{3.16}$$

$$f(T, p, V) = pV - nRT = 0 \tag{3.17}$$

The ideal gas EOS is a simple approximation functioning well in many cases. Due to its simplicity, however, it has many limitations. The ideal gas EOS neglects both molecular size and inter-molecular attractions. The EOS is most accurate for mono-atomic gases at high temperatures and low pressures, when interaction between molecules, dependent on molecule size, are minimal. The negligence of attractive forces between molecules renders the EOS unable to predict condensation. Additionally, real-gas pressures are often lower than for ideal gases due to the attractive forces.

To correct for the errors in the ideal gas EOS, the van der Waals EOS serve as a simple and much more accurate EOS for real-gas behaviour. The van der Waals EOS can be viewed as a fix for the ideal gas EOS' most notable flaws, as it includes particle size and attractive forces. These values must be supplied for all gases however, and the EOS looses the generality of the ideal gas EOS, which functions similarly for all gases. Furthermore, if modelling real gases, modern EOSs can prove much more accurate while only slightly more complicated. Examples of such are the Soave-Redlich-Kwong (SRK) EOS, which is specialised for the behaviour of hydrocarbons and the Peng-Robinson EOS, similar in many ways to the SRK EOS, but superior in predicting liquid densities, especially for non-polar species (Soave 1972, Donnez 2007, van der Waals 1873).

An exact explosion model can not be based on the ideal gas law, but requires detailed kinetics for every reaction along with the position and momentum of every particle. Such a

system is as of now impossible to design and would require immense computing power. For CFD codes to be valuable tools, they must balance the need for both accuracy and speed. While FLACS has the ideal gas EOS at its base, the code is equipped with multiple adjustments to handle real-gas behaviour, as discovered through extensive validation. The following example of a sub-grid model implemented in FLACS is given by Prankul Middha in his doctoral degree (Middha 2010).

Hydrogen, as a particle lighter than air, diffuses at a much quicker pace than oxygen and nitrogen. In a flame front moving through a hydrogen-air mixture hydrogen, rather than oxygen would diffuse into the flame. The effect would be a richer fuel mixture at the front, and a higher burning velocity where this phenomenon occurs, creating unevenness in the front as well. Fuels with a mass larger than oxygen observes the opposite effect. Oxygen diffuses into the flame front at a higher rate than the fuel, inducing a leaner fuel mixture and a lower burning velocity. A simple system at the base accompanied by properly designed sub-grid models to fix the most important problems can be more effective than a complex system as the standard. While FLACS can simulate explosions with grid sizes two orders of magnitude larger than the flame thickness using sub-grid estimation models, a more detailed code would require a much smaller grid and ultimately more computing power to simulate the same situation. A grid refinement by a factor of 10 would typically require 1000 times more grid cells and 10 times better time resolution, which amounts to 10,000 times more simulation time.

Based on the species' vapour pressure, a simple sub-grid model which could solve the condensation problem related to the ideal gas EOS could be designed. The problem is currently not solved in FLACS, as the pool model was designed for cryogenic fuels (LNG) initially and seems to have deficiencies for liquids with boiling points above ambient temperature. Today, FLACS only models evaporation of a pool without regard for the vapour-liquid equilibrium. The pool is designed to receive heat in the form of conduction from the ground, convection due to air movement and radiation from the sun. Energy is lost due to evaporation, and availability of energy represents the evaporation limitation.

An evaporation model as described might work well for species where the vapour pressure does not represent an obstacle. For these species in the current model, evaporation will proceed without regard for the vapour pressure, nor the absolute pressure for that matter. This was observed during the pool validation, described in Appendix B.3. A better model could be to use the vapour pressure as an equilibrium. The evaporation rate could be defined by the gas concentration and absolute pressure in the control volumes just above the pool. Condensation could be modelled by a negative evaporation rate. In such a case, mass would be transferred from the control volume above the pool to the pool, at a rate related to the difference between the partial pressure and the vapour pressure. A solution as the one proposed would provide a simple fix and allow for improved modelling of liquids with boiling points above ambient temperature.

Porosity model

The use of a distributed porosity model is according to the FLACS manual one of the key features distinguishing FLACS from other CFD codes (Gexcon 2019). The porosities allotted to the different cells permit FLACS to represent complex geometries on relatively coarse grids. While walls and larger objects are represented on grid, smaller objects are represented sub-grid. In simulations, a porosity field represents a local congestion and confinement, which allows sub-grid models to contribute with flow resistance, flame folding and turbulence generation in simulations.

Flame and explosion model

To estimate behaviour during explosions, FLACS relies heavily on the substances' laminar burning velocities, which are tabulated when defining each species. When a combustible mixture is ignited under quiescent conditions, the initial burning process is laminar, with a smooth flame front and propagation governed by thermal and molecular diffusion processes. The next phase in the explosion model is defined as quasi-laminar, where instabilities due to for example turbulence or molecular diffusion lead to a wrinkled flame surface. The quasi-laminar regime represents a transition from the laminar to the turbulent burning process.

The mentioned regimes are dependent on the species' pressure and temperature dependent laminar burning velocities, which through modifications presented by Bjørn J. Arntzen in his PhD thesis are combined to explicitly depend on pressure (Arntzen 1998). In FLACS, both the reactivity and the diffusion coefficients are also dependent on the species' laminar burning velocity. If accurate, such a model would effectively simplify the kinetics of the combustion and propagation processes. According to the FLACS manual, the model has been extensively validated, and multiple experiments are listed and described.

Validation

For a code to function properly, the developers must implement good models which then are adjusted after extensive validation. According to the manual, the FLACS code is well empirically validated for explosion scenarios. The main source of validation is a series of experiments with natural gas on scaled models of off-shore modules. This is not to say the models are without weaknesses. Following are some of the model weaknesses stated in the FLACS manual (Gexcon 2019). As stated earlier, the code is dependent on empirical values for the laminar burning velocity for many aspects of the model. The simplified and generic Le Chatelier's mixing rule is applied to predict flammability limits and is not accurate for mixtures at higher pressures and temperatures and excludes many substance-specific considerations. FLACS does not model detonations, when the flame propagation becomes super-sonic. However, by some adjustments in the scenario parameters, Hansen et al. demonstrated a way to model detonations using FLACS (Hansen & Johnson 2020).

Gas dispersion scenarios have also been validated through a broad range of land-based experiments. Still, the grid boundaries may be unreliable and should be placed some distance away from the situation observed, especially if wind is modelled. Another inaccuracy is of course the representation of complex geometry by solid blocks. The pool evaporation model is relatively new, and has been less validated than the explosion and dispersion models. The pool model has primarily been validated using LNG, and Gexcon acknowledges that the pool model might not function properly for fluids different in nature to LNG. For example, the pool model cannot handle preferential evaporation from multi-component mixtures (Gexcon 2019).

3.5 Relevant regulation

In this chapter, the relevant rules and regulations governing ship design and operation are discussed. The regulations have been adopted internationally through the International Maritime Organisation (IMO) and are often developed in cooperation with classification societies. Examples of such societies are Lloyd's Register, DNV GL and ABS, with headquarters in the UK, Norway and the US, respectively. These societies maintain the international standards by certification of ship design before construction, and the societies ensure continuing compliance by carrying out regular surveys. Classification of a ship is usually required to acquire marine insurance. In some cases, classification is demanded for ships to enter certain ports, being a certificate of the ships seaworthiness and integrity.

Before being classified, all ships introducing new technology, with regard to the power systems, not covered by current regulations require a risk assessment to be carried out. The application of all the fuels discussed in Section 3.3 except MGO must follow an alternative design approach, which includes performing a risk assessment (LR 2020). For LNG, rules are developed and included in the IGF code, but risk assessments are still required. The risk assessments can follow the standard IMO guidelines of the Formal Safety Assessment (FSA), as discussed later in this section (IMO 2018*b*).

3.5.1 IGF code and alternative design

The International Code of Safety for Ships using Gases or other Low-flashpoint Fuels (IGF code) came into force at the start of 2017 and regulates, as indicated by its name, the use of gases and low-flashpoint fuels in ships. The code contains mandatory procedures and standards for design, installation, operation and monitoring of machinery equipment and systems applying such fuels. Low-flashpoint fuels are fuels with flash points below 60 °C. The IGF code only contains detailed prescriptive rules for use of LNG as a fuel. In practise, these rules have become a standard to which class societies often look when evaluating other fuels as well, even though the rules are not universal. Hydrogen, for example, has very different properties than LNG. Fuels like hydrogen, ammonia and ethanol will all need to follow the rules of alternative design, regulated by SOLAS, the International Convention for the Safety of Life at Sea (IMO 2015, 1974).

Before standardised design procedures are developed for a given fuel, the alternative design procedure is the route to become classed. The basic principle of the alternative design procedure is approval of the vessel given a demonstration of safety and performance equal to or higher than the levels of conventional ships. The procedure follows the steps outlined in Figure 3.4.

An equal level of safety is not a well-defined measure. The Norwegian Centre for Transport Research found in 1998 that the Norwegian fatality rate for passenger vessels averaged at 0.6 per 1000 million passenger-kilometre from 1970-1994 (Assum 1998). The Norwegian Maritime Authority has previously required that vessels which transport passengers and follow the alternative design procedure operate at a risk level of maximum 1.0

fatalities per 1000 million passenger-kilometre more than a modern conventional vessel. Another measure, better suited for vessels not transporting passengers, is defining the fatal accident rate (FAR) among crew, namely the expected number of fatalities per 100 million work hours, roughly translating to the complete work careers of 1000 people. The European Union uses a slightly different measure, the number of annual fatalities at work per 100,000 employees. According to Eurostat, the average values for Europe and Norway are both around 1.65. (Eurostat 2018). This corresponds to FAR values around 1.0. Traditionally, maritime professions have had many times higher values primarily due to fatalities from fishing vessel accidents.

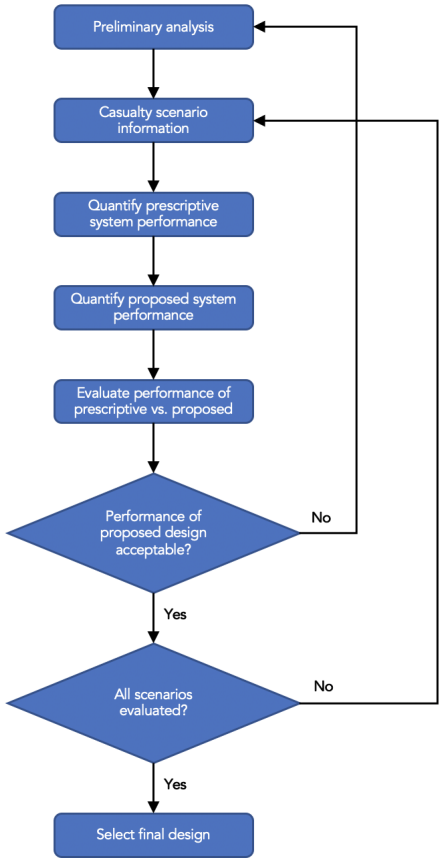

Figure 3.4: Illustration of the stages of the IMO alternative design procedure as described in SOLAS (IMO 1974).

The IMO FSA guidelines were revised in 2018 and set targets for risk levels of new vessels. For existing vessels, a fatality risk per year of 10^{-3} for crew and 10^{-4} for passengers is considered acceptable. The targets for new ships were adjusted to 10^{-4} and 10^{-5} for

crew and passengers, respectively (IMO 2018*b*). These targets are stricter than the values reflected by the 1000 million passenger-kilometre value of 1.0. During the last 20 years, risk acceptance in the population has decreased markedly. For traffic, death rates in Norway have decreased by a factor of 5 since 1970, to 108 deaths, the lowest per capita in Europe, and the rates reported by the Norwegian Centre for Transport Research may be considered as high today (SSB 2020). For Norwegian traffic, a possible average exposure to traffic among the population in the order of 30 minutes daily would correspond to exposure around 2% of the time. Considering a population of 5.3 million people, this compares 106,000 people constantly exposed. With 108 annual deaths, the annual fatality rate equals about 10^{-3}, similar to the earlier IMO tolerance criterion for members of crew. Here it should be noted that crew fatality rate would be per worker-year, while traffic exposure is constant. Thus the 10^{-3} annual fatality rate for crew would yield about 45 times more fatalities, assuming 1800 working hours per year. For a professional driver, spending 1800 hours in traffic a year, the FAR value would be around 10 and much higher than the target values discussed.

When applying by the alternative design procedure, the Norwegian Maritime Authority expects the involvement of an established class society, either by total certification or by giving an approval in principle (AIP) of the vessel or the relevant systems. To be eligible for an AIP, the following are expected: A detailed description of the vessel, a pre-HAZID, a HAZID, a gas explosion analysis and a risk assessment, along with documentation of the competence of the design team. This corresponds to the two first steps of Figure 3.5. A HAZID is a workshop where experts on the various parts of a system, along with other relevant people, come together to identify and discuss potential hazards and consequences, in a qualitative way. The risk assessment delves more deeply into the identified hazards, quantifying the risk associated with each. In sum, the risk must not exceed the limits of alternative designs, as mentioned earlier.

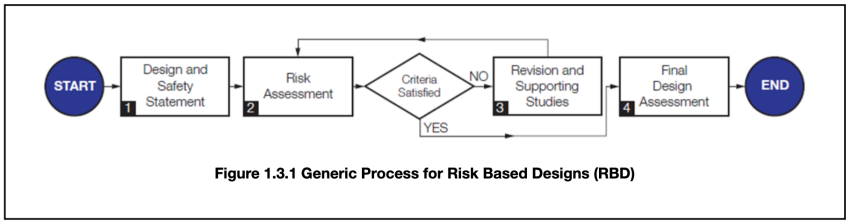

Figure 3.5: Generic process for risk based designs (RBD), from Lloyd's Register's RBD-procedure (LR 2018).

3.5.2 Use of fuel cells

The members of the IMO have not yet ratified rules for the use of fuel cells in seagoing vessels. Rules are under development. Lloyd's Register (LR) is currently developing new rules and has kindly allowed for insight into drafts of these, which in all likelihood are comparable to the IMO rules expected soon. In 2016, DNV GL developed its own rules

for fuel cell installations. In 2017, the European Maritime Safety Agency (EMSA), together with DNV GL, produced a report on the use of fuel cells in shipping, with regard to current and potential regulations and discussing safety aspects (Tronstad et al. 2017). The rules of most relevance to the thesis are discussed in the following paragraphs.

The rules of LR and DNV GL are similar to a great extent. Both sets of rules include the general IGF principle that no single failure should lead to a dangerous situation. The level of safety should be equivalent that of conventional vessels. The fuel cell holding space (FCHS), including eventual reformer units, must be located away from accommodation, service and machinery spaces. This area is designated as a hazardous area, and human interaction and presence should be minimised. The operation of the fuel cell system should be automatised where possible, especially control mechanisms. Alarms should sound both locally and at the bridge. Toxic or explosive gas accumulation should not be possible in the FCHS, which is to retain a simple geometric shape. The FCHS must also withstand shock waves and be protected from external damage. The space must be able to handle a maximum leakage scenario safely. Entrance to the fuel cell room should either be on deck or through an air-lock. Two fans with different power sources are required to ventilate the system. In case of failure of one fan, an alarm should sound. An inert atmosphere is an alternative safety measure. The FCHS must be able to contain leaks and fires. Naturally, the rules for the individual fuels used must also be followed. Both class societies stress that explosion or failure in one fuel cell unit should not be able to spread to other units. If malfunction is detected, the system must automatically shut down and the fuel be isolated. The system must be possible to shut down manually from outside the FCHS.

DNV GL further specifies that double piping or completely welded pipes are required for all fuel, either reformed or not. The society mentions nitrogen as a good inerting agent in the outer layer of double piping. Double piping regulation is especially important for hydrogen, which due to molecule size leaks easily compared to other gases. The fans mentioned earlier should be placed upstream rather than downstream of the potential leak. Fans may be sources of ignition and should, if possible, not come into contact with flammable gas atmospheres. DNV GL specifies that intermediate storage of reformed fuel must be located outside the FCHS. In general, no surfaces should reach temperatures higher than the auto-ignition temperatures of the fuels of the system, although DNV GL acknowledges that for fuel cells operating at higher temperatures, case-by-case risk assessments apply. If nitrogen is produced locally, the gas must contain a maximum of 5% oxygen.

LR further specifies that the FCHS should contain as little equipment as possible, and safe access should be possible for inspection. All fluid temperatures must be monitored. The concentrations of the inerting agent and product stream from the fuel cells must be controlled. Purging the system with ease must be possible. The inert atmosphere should be at a pressure higher than atmospheric. The reformer units should be kept as close to the fuel cells as possible, shortening hydrogen pipes.

In conclusion, the rules of LR and DNV GL agree in most aspects of fuel cell installation and operation. Relevant parts of the rules are included in this section, although the rules

cover much more. The option of alternative design is always available. If one can demonstrate an equivalent level of safety to modern conventional vessels, the rules should not be a hinder.

3.5.3 Use of ethyl and methyl alcohol fuel

On assignment by EMSA, LR and SSPA, a maritime consultancy, in 2015 produced a report on the use of ethyl/methyl alcohol as fuels in shipping (Ellis & Tanneberger 2015). According to the EMSA report, among class societies, only LR and DNV GL have rules on the use of ethyl/methyl alcohol. These are discussed below. The rules of LR cover only the use of methanol, which is similar to ethanol in many ways and may provide a good benchmark for an alternative design. The IMO is in the process of developing rules for use of these fuels. The IMO interim guidelines are currently under review, and LR has kindly allowed for insight into the proposed rules.

The EMSA report compares the DNV GL and LR rules. Although similar in many ways, there are notable differences. LR often favours a risk-based process, evaluating each case based on a risk assessment. DNV GL often has a more rules-based approach and includes specific ship type considerations. A notable gap in the rules is bunkering, which is not covered. It is noted that risk related to the bunkering situation is not usually within the scope of class rules or IMO documentation, but regulated by port authorities or regulator on land (Norwegian Directorate for Civil Protection (DSB) in Norway). However, regulation on bunkering was included in the rules by LR in the years following the report. Storage concentration of the fuels is also not mentioned. This is especially relevant for ethanol, which is often sold in bulk at 96%. On the other hand, concentrations lower than 100% would only lower risk (Ellis & Tanneberger 2015).

The proposed IMO rules build on standard IGF principles, e.g. that no single fault shall lead to a dangerous situation or unacceptable loss of power, that accumulation of gas must be prevented. Explosions and fuel spills must be contained and should not hinder operation. The rules are comparable to those currently developed by LR. The rules state, like for fuel cells, that the level of safety shall at least be equivalent to that of new vessels running on conventional fuel. The fuel storage room should be ventilated with 30 ACH and hold negative pressure, so that gases will be kept inside the room. The areas containing fuel lines are defined as hazardous areas. Double piping is required for all fuel pipes outside of hazardous areas. There must exist a minimum of two fuel tanks, although this is less strict if propulsion power is available from other sources. The storage tanks can be filled to 98% maximum. The storage room must contain a larger leak, with drains leading to another holding tank. The storage room and the fuel tanks must be closely monitored for gas concentrations, temperatures and pressures.

In the proposed IMO rules, ethanol and methanol are subject to the same set of regulations, without notion of their different properties. Toxicity is an area in which ethanol and methanol differ. According to the European Chemicals Agency (ECHA), methanol is a toxic gas, and gas concentrations above 200 ppm can be dangerous to humans. The same

does not apply for ethanol. The ECHA's stance is that neither ethanol or methanol spilled into water are toxic to fish, with LC50 (lethal concentration for 50% of the population) values above 10 g/l (ECHA 2020*b*,*a*). While there were few other studies on ethanol toxicity, Kaviraj et al. performed a comprehensive study in 2004 on methanol toxicity to multiple forms of freshwater aquatic life (Kaviraj et al. 2004). The group found that methanol is harmless up to concentrations of 24 mg/l. At higher levels, fish may see long-term effects from the exposure, but their results seem to further establish the LC50-levels of the ECHA. The studies indicate that ethanol and methanol fuel may be spilled into the ocean with limited cause for concern except for the immediate vicinity of the spill. However, the principle of the IMO MARPOL convention is to limit pollution from ships, and it is not likely that a flag administration will accept fuel being spilled into the nature (IMO 1973).

In the proposed rules, ventilation of 30 ACH is required for fuel storage spaces, without exception. However, in the IGF code, where LNG is regulated, it is mentioned explicitly that the level of ventilation can be reduced if other explosion prevention measures are in place (IMO 2015). The reason for omitting this point from ethanol rules is unclear. Ethanol and methanol can both be prevented from reaching flammable gas concentrations by lowering the environment temperature. Moderate refrigeration (or lack of heating) combined with a lower ventilation rate, e.g. 6 ACH, could likely be demonstrated to ensure a more than sufficient level of safety in the cool waters around Norway and thus be found acceptable in an alternative design approach.

3.6 Configuration of ethanol

In the CFD software FLACS, ethanol is not among the gases implemented with properties specified. Therefore, the required thermophysical properties had to be collected to properly define ethanol. This process is described in detail in Appendix A. To validate the species, simulations of explosion and dispersion scenarios were set up in FLACS. Overpressures and temperatures from deflagrations in a closed container were compared with experimental and theoretical values. Evaporation characteristics were also compared with reported values from experiments. The validation process is described in Appendix B. The implemented species was concluded to realistically represent ethanol in deflagrations, with the results of the simulations close to empirical and theoretical values.

The self-defined ethanol showed unrealistic behaviour with regard to pool evaporations. The validation experiments are described in Appendix B.3. Inherent problems of the FLACS software seemed to cause the deviations. During pool evaporation benchmarks, concentrations well above the vapour pressure were obtained in the simulations, not only for the self-defined ethanol, but also for hexane and heptane, which are among the predefined substances in FLACS. The results were shared with the FLACS support team, who observed similar results. At the time of finalising this work no final feedback on the problem had been received from the support desk. From past experience, it was suggested that the steel plate model for pool evaporation could have a flaw, however there was not enough time to explore this further.

To be able to perform risk assessments where liquid is spilled and may form a pool, evaporation rates presented in literature may instead be used as source terms for simulations. Lyulin et al. concluded that the initial evaporation rate of ethanol was 1.0 g/m^{2}s at 298 K (Lyulin et al. 2015). In another article, Raymond L. Smith found that the average evaporation rate over 15 minutes at 300 K was 0.37 g/m^{2}s (Smith 2001). From these results, gas concentrations in a ventilated room may be estimated. Ethanol pool evaporation can be modelled as an area leak from the ground, in which the leak rate is controlled to correspond to the empirical rates. The vapour-liquid equilibrium is not included in such a model, but given conservative estimates, the model should function sufficiently for the risk assessment.

Chapter 4

Methodology

This risk assessment followed the traditional procedure for risk assessments, in line with ISO 31000:2018 (ISO 2018). An illustration of the process is given in Figure 4.1. The methodology for the frequency and consequence assessments is discussed in this chapter, and this approach is used to establish a risk picture. In Chapter 5, the system is described in the following Chapter 6, the hazards are identified and discussed.

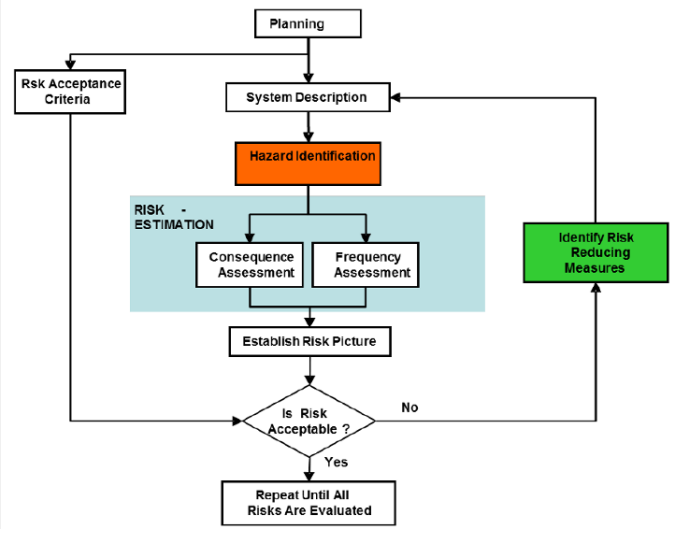

Figure 4.1: Illustration of the standard risk assessment methodology (ISO 2018).

4.1 Frequency assessment

Published data from the literature on leak frequencies of ethanol were not obtained. Similar data for other fluids has been collected in the oil and gas industry, and these frequencies are in this assessment applied for ethanol. The different procedures for estimating frequencies are described in the following paragraphs. Based on the frequencies from the oil and gas industry, LaChance et al. of the Sandia National Laboratories working on behalf of the US Department of Energy developed models to estimate leak frequencies for hydrogen for various sized holes based on the components in the system (LaChance et al. 2008). Using the model of LaChance et al., the hydrogen leak frequencies could be estimated based on a component count.

Alternative models to estimate ethanol leak frequencies were the RIVM, HSE, OGP and PLOFAM models. A summary of the models is presented by LR in a report for the Norwegian Directorate for Civil Protection (Kristiansen et al. 2017). The RIVM (Rijksinstituut voor Volksgezondheid en Milieu) model, is the simplest of the models mentioned, assigning frequencies based on equipment types rather than individual components. The model is best applied when there are few leaks possible outside of the equipment types included in the model. The model gives frequencies for instantaneous leaks of all content, steady state leaks releasing all content over 10 minutes and continuous leaks from a 10 mm hole. The model does not account for leaks as a result of external damage, like collisions, shocks, corrosion, vibrations or faults from inspection. The model is based on leaks from ageing, design errors and wear and tear (RIVM 2009).

The HSE (UK Health and Safety Executive) model is based on data from facilities in the UK. It is more detailed than the RIVM model by including data on flanges and valves, both missing in RIVM. HSE is therefore better suited for design specific and nuanced frequencies for major events. The frequencies are mostly independent of equipment size and depends on system pressure, temperature and fluid density. To provide a better picture of the leak frequencies, the HSE method demands a more complex part-count than RIVM (HSE 2017).

The OGP (International Association of Oil & Gas Producers) model is based on the same data as the HSE. The OGP model delivers frequencies for many more components than the HSE model but has no frequencies for storage tanks. The frequencies of various hole sizes are functions of component dimensions (OGP 2010).

The PLOFAM (Process Leaks for Offshore installations Frequency Assessment Model) model is the most validated and detailed method of those discussed. The model is based on comprehensive offshore data from the UK and Norway and validated against data from onshore industry as well. For each equipment dimension, the frequency is a continuous function of hole size Fossan & Sæbø (2016). This is the most detailed model, but also the most sophisticated. For this thesis, the RIVM model was used. The ferry of this thesis is only a concept vessel and detailed information on the components of the system were not available. Without a complete list of components and sizes, a simple model is to prefer.

4.2 Consequence assessment

Based on the potential hazards identified in Chapter 6, the consequences of each event were estimated quantitatively and the overall risk to crew and passengers was estimated. The different parts of the vessel considered to be potentially hazardous were modelled in 3D in the FLACS CFD code. Human health can be threatened by exposure to fire, pressure waves or projectiles. Pressure waves of 0.40 bar or more were assumed fatal, in accordance with estimates by the US National Academy of Medicine (IOM 2014). According to OGP (434-14), an pressure wave of 0.5 bar is estimated to be 50% lethal for people outdoors in the open, 100% if close to adjacent buildings (OGP 2010). The measure of 0.40 bar was concluded a sufficient measure on human fatality due to pressure waves. Direct exposure to hydrogen jet-fires or gas cloud explosions with hydrogen concentrations above 8% were also assumed fatal, and the same would apply for ethanol fires in clouds above LFL.

The probability of ignition should be included in the risk analyses concerning flammable gases, as the consequences of instant and delayed ignition will differ. An instant ignition might produce a jet flame, while a delayed ignition scenario in which the flammable gas can mix with air before ignition, can cause explosions.

In a Lloyd's Register report for the MoZEES project, Olav R. Hansen proposed a model to estimate hydrogen ignition probability in 2018 (Hansen 2018). The model was published in a confidential LR report, but the findings were in 2020 published in an article by Aarskog et al. (Aarskog et al. 2020). According to the model, the probability of ignition for a leak in an open environment could be characterised by Equation 4.1.

$$P_{ignition,freejet}(rate) = Minimum(1.0; 0.55 \cdot rate^{0.87}; 0.267 \cdot rate^{0.52}) \quad (4.1)$$

The rate in the equation is the hydrogen leakage in kg/s. The model was based on OGP ignition probabilities (434-6) for methane on offshore platforms and adjusted for hydrogen, and it has since 2018 been regularly applied for hydrogen risk assessments at LR (OGP 2010). The Hydrogen Risk Assessment Model (HyRAM) of the Sandia National Laboratories in the US is based on an alternative model, proposed by Norsk Hydro and DNV in the European HySafe project and described in 2006 in a report by Andrei V. Tchouvelev (Morales et al. 2008, Tchouvelev 2006). A graph illustrating the two models is given in Figure 4.2. The two models have similarities, but one major advantage of the model of Hansen is that it is continuous rather than a step-function as function of leak rate.

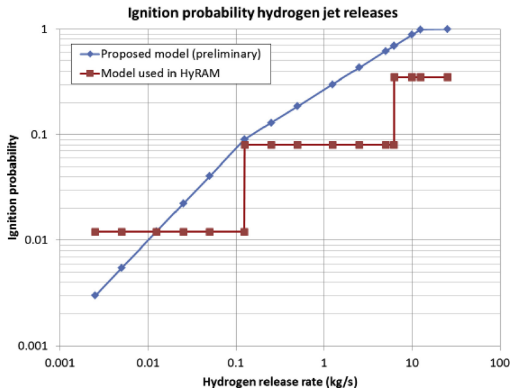

Figure 4.2: Comparison of the proposed ignition model of Hansen and the model used in HyRAM of the Sandia National Laboratories (Aarskog et al. 2020). Used with approval by Elsevier.

4.3 Establishing risk picture

By combining frequency and the consequent assessments, the risk matrix often used by Lloyd's Register for risk based design processes is shown in Figure 4.3 (LR 2020). The red region signifies unacceptable risk levels, the yellow region represents risk levels close to the unacceptable level. Due to uncertainties regarding the accuracy of risk assessments, events placed in the yellow region during a HAZID might in reality belong in the red region. Based on a cost-benefit analysis, the risk levels in the yellow region should therefore be lowered further unless the cost to do so is documented to be disproportional (ALARP process – keep the risk as low as reasonably practical). The green region indicates broadly acceptable risk levels and no further measures are required. The higher limit of the yellow ALARP region is set to the upper acceptable risk levels, while the lower limit is by definition set to an annual fatality rate of 10^{-6} (IMO 2018*b*).

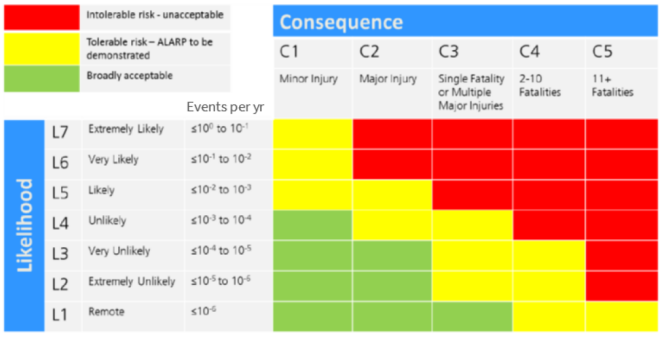

Figure 4.3: Example of a risk matrix used to categorise the potential hazards in line with the IMO FSA guidelines (IMO 2018*b*). The actual matrix shown is the one used by Lloyd's Register during risk based design work (LR 2020).

The basis for the tolerable risk levels is found in the discussion in Chapter 3.5. As earlier discussed, the Norwegian Maritime Authority has previously practised allowing 1.0 extra fatality per 1000 million passenger-kilometre for alternative design vessels compared to modern vessels using conventional technology. This measure could be used as the upper tolerance limit, as this vessel applies a new technology. The corresponding value for crew would be a FAR value around 1.0. However, the concept ferry should be able to comply with the recommendations from the IMO. Existing vessels are required to comply with maximum annual fatality rates of 10^{-3} and 10^{-4} for crew and passengers. The targets for new vessels are one order of magnitude lower. For the risk matrix, the IMO target values were set as the lower limit for the ALARP region, while the requirements for conventional ships were set as the upper limit. For new vessels using conventional technology, the lower limit is constant for both crew and passengers, at an annual fatality rate of 10^{-6}. For vessels using new technologies, a higher risk should be expected. If compliant with the new targets of the IMO, the risk was therefore assumed to be sufficiently controlled.

The risk matrix is a useful tool to qualitatively sort and prioritise scenarios during a HAZID. The identified scenarios of concern should then be assessed in more detail, using frequency and consequence assessments, to establish a more accurate estimate of fatality risk to crew and passengers, in order to confirm that the risk is within the acceptable limits.

Looking into the Norwegian Public Roads Administration's database for ferries and considering the less busy ferry connections in terms of passenger numbers, the assumption that the average passenger number equals 10% of the passenger capacity seems good (Vegvesenet 2020). As is discussed further in the next chapter, when describing the ferry systems, the concept ferry is inspired by MF Glutra, a Norwegian ferry (first LNG-fuelled ferry in the world). Based on information on MF Glutra, an average of 30 passengers were assumed on board during each crossing. The speed of 11 knots is assumed for the concept ferry and a duration of about 40 minutes for the crossing. This corresponds to a distance of 14 km for the connection. By assuming 15 hours of operation each day, about 22 crossings could be made, transporting 660 people daily, 360 days of the year. This relates to about 3.3 million passenger-kilometres per year. One passenger fatality would be acceptable every 303 years, given 1 fatality per 1000 million passenger-kilometre. Given 30 passengers, the individual fatality rate would be 1.8e-4 per year during the time the ferry is in operation (assuming a person 24/7 on board a ferry in operation). For passengers, the targets set by IMO for new vessels are in this case stricter with regard to passenger safety than the previous practise of 1 additional fatality per 1000 million passenger-kilometre for vessels utilising new technology.

MF Glutra had 5 crew members, but as the kiosks on many connections have now become self-operated and operation in general has become increasingly automated, a smaller number of crew was assumed. 3 members of the crew working 15 hours per day, or 9 employees working on average 5 hours per day, for 360 days each year (3 shifts) equals 16,200 worked hours yearly. A FAR value of 1.0 equals 1.0 fatality per 100 million worked hours, corresponding to one single crew fatality every 6200 years. This would correspond to and the individual acceptable fatality frequency per year (if 24/7 on a vessel in operation) for the three crew-members would be 8.7e-5. For this case, the FAR criterion is marginally

stricter with regard to crew safety than the targets of the IMO. Still, the IMO targets of 1.0e-4 was used for the green region of the risk matrices.

In this discussion it should be kept in mind that the tolerance criteria considered for alternative design are mainly related to hazards from the fuel. As there are many more risks to crew and passengers which are not related to fuel, the alternative design tolerance criteria should preferably be lower than the IMO requirements. Still, for the total risk exposure for vessels utilising new technology it is considered reasonable to compare to risk levels considered acceptable on existing (modern) vessels rather than IMO target values for new vessels.

Chapter 5

System description

5.1 Inspiration

In this thesis, the ethanol system was considered for a double-ended ferry. The ferry design was inspired by that of MF Glutra, the world's first LNG ferry. The ferry has been described in detail in the SINTEF report by Einang et al. in 2000 (Einang & Haavik 2000). The ferry is a double-ended car/passenger ferry with capacity for around 100 cars. The ferry took a year to build and was set in operations in February 2000. The costs for this first LNG ferry were 30% higher than estimated for a similar diesel-powered ferry.

The specifications of the ferry are well documented, and the operation is of little complexity. The original layout of this ferry is shown in Figure 5.1. The ferry had electric thrusters in both ends. These were twin propellers, able to thrust in both directions, with a combined maximum load of 2.0 MW. The LNG is stored in two large cryogenic, vacuum insulated tanks, one on each side of the ferry, for stability and redundancy reasons. Each tank could contain 32 m^3. Above the tanks, the ferry had four different gas engines, each capable of supplying 675 kW. The engines charged a battery, which in turn supplied the thrusters along with the rest of the vessel with electric energy. Two and two gas engines shared gas masts for emergency venting near the top of the ferry, as illustrated in Figure 5.1. The gas engines were placed in four different rooms at the opposite side of the ferry from where passengers and control functions were located. MF Glutra traversed the Norwegian route of Sølsnes–Åfarnes. According to Fjord1, the 2020 operator of the route, the time required for the crossing is 13 minutes, with 7 minutes for loading off and on the vehicles at each end, resulting in 26 minutes operation and 14 minutes rest during a round-trip.

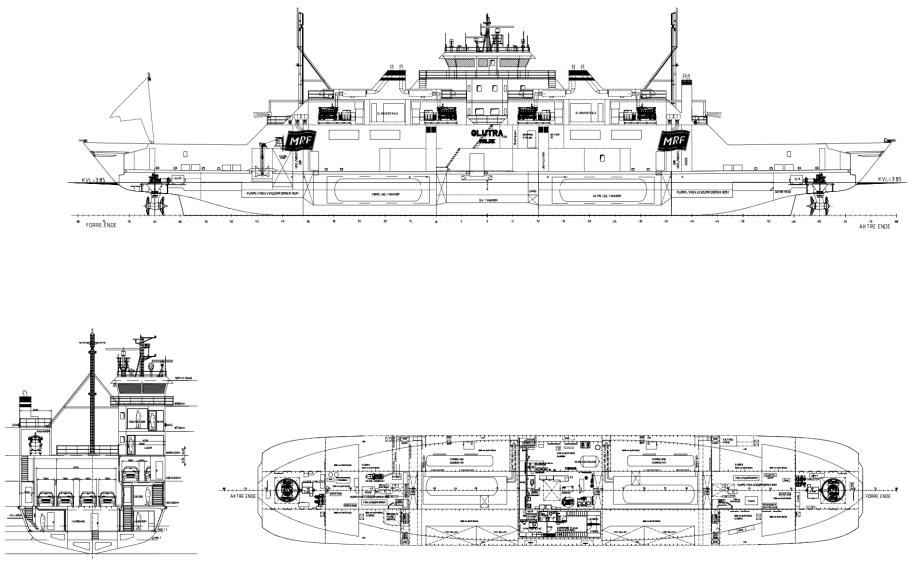

Figure 5.1: Layout of the ferry MF Glutra, as designed in 2000 (Einang & Haavik 2000). Used with kind approval by SINTEF.

MF Glutra, the first LNG ferry, was designed with safety in mind. The ferry was designed to minimise the risk of explosion, especially by limiting potential gas volumes by minimising the size of the rooms where gas could leak. The ferry was designed with redundancy throughout its energy systems. All engines and both fuel tanks were separately placed in individual rooms. All gas pipes had double-walled piping, so that a leak would be collected in the outer layer and vented. The ship was built to withstand any potential explosion, which should not hinder further operation. All areas exposed to potential gas leakage were furnished with gas detection sensors, with alarms at 20% of LFL.

In 2015, the IGF Code was ratified by the IMO, although the first draft version was proposed to IMO (by Norwegian Maritime Authority) as early as in 2004. In the code, requirements for ships using low-flashpoint fuels are specified, for LNG requirements are specified in detail. Many of the safety measures adopted by MF Glutra were maintained in the IGF code. As MF Glutra was a test ferry operating a shorter ferry connection, later LNG ferries have been built to traverse longer crossings. Today, a significant fraction of the shorter connections along the Norwegian coast have been electrified. Ferries must comply with the requirements of the IGF code (4.3). More modern ferries have managed to satisfy the requirements while placing fuel systems and engines below deck instead employing one side of the vessel for the sole purpose, as was done with MF Glutra.

5.2 The concept ferry

The concept ferry of this thesis is powered by fuel cells connected to two reformer units. This ferry differs in several aspects from MF Glutra. Modern ferries corresponding to MF Glutra are presently designed more symmetric, with a more efficent hull and with cars on one deck only to allow for more efficient loading/unloading. MF Moldefjord, pictured in Figure 5.2, is designed with these characteristics. MF Moldefjord travels for 35 minutes between its destinations at a speed of 11 knots. It is powered by a 2.0 MW LNG system (Blaalid 2010). A modern MF Glutra would probably look more like MF Moldefjord. The concept ferry layout is something in-between these two ferries. The size of the ferry remains similar to that of MF Glutra, at about 100 m long and 16 m wide. Short connections like Sølsnes–Åfarnes are these days electrified. Therefore, this thesis considers a longer connection, with travel time measuring 38 minutes instead of 13, more similar to the Molde-Vestnes connection where MF Moldefjord operates. As with MF Glutra, the ferry is assumed to spend 7 minutes in each port for unloading and loading. A complete cycle then requires 45 minutes.

Instead of four rooms for the gas engines, the ethanol ferry is to contain both the reformers and the fuel cell cabinets in the same room, defined as the fuel cell holding space (FCHS). For practical reasons and to make room for passengers above deck, this space is placed below the car deck. As MF Glutra travelled at 16 knots, while the concept ferry only at no more than 12 knots, less power will be required. As the required power tend to be proportional to square of the operating speed, the required power may be only 60% compared to Glutra.

A 1.5 MW system was thus assumed sufficient for the concept ferry. The fuel cells of the concept ferry run continuously and charge a central battery which in turn supplies the thrusters. The set-up is similar to that of MF Glutra. As ethanol works with standardised fuel tanks without need for isolation, the tanks would not represent a major expense as for cryogenic LNG or hydrogen tanks. By regulation, two separate tanks are required, and two fuel tanks of 32 m^3 m3 each are assumed as for MF Glutra. As ethanol does not require vacuum-insulated walls, the tank capacity will be higher than for cryogenic LNG tanks occupying the same volume. LNG will also expand more due to heating, and tanks cannot be filled to the same level as e.g. ethanol.

Ethanol has been used in vehicles in Brazil for years, fuelled at normal pumps. The fuel could be supplied from fuel trucks by the ship-side. The ferry is designed to store ethanol as a 96% mixture of ethanol and water. Due to the azeotropic limit, this is the highest concentration which can be produced by means of distillation.

Figure 5.2: MF Moldefjord. Photo: Peter Fiskerstrand. Available at Wikimedia Commons.

5.3 The power system

Figure 5.3 below presents a process flow diagram of the main parts of the power system. The average engine load for operation at sea is in the concept ferry assumed to be 55%, operating at 50% load during standard travel and at higher loads during manoeuvring, necessary close to harbour. The ferry rests in harbour for 16% of operation due to unloading/loading.

5.3.1 The battery

The batteries are partly meant as redundancy for the fuel cell system and ensure safe travel to port in case of problems. Thus, there should always be available battery capacity to bring the ferry safely to nearest port. This is similar to 20 minutes of travel. The batteries are assumed to be able to transport the ferry for a minimum of 40 minutes. At an average load of 830 kW, this amounts to 550 kWh. In an emergency, the vessel might operate at lower speed to reduce power consumption, thus smaller batteries may be possible. By regulation, the batteries must be organised in at least two independent circuits, for sake of redundancy. If one circuit fails, the other will manage to provide power given that both batteries are independently connected to the fuel cells. However, due to an energy demanding cold-start, larger batteries are beneficial. The capacity of the batteries is not considered further. Based on the assumptions regarding the ferry operation, the average power supply to the battery is assumed to be 690 kW.

The battery efficiency for a charge and discharge is assumed to be 95%, given the rapid charge and recharging necessary. This is a conservative assumption, given Li-ion batteries can have efficiencies at 99% (BU 2017). A hybrid system would have several advantages to the current set-up, where the fuel cells directly powered the thrusters and excess energy charged the system, while periods with high loads would see power arrive from both the cells and the battery. In this case, for sake of simplicity, the fuel cells would only charge the battery. The designs would be similar with regard to safety, and so the simpler version is chosen for this thesis. By these assumptions, the fuel cells have to steadily supply at least 720 kW. While there are clearly hazards related to large batteries, it is considered that these are handled by built in safety systems from the battery manufacturer, and that safe operation is ensured by the battery management system.

5.3.2 The fuel cells

Solid-oxide fuel cells are chosen as the best alternative for the fuel cells. The cells operate at high temperatures, and the products from the reformer units can be sent straight to the fuel cells. PEMFCs are a good alternative to the SOFCs, but would require an additional condenser unit, compressor unit and a water-gas shift reactor to process the reformer product stream. Furthermore, SOFCs generally have a higher electrical efficiency than PEMFCs. The disadvantages of SOFCs mentioned in the EMSA study on use of fuel cells in shipping are economic cost relative to other fuel cells, the fuel cells' tolerance to

cycling, along with a lower safety score due to high-temperature operation.

The safety of the system is handled by this thesis and cycling is also avoided by design. The economic cost remains a disadvantage. The cost of the SOFCs are, however, assumed lower than the combined cost of PEMFCs, a water-gas shift reactor, a condenser unit and an extra compressor. The electric efficiency of the fuel cells are assumed to be 60%. SOFCs reportedly vary in electrical efficiency between 50-70%, as discussed in Chapter 3.1.3. The fuel cells operate at 1020 K. If generally operating at 75% load when delivering 720 kW, modules able to produce 950 kW of power are required.

Bloom Energy, an American SOFC supplier, provides the Energy Server 5 system. These servers maintain electrical efficiencies of 52-65%, and a 950 kW system would demand a footprint of 45 m^2, assumed to consist of 36 separate units. As mentioned in Chapter 3.5.2, an explosion must not be able to spread from one unit to another. In this case, the safety of the system is not assumed to worsen by placing the units close. According to Bloom Energy, the servers are normally placed close together outside, in publicly accessible areas. This assumption is discussed further in Chapter 6. The optimal pressure for gaseous fuel entering the servers are about 2 bar, according to the product data sheet, although the modules may operate with pressures up to 2.2 bar. The cells are designed for natural gas, but can handle hydrogen as well, as the natural gas is converted to hydrogen inside the cells (Bloom Energy 2019). Therefore, it is assumed that the size of the modules probably could be reduced somewhat by running on pure hydrogen.

To maintain a pressure inside the operating window of the fuel cells, a pressure drop of 0.3-0.5 bar is assumed for the reformer units. The fuel cells are assumed capable to heat the incoming hydrogen and steam. An alternative would be to utilise the steam exhaust from the fuel cells to heat the hydrogen, although this might add to system complexity, and care should be taken not to increase hydrogen leak propensity, as discussed in Chapter 7. Bloom Energy does not mention the air supply required for the SOFC units, and they seem able to compress the air entering. In the concept ferry, an external compressor was assumed required, although this assumption should not affect the risk assessment. Bloom Energy does not include information on the system safety in the data sheet (Bloom Energy 2019). To be able to place the fuel cells close together in public areas, the units should maintain a high level of safety. Still, the risk assessment should account for the amounts of hydrogen available in the fuel cell modules.

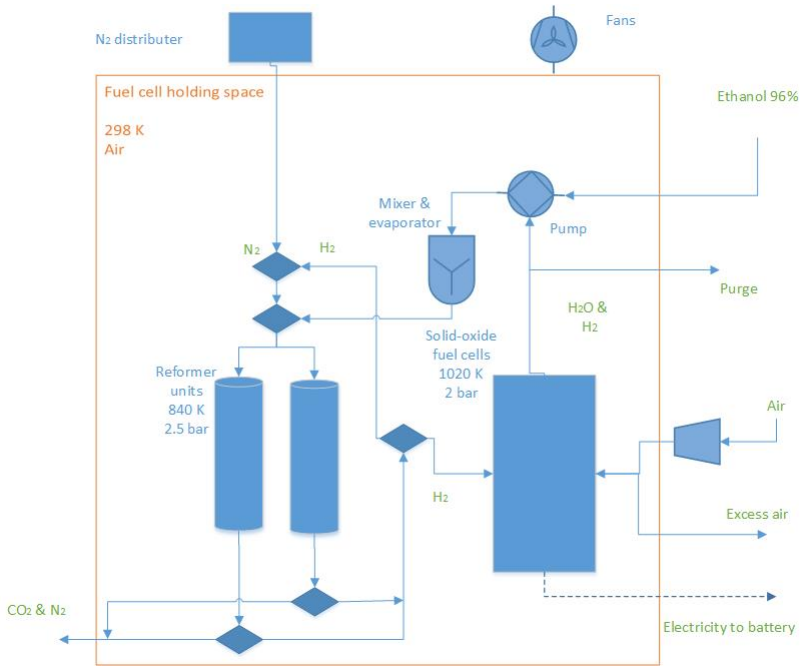

Figure 5.3: A process flow diagram of the high temperature space and surrounding units.

5.3.3 The reformer units

Based on the fuel cell efficiency, the reformer units have to supply hydrogen with a lower heating value of 1200 kW during normal operation. For the ability to utilise 90% of the fuel cell load range, as is desired in this case, the heating value must be increased to 1400 kW of hydrogen. The latter amount corresponds to a hydrogen stream of 11.6 g/s, or 5.8 mol/s. The reformer units, operating at 2.5 bar and 850 K, are assumed to produce hydrogen at 98% purity, as was the case with He et al. at similar pressures and a steam to carbon ratio of 3 (He et al. 2010).

He et al. observed reforming cycles of up to 110 minutes. Due to degradation of the adsorbent material, the duration of the cycle declined to 20 minutes after eight runs (He et al. 2010). In this case, the problem of degradation is assumed solved to some degree. The potential reformer cycle is assumed to be 80 minutes reforming before regeneration is necessary. Pushing the limits of this cycle may quickly yield higher concentrations of CO and methane and encumber the regeneration process. Therefore, one reformer is in the cycle assumed to operate for 60 minutes, then heated up for 5 minutes, 30 minutes regeneration follows before 15 minutes of catalyst recovery. The process has a margin of 10 minutes to smooth the transitions.

In the regeneration process, proceeding at 1040 K, He et al. utilised argon to sweep the reformers of CO_2 and hydrogen to reduce any oxidised catalyst (He et al. 2010). For this

case, nitrogen produced locally is used to sweep the reformer units. Then, in a separate catalyst recovery process, some of the hydrogen stream leaving the reformer in operation would be sent to the regenerating reformer to reduce the catalyst. This hydrogen will afterwards rejoin the stream entering the fuel cells after passing a small compressor unit. The catalyst recovery phase can proceed as the temperature decreases back to 850 K. The nitrogen used can either be dispersed or utilised to some degree in the inerting systems. In this case, the nitrogen and the CO_2 are assumed released into the atmosphere. The reformer cycle is illustrated in Figure 5.4.

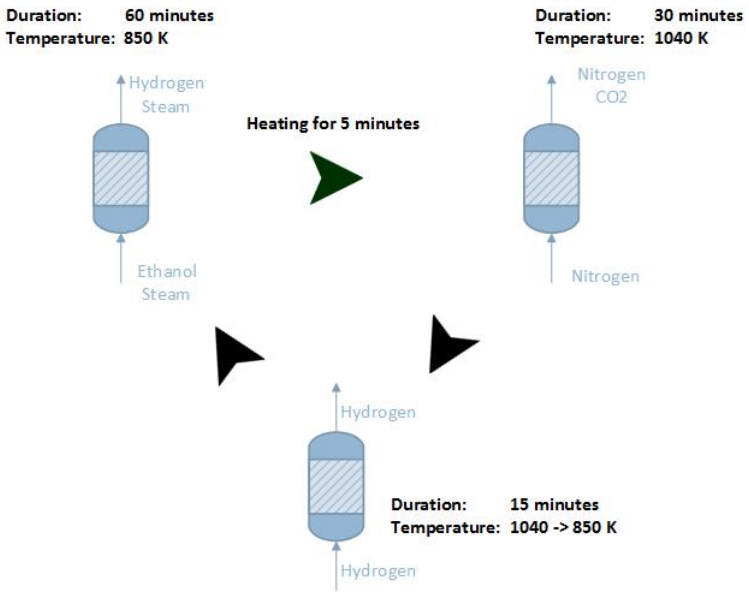

Figure 5.4: A process flow diagram illustrating the different stages of the sorption-enhanced reformer cycle.

The impurities of the reformer product stream are assumed to comprise 1.1% methane, 0.30% CO and 0.60% CO_2 and constitute the remaining 2% of the products excluding the excess steam. This stream is sent directly into the SOFCs, where the impurities are reformed into CO_2 and hydrogen as described in Chapter 3.1.3 on fuel cells. Based on the hydrogen content of methane in addition to the hydrogen stream, the ethanol required corresponds to 0.97 mol/s, or 45 g/s.

If hydrogen were to be utilised for heating, more ethanol would be required. In the concept, heat generation for the reformers is supplied by the battery or excess heat from the fuel cells. The risk of using hydrogen for heating makes electric heating seem a better choice in this case. The full load streams of the power system are illustrated in Figure 5.5. The figure omits the air streams to and from the reformer, along with the flows during the regeneration of the reformers.

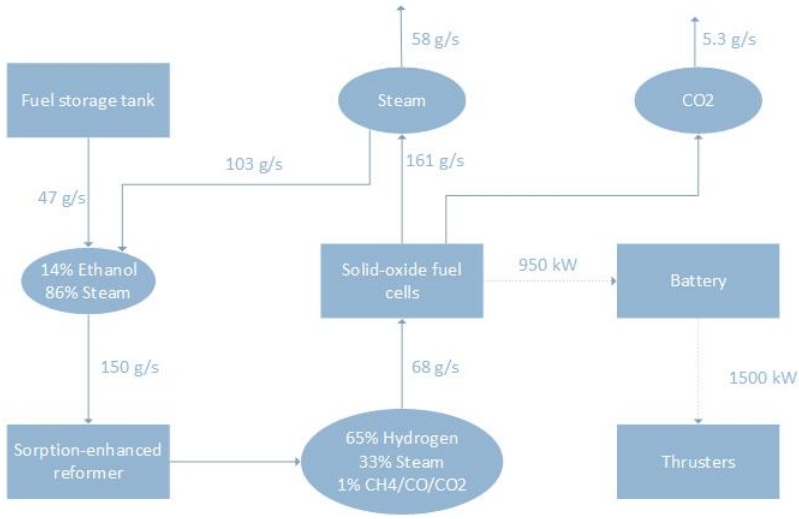

Figure 5.5: A process flow diagram illustrating the main mass and energy streams of the power system. Rectangles represent units and ellipses represent fluid mixtures.

Based on the amount of catalyst and a catalyst/dolomite density of 3.0 g/cm^3, the reformer used by He et al. was only 2.0 cm tall with an area of 2.0 cm^2. The flow consisted of 21 ml/min N_2 and 5.7 g/h of liquid mixture, in total 0.28 mol/h. By considering the flow rate per gram catalyst, the reactor was scaled to accommodate a flow of 0.97 mol/s of ethanol and 5.8 mol/s of steam. The volume required would correspond to around 0.35 m^3. If using the same relation between area and height as He et al., the concept reactor units scale to 59 cm in height, with a radius of 43 cm.

For the reformer units of the concept, a height of 2.0 m was assumed and a radius of 30 cm, 0.57 m^3 in total. This ratio gives a larger volume and a more cylindrical form. A longer unit would lead to a larger pressure drop and allow for higher velocities. This drop is assumed adjusted to match 0.3 bar, as mentioned earlier during the discussion on fuel cells. The void fraction is assumed to be 0.40, resulting in 0.23 m^3 of available space for gas flow. The reformer would have a container able to set the reactor heat. The container is assumed to double the reactor volume. The total size is assumed to be 2.2 m in height and 40 cm in radius.

In an extensive discussion on the matter, Donati et al. explains the complexity of scaling reactors (Donati & Paludetto 1997). The procedure is mainly based on experience. In practise, industrially scaled technologies seldom relate to laboratory equipment and kinetic data is peculiar to the system observed and scaling may affect other aspects of the system, e.g. transport phenomena and fluid dynamics, in different ways than the chemical reaction. A different type of reactor or other related apparatus may be better suited for the scaled operation, in turn affecting the system. In addition, the amount of impurities in the

system along with the catalyst ageing/deactivation processes are likely to differ from the laboratory experiment when scaled. The system presented by He et al. has not been scaled in a pilot plant and therefore lacks evidence that the results are reproducible when scaled.

The residence time of the reactor of He et al. is 1.5 ms. The residence time is a measure of how long the flow remains in a given control volume. When the control volume is a reactor, it becomes the time available for the reactants to react. As He et al. leaves out mention of the void fraction, this parameter is not considered. With a 5.4 ml/s flow and a 4 cm^3 reactor, the residence time becomes 0.74 s. For the reformer described in this section, a 0.19 m^3/s flow passes through a 0.57 m^3 reactor, corresponding to a residence time of 3.0 s. By these measures, the reactor size is conservative with regard to size. Due to the uncertainties in the process of reactor scaling and in the scalability of this particular reaction, an assumed conservative reformer unit size was considered a good choice for a safety analysis of the system.

The steam required for the reforming is recycled from the fuel cell exhaust, as illustrated in Figure 5.5. Some water enters the cycle from the ethanol fuel mixture and a corresponding amount is purged after the fuel cells, in addition to the water produced in the process. Excess water is purged from the fuel cell exhaust.

A buffer tank is initially not assumed necessary. According to Faanes et al., the purpose of such tanks is to exploit the volume to provide smoother operation and avoid propagation of disturbances (Faanes & Skogestad 2003). The reformers would in all probability not produce a perfectly homogeneous and steady stream. Switching from one reformer to the other would disturb the flow and a buffer tank could be designed to provide a further pressure regulation before the fuel cells. On the other hand, SOFCs are highly fuel flexible and the SOFC units are assumed to handle minor disturbances. A potential buffer tank will be further discussed during the hazard identification process.

The sorption-enhanced system could in theory capture and the CO_2. Given that the ethanol is produced from biomass and renewable energy, such a process could result in so-called CO_2 negative emissions. In that case, the CO_2 and nitrogen stream from the regeneration cycles would enter a CO_2 stripper column and be exposed to an amine solution designed to capture the greenhouse gas. This amine solution could then be stored and switched with a new amine solution when the ferry rests in harbour. Such a process could become viable if a CO_2 market was available. However, such a process was not considered further in this case.

5.4 Safety considerations

Before defining the concept ferry further, an early risk evaluation was performed. Three different areas were considered potentially hazardous: The two fuel storage holding spaces (FSHS), the fuel cell holding space (FCHS) and the car deck (during bunkering only). Models for these areas were designed in the FLACS CFD model. The concept ferry was aimed designed in accordance with the draft regulations for fuel cells and ethanol discussed in Chapter 3.5. All ethanol pipes are double-walled with inert atmospheres. As ethanol is liquid at room temperature, the outer pipes lead leaks to the drainage tank, which by the proposed regulation for use of ethanol has an inert atmosphere. If ethanol starts accumulating in the tank, the fuel supply should be closed off and vessel should be repaired. Sensors detecting liquid leaks are present in the the pipes. Double-walled pipes with inert atmospheres are not considered potentially hazardous in case of a leak.

5.4.1 Fuel storage holding space

In the FSHSs, the storage tanks are single-walled. This allows for spills to reach into the surrounding rooms. The risk level posed by such leaks is assessed in Chapter 6. By draft rules, the FSHS should have a ventilation level of 30 ACH, delivered by two fans connected to different electrical circuits. Each fan should have a capacity to deliver 30 ACH to secure redundancy in ventilation. The fans are placed downstream of the FSHS and produce a negative pressure in the room to prevent potential gas concentrations developing from exiting the FSHS. The atmosphere inside the tank is inert. As a further safety measure not explicitly considered in the draft rules, the FSHS temperature is proposed kept at 10 °C, well below the flash-point of ethanol. Crew should not need to enter the FSHS during operation.

All pipes connected to the storage tank are connected to the top of the tank, and a pump will actively extract the fuel. By this design, the connection and the pipes can only leak while the pump is active. This is a common arrangement. If the pump is located at a lower level than the storage tank, leaks would continue by hydraulic head pressure, even as the pump has been shut off. A valve connecting the ethanol supply pipe to the atmosphere would solve this problem, given that the valve automatically opens when a leak is detected. In this case, the FSHS and FCHS are at the same deck level, and the pump could be placed above the storage tank if considered inherently safer.

Including a tank connection space (TCS) at the end of the tank would be an option. The purpose of a TCS is to collect small leaks where they most frequently occur, by the tank connections. By regulation, the area surrounding the tank is a hazardous space requiring 30 ACH of ventilation. A solution where the TCS is ventilated with 30 ACH and the rest of the FSHS with 6 ACH could be approved by alternative design if an equivalent level of safety can be demonstrated. Such a solution can be less expensive and generate less noise than continuously ventilating the whole FSHS with 30 ACH.

The option proposed in this thesis is the combination of keeping the temperature in the

FSHS below the flash-point and maintaining a reduced ventilation. The room could be kept at the same temperature as the seawater outside, in Norway this would be well below the flashpoint of ethanol most of the year, with a refrigeration system activated in periods when the sea temperature would exceed the flashpoint of 13 °C. The ventilation system could then be selected to ensure a non-flammable atmosphere also for warm days assuming failure of refrigeration system. The different solutions are discussed further in the hazard identification discussion in Chapter 6. A TCS is not included in the initial design.

The drain leading to the drainage tank is placed below the tank connections. The drainage tank is only designed to contain the volumes of smaller spills. The drainage tank must according to the draft ethanol rules of LR follow the same rules as a fuel storage tank, and its atmosphere will be inert. The drainage tank itself was not considered potentially hazardous. In the event of a complete tank rupture, the drain will fill up and the ethanol will remain in the FSHS. In such a scenario, the ethanol evaporation must be controlled by the refrigeration and ventilation systems until the ethanol can be pumped out when docked.

Regarding the drainage tank, an alternative measure to inerting the tank that should be considered would be to partially fill the drainage tank (and potentially the deck below the fuel tank) with some water, so that an ethanol spill would be diluted in water. This would increase the flash point significantly. For 50/50 mixtures of ethanol and water, the flash-point increases to 20 °C compared to around 13 °C for pure ethanol.

Flammable atmospheres will this way be prevented inside the FSHS.

5.4.2 Fuel cell holding space

Inside the FCHS, the pipes are single-walled. Due to the small size of the molecule, hydrogen may have a higher leak propensity compared to other gases, and smaller leaks must not be able to develop into hazardous situations. Sensors monitor gas concentrations at the inlet and outlet of the reformer units. Solenoid valves, electrical open-close-valves, are paired with sensors and will close off the system in case of a malfunction. Each segment of the hydrogen piping system has valves mechanically closing in case of a pressure drop, which would develop in case of a larger leak or a burst. The FCHS has a simple geometrical shape to prevent leaks from accumulating, and the space is ventilated with 30 ACH. The exiting air is sent out away from the ship-side and assumed to be non-flammable. This is due to the assumption that the hydrogen available to leak would not manage to develop significant (flammable) concentrations in the room. The FCHS is a restricted area during operation.

The FCHS walls are assumed to be similar to the bulkheads of the ships. Hydrogen is transported at temperatures just above its auto-ignition temperature of 830 K. If a leak occurs, the hydrogen would have to mix with air to be able to ignite. The hydrogen amounts available to leak are small compared to the volumes of surrounding air and the temperature would quickly drop in the process. Auto-ignition is therefore not expected in this case. Given an auto-ignition, a jet flame would develop until the hydrogen stream were closed

off. As the area is restricted, the jet flame would not be of any danger to crew or passengers.

The temperature of the FCHS is in this case set to 298 K. An alternative would be to keep the temperature at 850 K. Due to multiple high-temperature streams and with both the SOFC-modules and the reformers operating at 850 K or higher, such an option could be viable. Both the SOFCs and the reformers would have benefited from a higher base temperature and it would allow for a quicker and lighter start-up process if the room is kept at high temperatures overnight. Such a redesign and optimisation of the system could likely simplify systems and save space, but would require a close cooperation with fuel cell developers and be costly. Heat recovery systems were not included in this thesis and the alternative solution was not exploited further.

Inside the FCHS, there is a potential for leaks of hydrogen rich fuel mixture into the room. The available volumes, and thus the explosion potential, is however limited.

5.4.3 Car deck

For bunkering, a fuel truck is assumed to provide the ethanol to the ship-side when the ferry rests in harbour, typically during night-time as is done for LNG-ferries today. The area around the truck is sealed off, providing a safety zone in case of fire. The filling hose would typically connect inside at the car deck. Any spill by the connection would fall onto the car deck. The deck is assumed to incline about -1% from the centre-line of the ferry towards the walls, to lead rainwater and potential bunkering spills to the sides.

Possibility for generation of explosive atmospheres with spills during bunkering is assumed low, due to the open design and expected moderate temperatures when bunkering during night-time.

5.5 Nitrogen systems

In theory, the products of fuel cells are nitrogen and steam. However, the fuel cells require surplus oxygen, thus the nitrogen cannot be used further in inerting processes. The supplier of the SOFCs does not specify the required air flow, but from the study by Janardhanan et al. the ratio of excess air relative to the stoichiometric amount seems to be between 2 and 3 for SOFCs, although it is stated that SOFCs running on pure hydrogen will require higher flows (Janardhanan et al. 2007). In any case, the exhaust leaving the fuel cells has a higher oxygen content than acceptable as an inerting agent. Therefore, the fuel cells could not be utilised to produce nitrogen as a by-product.

The ferry requires nitrogen as an inerting agent for the atmosphere inside tanks and potentially also for double-walled pipes, unless these are properly ventilated. In addition, nitrogen is the flushing agent of the reformer regeneration process. The FCHS, where the fuel cells and the reformers are located, could have either an inert or an air-based atmosphere. An inert atmosphere would be more expensive than using air but potentially increase the level of safety. On the contrary, an inerted room would represent a risk of asphyxiation for crew potentially entering the FCHS for inspection or maintenance. In this case, an air-based atmosphere is chosen. If the explosion risk with the air atmosphere turns out to be significant, the choice could be reconsidered at a later stage. The nitrogen for inerting purposes could be supplied by standard high-pressure tanks. If using a sensor to monitor partial pressures in the tanks and double piping, the nitrogen might be to a great extent be recycled and re-compressed. However, such cylinders would require much space, be expensive to acquire and require their own set of logistics when refills are necessary. Local nitrogen production on the vessel is therefore assumed to be a better option.

As ethanol is consumed at a rate of about 50 g/s, nitrogen gas at a rate of 3.9 l/min would have to be added for the pressure to remain stable. He et al. regenerated their reformer by an inert stream of 60 mL/min (He et al. 2010). Given the discussion on reformer size in Chapter 5.3.3, the corresponding stream for the larger system would be 1.8 l/s. This amount would only be required for half of the time, during regeneration of one of the reformer units. The required potential for nitrogen production, including the required nitrogen for the outer rooms in the double-walled pipes, was estimated to be 1.9 l/s.

A small nitrogen production unit would be located outside the FCHS. A unit only producing 0.11 m^3/min with a quality just above 95% is assumed affordable and it would require little space relative to the cylinders. The SEPURAN N2 4“ membrane module is an example of a product in the market that would fulfil the requirements. At 87 cm in length, it would manage to produce up to 2.5 l/s at 7 barg (EI 2020). A unit of similar size to the SEPURAN N2 4” but with an incoming pressure of 2.5 barg is in the concept assumed to satisfy the demand.

As the system is small in size and not assumed a major expense, two membrane modules could be installed to provide redundancy in the nitrogen systems. If only one module is available, any failure would cause a shut-down of the fuel cell systems and a break from operation due to necessary maintenance. In this case, one module was assumed sufficient.

5.6 Area design

In this section, the areas considered potentially hazardous are defined in detail. The designs presented have not been discussed with naval architects and would in all probability have to be adjusted for a real vessel. The designs were in this thesis assumed to function with regard to demonstrating the safety of the power system.

5.6.1 Fuel storage holding space

The two fuel storage holding spaces (FSHS) primarily hold the ethanol container tanks. These are similar to those of MF Glutra and the rooms are placed along the centre-line of the vessel. From Figure 5.1, the rooms were approximately 3 m high, 12 m long and 4 m wide. The container tanks are cylindrical and 9 m in length. To hold 32 m^3, the inner diameter of the tanks must be about 2.2 m. The tanks rest on one of the sides of the rooms. The tanks are connected to a bunkering pipe and to an ethanol supply pipe. A third pipe supplies nitrogen gas to the tanks, to replace the volume of ethanol extracted and ensure an inert atmosphere. To avoid excessive piping in the room, the pipes are sent towards the roof. The pipes for ethanol supply and nitrogen inerting are transported along the roof to the FCHS, while the bunkering pipe moves through the roof of the FSHS towards the connection at the car deck. The set-up is equal for the two storage rooms and is illustrated in Figure 5.6.

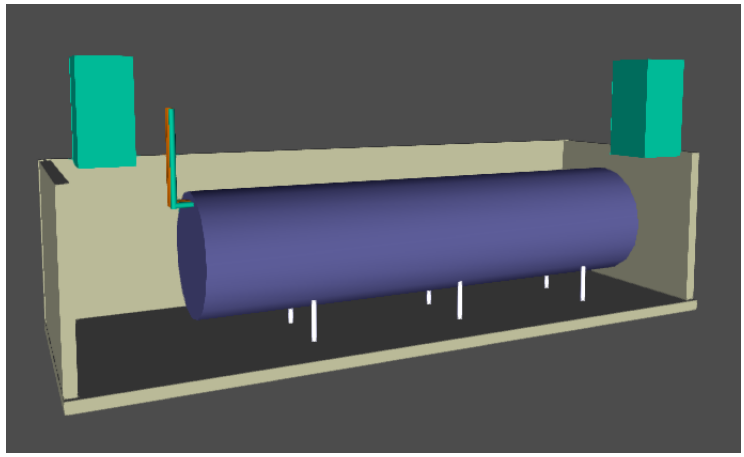

Figure 5.6: An illustration from FLACS of the set-up of the fuel storage holding space. The roof and one wall were removed for sake of visibility.

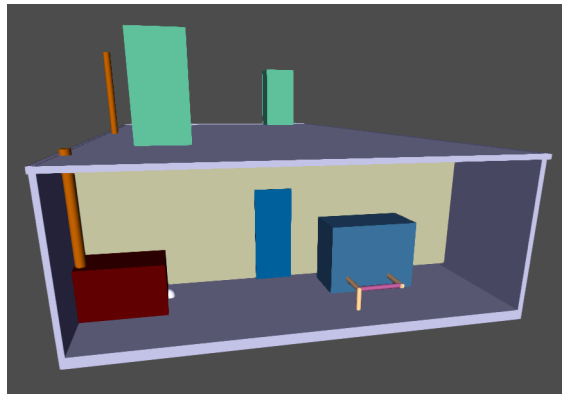

Figure 5.7: An illustration from FLACS of the set-up of the room outside the FCHS. The front wall was removed for sake of visibility.

5.6.2 Fuel cell holding space

In contrast to the gas engines of MF Glutra, the outer room containing the FCHS is situated below the car deck, between the two FSHSs. The FCHS is itself a smaller room encompassing the reformer units and fuel cell modules. A nitrogen production unit is situated in the outer room, connected to a compressor for air supply. The compressor additionally supplies the FCHS with pressurised air for the SOFC modules. Incoming ventilating air would enter the FCHS through a shaft on one side of the room and exit through a similar shaft at the other end. The fans are placed upstream of the FCHS. A pump unit would be connected to fuel pipes coming down from the ceiling with supply of ethanol. The FCHS is assumed to be 13 m long, 8 m wide and 2.7 m high, while the section outside the FCHS would only be 3 m long, 8 m wide and 2.7 m high. The ceiling height is lower than in the FSHSs to minimise the volume of the FCHS and lower the air flow required for ventilation. An illustration of the room is given in Figure 5.7. In the figure, the nitrogen unit is situated next to the compressor unit supplying air to the SOFCs. On the left, the pump supplying ethanol is situated.

The main components of the FCHS are the twin reformer units along with the SOFC modules. Space for a compressor, a mixer and heat-exchange capabilities is also necessary. The modules have an assumed combined footprint of 45 m^2, with a height of 2.2 m. These are organised in six rows of six modules, and the rows are grouped into three groups to ensure access for maintenance. The reformer units are cylinders 2.2 m tall and have a 60 cm inner, and 80 cm outer diameter. Additionally, units for mixing ethanol and steam and evaporation are placed next to the reformer units. The fuel cells are connected by a main air pipe to the outer room. The same applies to the reformer units, although with nitrogen pipes. CO_2, nitrogen and other gas evacuated from the FCHS are released together with the ventilation air. An illustration of the set-up is given in Figure 5.8.

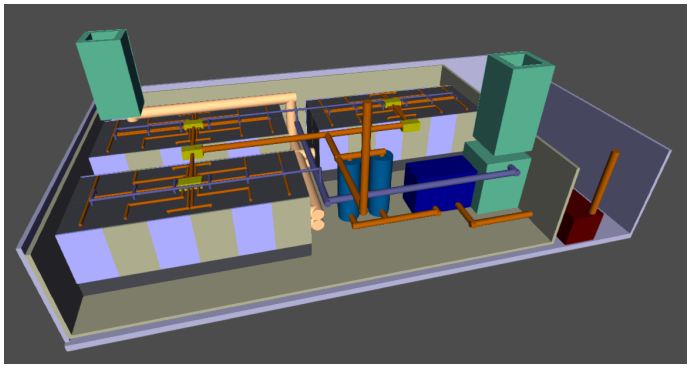

Figure 5.8: An illustration from FLACS of the set-up of the fuel cell holding space. The roof and a side wall were removed for sake of visibility.

5.6.3 Car deck

The central 40m of the 100 m long ferry deck is covered by the superstructure, representing a ceiling 5 m above the deck. The bunkering station is assumed to be placed at the end of the covered part of the deck. The bunkering rate is assumed to be 60 m^3/h and the hose diameter 63 mm. The rate is higher than for LNG-tankers and similar to rates found for methanol supplied from trucks (Forsman & Algell 2013, Knudsen et al. 2017). During bunkering, two people are assumed to monitor the situation; one by the truck and one person on the ferry. The FLACS model used to simulate the bunkering situation is illustrated in Figure 5.9.

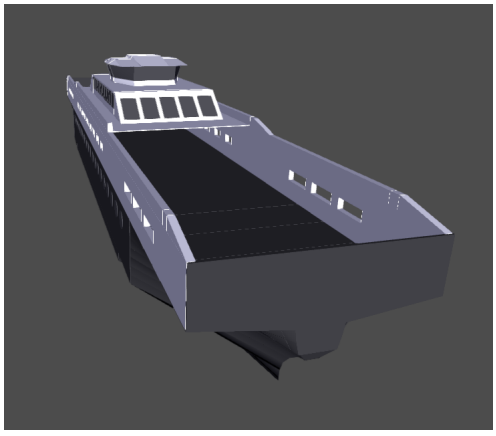

Figure 5.9: An illustration from FLACS of the geometry model used to simulate the bunkering scenario.

Chapter 6

Hazard identification

6.1 Fuel storage holding space

In the concept ferry, the fuel storage holding space could, by regulation, be suited with ventilation at 30 ACH and a drain. In this thesis, a temperature lower than the flash-point of ethanol was proposed as an additional safety measure. The volume of the room is 144 m^3, and according to FLACS 34 m^3 of these were filled, primarily due to the storage tank. If not considering the drain, the surface of the floor is 48 m^2. Given the initial and maximum rate of ethanol evaporation, as discussed in Chapter 3.6, a floor entirely covered by ethanol at 298 K could give an evaporation of 0.048 kg/s ethanol gas at the maximum rate, corresponding to 25 l/s ethanol gas.

Ventilation would be supplied by two fans, each capable of delivering 30 ACH and connected to different circuits for redundancy in case of electrical failure. To ventilate at 30 ACH, the fans must deliver 920 l/s of air. If the ethanol in the room were allowed to evaporate indefinitely at the maximum rate, the system would reach steady state when 25 l are removed from the room every second by ventilation. If the room is well mixed, the maximum gas concentration of ethanol that could by this assumption develop would be a gas fraction of 25/920, or 2.7% of the room, although some volumes would probably have higher concentrations, due to insufficient mixing. The LFL of ethanol is higher, at 3.3%, and simulations should assess the volumes of flammable clouds able to form under these conditions.

In reality, as discussed in Chapter 3.6, the evaporation rate would quickly drop, seeing an average rate of around 0.018 kg/s in the first 15 minutes, if the entire floor is covered by the ethanol pool. In the FSHS, ventilation would alone be able to maintain a non-flammable atmosphere during such a worst-case spill.

Another aspect to consider is that a major spill, e.g. a severe low-probability tank failure, would be required to fill the entire floor with ethanol. A spill from the fuel line tank

connection would at maximum be of the order the pump rate of 50 g/s, creating only a very limited pool area with the majority of spill being collected in the drainage tank. The likely evaporation rate for such a worst-case fuel line spill at 25 °C would likely be one order of magnitude lower, i.e. of the order 2-5 g/s, or 1-3 l/s. To keep the atmosphere non-flammable would only require 30-100 l/s ventilation, or 1-3 ACH, i.e. much less than the 30 ACH specified in the draft rules.

With a major release during bunkering, much higher spill rates (13 kg/s) could be seen, this could create a much larger pool on the floor and potentially lead to a hazardous situation if the FSHS is at room temperature without sufficient ventilation. As there will be no passengers and only essential crew during bunkering, risk should be limited. Gas alarms will likely sound prior to explosive atmospheres developing.

As discussed, in addition to ventilation, drainage tank and detection to activate shut-down of pump it was planned to keep the temperature in the FSHS below the ethanol flash point. If the temperature can be kept below 13 °C, this would prevent the generation of flammable atmospheres inside the FSHS. As this is a safety measure not required in the draft rules it would be expected that this measure could justify implementing a reduced ventilation rate in the FSHS, for instance 6 ACH.

At the Norwegian coast where the ferry would be expected to operate the sea temperatures are below 13 °C, the ethanol flash point, most of the year and will seldom exceed 16 °C, even at the surface. If the FSHS is thermally connected to the sea water below the vessel, the FSHS temperature would seldom exceed the ethanol flash point, and if it does, it would only be by a few degrees. Thus, a refrigeration system to keep FSHS temperature below 13 °C would only need to be active a small fraction of the year and would only need a limited power supply.

With the combined thermal control maintaining temperature in the FSHS below 13 °C combined with e.g. 6 ACH ventilation, the explosion risk should be controlled for any type of leak event, even the catastrophic tank failure.

A failure of the fan(s) would still not lead to a flammable atmosphere, while given a failure of the refrigeration system there will be a minor possibility for the development of flammable atmosphere (combination of tank failure that will overflow the drain tank and exceptionally high temperature in the sea heating of FSHS to lead to evaporation beyond what can be handled by the 6 ACH fans).

With temperature control fires will be low likelihood but possible if there is a strong ignition source. If this would happen there would be a need to fight fire by reducing oxygen access (stop ventilation) and use water mist or inert gases to cool and quench the fires.

6.2 Fuel cell holding space

In the FCHS, the required level of ventilation is also 30 ACH, while there would be much less available floor surface area compared to the volume of the room. Therefore, ethanol evaporation does not constitute a hazard, as discussed in the previous section, the maximum spill rate is also limited to the pump rate (50 g/s) and could be quickly shut-down at gas detection.

The available hydrogen could represent a potential risk. The reformer unit contains the largest available amounts of hydrogen, as the pipe segments are separated by valves which would close in case of larger leaks.

As described in Chapter 5.3.3, the reformer units contain 0.23 m^3 of products and reactants. The product stream consists of close to 2/3 hydrogen. By assuming reactants and products each make up half of the unit, 1/3 of the reformer volume would be hydrogen. If a leak were to happen by the outlet of the reformer, some of the ethanol would react before leaking into the room. By assuming that all of the ethanol in the reformer would react to become hydrogen, 2/3 of the total reformer volume could leak as reactive hydrogen. 2/3 of 0.23 m^3 corresponds to 0.15 m^3. By the ideal gas law, the volume amounts to 4.7 mol when at 2.2 bar and 850 K. 4.7 mol or 9.4 g is therefore the theoretical maximum amount of hydrogen available to leak. In reality nearly half of the hydrogen would be expected to remain inside the reformer as gas will not be pushed out after the pressure has fallen to ambient levels (1.0 bar). 5 g of hydrogen is a negligible amount inside the FCHS and should be of no concern. In Chapter 8, simulations are shown to illustrate the limited hazard from such a release.

In Chapter 5.3.3, the placement of a buffer tank after to the reformer units is discussed. Such a tank can provide a more stable flow to the SOFCs from the reformer units. On the other hand, the tank may represent a potential hazard, as it holds large volumes of hydrogen relative to other units in the setup. The volume required to stabilise the flow from the reactor units was not assumed to be large. Literature on the matter was scarce, although B. Sigales discussed 5 minutes residence time to be sufficient for liquid products moving to other process units (Sigales 1975). Gases are more turbulent than liquids and level out local differences much quicker. In addition, the SOFCs are flexible with regard to fuel input and would not require perfectly calm inlet streams. A tank designed for a residence time of 10 s was chosen to observe in simulations.

The product flow of 8.7 mol/s corresponds to 0.28 m^3/s, of which 0.187 m^3/s is hydrogen. Given the residence time, the tank would room 2.8 m^3. As discussed in Chapter 7, holding tanks fail at annual rates of 1e-6 or lower. The leak would most probably be located by the connections. A pipe diameter of 0.10 m was assumed, forming the basis for the leaks. However, the tank should preferentially designed so that the valve closing the tank to the pipe is located inside the tank. If the pipe fails and the pressure difference becomes large (¿1 bar), the tank will close. The buffer tank is therefore subject to holding tank leak frequencies. As with the reformer, the contents will only leak when there is a pressure gradient. At 2.2 bar, 55% of the contents can leak instantly. By the ideal gas

law, 1.87 m^3 hydrogen corresponds to 116 g at 2.2 bar and 850 K. 55% of this (64 g) would realistically leak. 64 g of hydrogen will quickly mix in the FCHS and should not be able to develop flammable volumes of concern. This is proved by simulations in Chapter 8.

In hydrogen at room temperature, the speed of sound is roughly 1200 m/s and much higher than in the other fuels discussed in Chapter 3.3. In high-temperature hydrogen at 850 K, the speed increases to roughly 2200 m/s. Due to the fraction of denser water vapour in the mixture, the sonic release velocity of the mixture will be around 1150 m/s. This is a very high velocity which will ensure immediate strong mixing and dilution in air.

To conclude, due to the limited volume and pressure of the buffer tank, the risk related to leaks will be demonstrated as low. It may thus be acceptable for the buffer tank to be placed inside the FCHS. However, since draft rules require it placed outside the FCHS an alternative design safety justification would be required for the buffer tank to be accepted inside the FCHS.

The safety of the fuel cell units have not been assessed. The volume of hydrogen inside each unit is however very small and a release into the FCHS would be of negligible concern. Due to the high temperature inside the SOFC unit it can be expected that a leak inside the cabinets would ignite, this could potentially cause some local damage to the units.

6.3 Car deck

A spill of ethanol from the fuel hose onto the car deck during bunkering represents a potentially hazardous situation. The fuel is supplied at a rate of 60 m^3/h, corresponding to 13 kg/s. While bunkering, two people are expected to monitor the process. A hose rupture would as a consequence quickly be discovered and the pump stopped. If 10 s is assumed to be a conservative estimate for how long a ruptured hose would be allowed to leak the spill could at most amount to 0.16 m^3 of spilled ethanol, due to the 96% concentration. If evenly distributed, the spill could perhaps produce a 2 mm layer across 80 m^2. By assuming the evaporation rates presented in Chapter 3.6, the maximum evaporation rate would in that case be 0.080 kg/s, given a temperature at 25 °C. At this rate, the ethanol would completely evaporate in 26 minutes. Given calm condition, with a wind speed of 0.5 m/s, the air would move across the spill in only 20 s, assuming a circular pool. The conditions would therefore compare to a minimum 180 ACH, as the air would move quicker across the shorter stretches of the pool. At maximum rate, only 0.85 m^3 (1.6 kg) would manage to evaporate during one such air change. As the LFL is 3.3%, that could produce a maximum flammable volume of 26 m^3, which would be spread out thinly across the 80 m^2 pool.

In reality, the temperature in Norway rarely reaches 25 °C at night, and wind conditions by the coast are generally above 0.5 m/s. Thus, the scenario visualised would be rare. The pool cannot continue to evaporate at maximum rate when the ethanol partial pressure above the pool begins to rise, as the vapour-liquid equilibrium shifts. The bunkering situation was ultimately presumed safe. By these calculations, a sloping deck was considered unnecessary as a safety measure, although some slope should in any case exist to remove rainwater. With regard to simulations, the scenario depicted was modelled to verify the result. An ethanol area leak was used instead of the pool evaporation model. The results are discussed in Chapter 8.

Chapter 7

Frequency assessment

The frequency assessment was based on two different models. For hydrogen, the model developed by LaChance et al. was applied, while for ethanol, purple book models of RIVM was applied. In Table 7.1, relevant ethanol frequencies for the system are given. In Table 7.2, relevant hydrogen frequencies for the system are given.

7.1 Ethanol frequencies

The units able to leak ethanol were the two storage tanks, the pipelines inside the FCHS, the reformer units, the pump pulling ethanol from the storage tanks, the heat exchanger inside the FCHS and the hose supplying ethanol during bunkering. The storage tanks were assumed single-walled, the frequency for pipelines was adjusted based on a length of 3 m, the pump was assumed centrifugal and the frequency for bunkering was adjusted based on a three hour bunkering process. The double-walled pipes are not included in the assessment, as the outer shell was expected to be able to lead leaks out into the air, liquid leaks should end in the drainage tank.

The tolerance level for one crew-member fatality of 3e-4 per year gives an indication of the maximum tolerable frequency for major accidents. For the tanks, most leaks would occur related to the tank connections and be relatively small. The expected annual frequency for catastrophic leaks from each tank is 1e-5 (two types of events, each of 5e-6 per year), thus for two tanks the frequency is 2e-5 per year. Scenarios with frequencies this low could have severe consequences without exceeding the tolerance criterion, however, for the actual case it is still believed that a tank rupture scenario could be managed safely.

Leaks should also be expected, and managed safely, from the pipes inside the FCHS. One of the reformer units should also be expected to fail catastrophically at an annual rate of 2e-5, based on the RIVM frequency model.

Table 7.1: Leak frequencies based on the RIVM model (RIVM 2009).

Unit	Event	Frequency in annual occurrences
Single containment atmospheric tank	Instantaneous release of entire contents	5e-6
	Release of entire contents in 10 min. in a continuous and constant stream	5e-6
	Continuous release from a hole with an effective diameter of 10 mm	1e-4
Pipelines	Rupture in the pipelines	3e-6
	Leak with an effective diameter of 10% of the nominal diameter, up to a maximum of 50 mm	2e-5
Reactor and process vessels	Instantaneous release of entire contents	5e-6
	Release of entire contents in 10 min. in a continuous and constant stream	5e-6
	Continuous release from a hole with an effective diameter of 10 mm	1e-4
Centrifugal pumps and compressors	Catastrophic failure	1e-5
	Leak (10% of diameter)	5e-5
Pipe heat exchangers where the hazardous substance is located inside the pipes and where the casing has a design pressure that is greater than or equal to the maximum pressure of the hazardous substance occurring in the pipe	Rupture of 10 pipes at the same time	5e-6
Bunkering hose	Rupture of hose	1e-5
	Leak in hose with an effective diameter of 10% of the nominal diameter.	1e-4

The reformer units contain hydrogen as well, and the lower parts of the reformer would be considered with hydrogen leak frequencies. Catastrophic leaks would have a frequency of the order 1e-6 per year, smaller leaks from tank connection a somewhat higher frequency. The pump expected failure rates are estimated to about 6e-5 times yearly. The heat exchanger inside the FCHS handling ethanol would also see low failure rates at the similar range. Here it should be noted that the pressure in the systems is relatively low, only 2.2 bar, while many of the frequencies, in particular for hydrogen systems, are developed for system pressures of 100s of bar. It can thus be assumed that real frequencies may be even lower than those estimated.

For the bunkering hose rupture frequency is estimated to 1e-5 per year, with smaller leaks occuring with a frequency of 1e-4 per year.

Table 7.2: Leak frequencies based on the hydrogen model of LaChance et al. (LaChance et al. 2008).

Unit	Release size [%]	Leak frequency in annual occurrences
Cylinders	0.01	1.18e-6
	0.1	9.98e-7
	1	6.80e-7
	10	3.90e-7
	100	2.09e-7
Pipes	0.01	8.78e-6
	0.1	4.57e-6
	1	1.80e-6
	10	9.12e-7
	100	6.43e-7
Joints	0.01	7.05e-5
	0.1	3.56e-6
	1	7.80e-6
	10	6.96e-6
	100	6.21e-6
Valves	0.01	5.71e-3
	0.1	7.50e-4
	1	9.92e-5
	10	4.13e-5
	100	1.49e-5
Instruments	0.01	8.31e-4
	0.1	2.78e-4
	1	1.73e-4
	10	1.84e-4
	100	1.11e-4

7.2 Hydrogen frequencies

With regard to estimating hydrogen leak frequencies, the SOFC modules represents a challenge as the detailed layout is not known. In all probability, there are several ways hydrogen can leak inside the SOFC modules. However, due to the small amounts of hydrogen in each module, fuel cell leaks are not considered as potentially hazardous. Hydrogen from the SOFCs would probably ignite upon contact with air and therefore unable to develop larger volumes of flammable gas. With 36 SOFC modules, all of these would require pipes, joints and valves, in addition to those required by the reformer units and the surrounding system. The number of components is estimated in Table 7.3.

The reformers were considered as cylinders. According the the RIVM procedure, one can roughly assume a ten times higher frequency for process units rather than storage units. This rule of thumb was applied for the reformer units. A count of these parts is presented in 7.3.

The estimated frequencies indicate that a hydrogen leak somewhere in the FCHS could take place every 5 year, most of these would however be small. There is also a possibility that system details (leak points) may have been underestimated, and that the leaks will be more frequent, on the other hand, pressures are as mentioned low, and the predicted frequencies may therefore be too high. As the amount of hydrogen available given a leak is low, the consequences can likely be kept limited.As there will be no people present in the FCHS during operation, the potential for fatalities should be negligible if the FCHS walls/decks can maintain its integrity through the incidents.
Table 7.3.

By looking at these frequencies, the FCHS must obviously be able to prevent events from producing dangerous situations. Leaks will happen frequently, and at the temperatures of the process the room was required to have an inert atmosphere, as the hydrogen would auto-ignite in the room, at the temperatures of the processes. None of the events should be allowed to cause fatalities. If, as likely, only one of the crew managed the room surrounding the FCHS, a worst-case event happening rarer than 1e-4 times a year could in theory be allowed to break the FCHS, creating a dangerous situation in the outside room. This would be relevant for the event of a complete rupture of a reformer unit.

Table 7.3: Component count and indicative total leak frequencies for all hydrogen systems based on the hydrogen model of LaChance et al. (LaChance et al. 2008).

Unit	Count	Release size [%]	Leak frequency in annual occurrences
Cylinders	2	0.01	2.36e-5
		0.1	1.96e-5
		1	1.36e-5
		10	7.80e-6
		100	4.18e-6
Pipes	31	0.01	2.72e-4
		0.1	1.41e-4
		1	5.58e-5
		10	2.82e-5
		100	2.00e-5
Joints	60	0.01	4.23e-3
		0.1	2.14e-4
		1	4.68e-4
		10	4.18e-4
		100	3.73e-4
Valves	30	0.01	1.72e-1
		0.1	2.26e-2
		1	2.98e-3
		10	1.24e-3
		100	4.47e-4
Instruments	5	0.01	4.16e-3
		0.1	1.39e-3
		1	8.65e-4
		10	9.20e-4
		100	5.55e-4

Chapter 8

Consequence assessment

In the following CFD simulations using FLACS are used to evaluate risk aspects identified during the hazard identification. Simulations have been performed in three different areas, including:

- Ethanol spills in the FSHS to evaluate potential for generation of flammable atmospheres.
- Hydrogen releases inside the FCHS to evaluate potential explosion risk from releases.
- Ethanol spills at the car deck to consider possible hazard scenarios during bunkering.

The motivation for the simulations, information about the setup and results will be presented for the different areas.

8.1 Simulations of ethanol spills in the FSHS

8.1.1 Procedure

The proposed safety philosophy to limit risk from ethanol spills in the FSHS were the following:

1. Keep temperatures below 13 °C flashpoint. This will prevent flammable atmospheres to develop.
2. Maintain moderate ventilation of 6 ACH. This will limit risk if refrigeration should fail.

3. Drainage tank to collect spilled ethanol and limit floor area exposed. This will minimise pool evaporation. If the drainage tank is partially filled with water, this will further increase flashpoint (reduce evaporation).
4. Gas detection in drainage tank and FSHS (20% LFL) will stop pump and end spill of ethanol (except for tank failures).
5. Double piping of bunker line will prevent leaks during bunkering (it is assumed that proper safeguards to avoid overfilling are implemented).
6. Fire-fighting system (water).

If temperature control (1) is successful, obtaining flammable concentrations inside the FSHS will not be possible, and explosions and fires will be prevented. A fire could however be initiated by a strong ignition source (e.g. open fire), but the fire-fighting system (6) is expected to handle this.

Only if the temperature control (refrigeration) should fail, there would be a possibility for generation of flammable atmospheres:

1. About $\frac{1}{3}$ of the year the sea-temperature can potentially be higher than the ethanol flashpoint, so that there is a possibility for generation of flammable atmospheres. With passive cooling from contact with hull, the temperature would seldom be significantly higher than the ethanol flashpoint and never as high as 20 °C.
2. Leaks from pump or fuel lines have the highest frequencies (of the order 1e-4 per year). These leaks would be sized similar to the pump rate (0.05 kg/s) and would be stopped quickly at confirmed detection. The spill would create a small pool (likely less than 5 m^2) and be collected in the drainage tank. To demonstrate that this scenario is sufficiently safe, a simulation of a 5 m^2 pool evaporation (using fixed worst-case rate 0.001 kg/m^2s, i.e. 5 g/s) is performed in a room with ventilation of 6 ACH – see scenario 700002. This will be representative for pool evaporation in 25 °C.
3. Small leak from tank (10mm-frequency 1e-4/year) would by the Bernoulli equation give a leak rate of the order 0.25 kg/s or less. With this rate it would take almost 1h to spill 1m3 ethanol, and several hours to fill a drainage tank. The vessel can be taken out of service and the leak scenario can be managed safely prior to any escalation of the scenario.
4. For a catastrophic tank failure to develop flammable atmospheres the refrigeration system must fail and the temperature on the day must be higher than the ethanol flash point. The failure itself is a rare incident (frequency of 2e-5 per year), and the combination of these three events would be even more so. A tank failure is simulated in scenario 700001 (fixed worst-case rate 0.001 kg/$m^2 s$, i.e. 48 g/s, 6 ACH ventilation).
5. 0.37 g/m^2s is a more realistic evaporation rate for ethanol at 25 °C. Scenario 700012 is similar to 700001, but with the more realistic rate (0.018 kg/s)

6. Scenario 700007 is similar to 700001, but with 30 ACH instead of 6. This is to simulate the relative effect of the ventilation power given a catastrophic failure. Scenario 700008 is similar to 700007, but with the lower evaporation rate of 0.018 kg/s instead of 0.048 kg/s.

7. A catastrophic failure is rare to the extent that flammable clouds are acceptable. Scenarios 700009, 700013 and 700014 model the potential explosions, given an ignition of the flammable clouds produced in some of the catastrophic failure scenarios. Based on the results from the validation simulations in Appendix B, the highest explosion pressures are produced at an equivalence ratio of $\phi = 1.2$. Given ventilation of 6 ACH, a catastrophic failure will by both evaporation rates discussed (48 g/s = 26 l/s & 18 g/s = 10 l/s) be able to reach high equivalence ratios, by looking at the steady state result of the ventilation (183 l/s) and the evaporation. The simulations quantify the potential consequences given the different worst-case scenarios and assure that the hull of the vessel is not in danger of breaking.

8. The spill scenarios mentioned above model the ethanol evaporation as an area leak from the floor. The pool evaporation model in FLACS is not properly validated for substances with flash-points at ambient temperatures, and errors were experienced using the defined ethanol substance. Heptane and hexane were tested as a potential substitute for ethanol in the pool evaporation model. The results were unreliable (evaporation seemed to proceed independently of vapour pressure) and are discussed at the end of Appendix B.

Table 8.1: An overview of the simulations performed in the fuel storage holding space.

Fuel storage space		**Simulation parameters**			
Scenario number	Description	Release [kg]	Duration [s]	T [K]	Ventilation [ACH]
700002	Ethanol area leak by tank connections	0.005/s	900	298	6
700001	Ethanol area leak across floor	0.048/s	900	298	6
700012	Ethanol area leak across floor	0.018/s	900	298	6
700007	Ethanol area leak across floor	0.048/s	900	298	30
700008	Ethanol area leak across floor	0.018/s	900	298	30
700009	Ethanol explosion	1.71	10	298	0
700013	Ethanol explosion	15.9	10	298	0
700014	Ethanol explosion	10.6	10	298	0

8.1.2 Simulation results

Scenario 700002

A leak from one of the tank connections is among the more likely events in the FSHS (about 1e-4 occurrences per year). The largest of these leaks would come from a rupture of the bunkering line during bunkering (13 kg/s). The bunkering situation is expected to be monitored by two trained personnel and would therefore quickly be stopped. The other event would be a rupture from the line supplying ethanol to the SOFCs (0.05 kg/s). This leak would instantly be stopped due to the disconnection of the pump from the ethanol storage due to the break. The ethanol already in the pipe can leak onto the floor of the FSHS.

Scenario 700002 was assumed to represent both the events described. Both events would be safely controlled if the refrigerating system functions properly. In the scenario, the refrigerating system is assumed to fail, and the temperature in the room was set to 25 °C. The leak was assumed to form a 5 m^2 pool on the floor. The evaporation rate was set constant at 5 g/s and ventilation at 6 ACH.

The geometry is illustrated in Figure 8.1. The arrows indicate the two leaks. The one from the floor represents the evaporation from the 5 m^2 pool, and the other represents the air entering the room. The grid cells were 25 cm in the X and Y directions. In the Z direction, the cell length was 15.0 cm. The Z direction has a finer grid to allow for a more detailed description of concentration layers in this direction, considered of most importance for both the evaporation and ventilation.

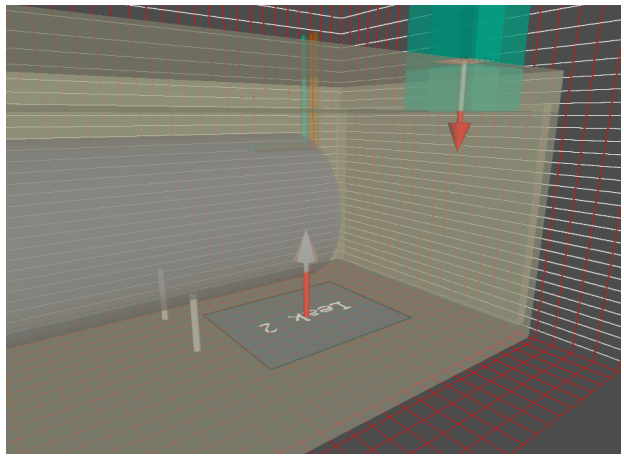

Figure 8.1: Illustration of scenario 700002.

As assumed prior to the simulation, this scenario cannot produce larger flammable volumes. In Figure 8.2, Q9 inside the FSHS is given over time. Q9 is the equivalent stoichiometric cloud size and is expected to give the same explosion consequences as the

actual dispersed cloud. As clouds are very different in shape and composition, Q9 is a way to compare the reactivity of different clouds by their equivalent stoichiometric volume (Hansen et al. 2013). The maximum equivalent stoichiometric volume present from this scenario was 0.6 m^3. In a room of 110 m^3, this amount is not considered a hazard. More than 10 minutes were required to reach these levels. The drain is assumed able to remove the smaller and more frequent leaks, as simulated in this scenario, before 10 minutes has passed. The early spike in Q9 volume from Figure 8.2 is assumed a result of ventilation patterns not having established themselves yet, as the two leaks initiate simultaneously.

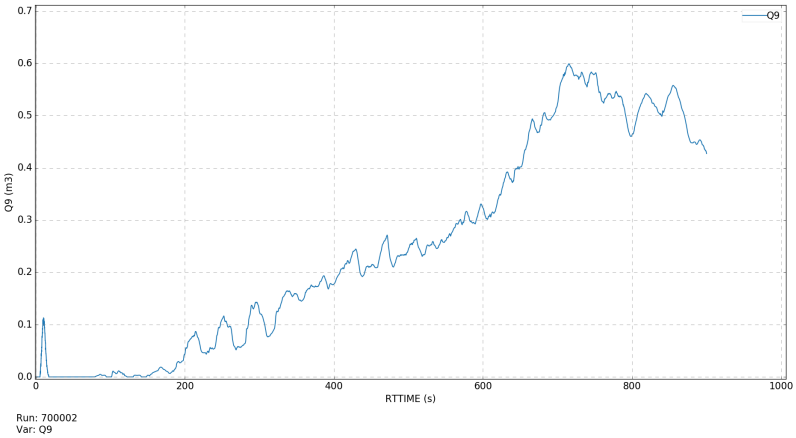

Figure 8.2: The equivalent stoichiometric cloud volume (Q9) over time in scenario 700002.

The scenario demonstrates that the frequent leaks can be considered not to be potentially hazardous, even if the refrigeration, the main safety measure, should fail. Both the temperature and the evaporation rate in the scenario was set to unrealistically conservative levels. Even so, the leak did not manage to develop flammable volumes of concern.

Scenarios 700001 and 700012

Scenarios 700001 and 700012 both simulate the event of a catastrophic tank failure. In such a case, the contents of the tank would spill onto the floor of the FSHS. The drain would fill and ethanol would evaporate from the whole surface of the floor. Under normal circumstances, a catastrophic failure would be controlled by the refrigeration system. The ferry would manage to reach shore and safely pump out the ethanol. For the situation to potentially become hazardous, both a failure of the refrigeration system and high seawater temperatures must coincide.

The scenarios differ only in the rate of evaporation. In 700001 the rate is at the maximum rate observed for ethanol at 25 °C (48 g/s), while the rate of 700012 is the observed average rate for the first 15 minutes of evaporation (18 g/s), also at 25 °C. Otherwise, the

scenario is similar to 700002 with regard to grid and ventilation. Figure 8.3 provides and illustration of the scenarios. As the figure indicates, the evaporation is also in these scenarios modelled as an area leak from the floor. In contrast to 700002, the leak covers the whole floor surface.

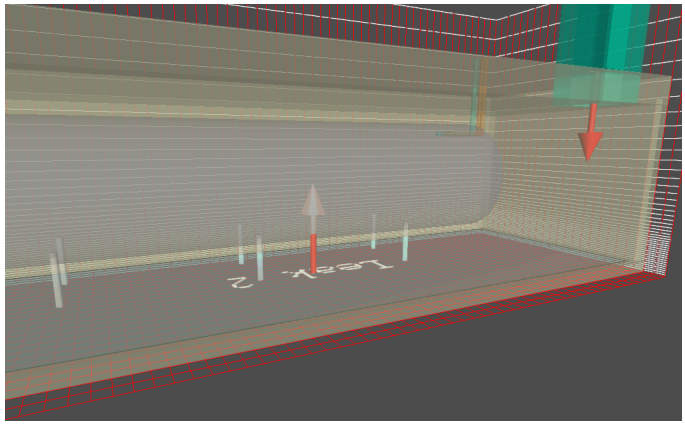

Figure 8.3: Illustration of scenarios 700001 and 700012.

Both scenarios were prior to the simulations expected to produce flammable atmospheres. If the room were perfectly mixed, the steady state concentrations would be 12.4% for scenario 700001 and 5.2% for 700012. The concentrations correspond to equivalence ratios of 1.9 and 0.8, respectively. Both those concentrations would produce explosions if ignited.

The scenarios did not manage to produce realistic results. The concentration levels from scenario 700001 are illustrated in Figure 8.4. From the figure, it is apparent that the ventilation was too low to stir the room. The ethanol is heavier than air and would probably remain closer to the floor, but the layered composition presented is too perfect to be realistic. The ventilation inlet was moved to one of the walls, close to the floor, in an attempt to provide a better angle for mixing, but the results were the same.

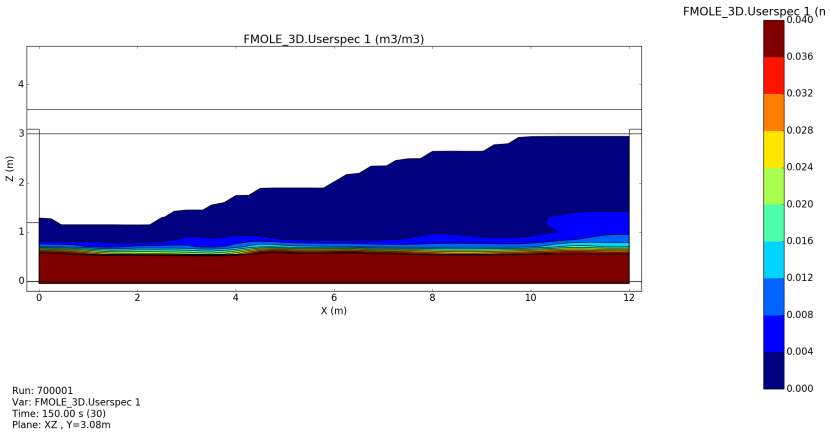

Figure 8.4: The concentration volumes at 150 s in scenario 700001.

The failure of scenarios 700001 and 700012 to produce results was not considered problematic, as these scenarios in any case would be expected to produce large amounts of flammable ethanol mixtures. The results would only serve to affirm the estimates. The potential consequences of an ignition of the estimated clouds from these scenarios would in any case be investigated. This is done in scenarios 700013 and 700014.

Scenarios 700007 and 700008

Scenarios 700007 and 700008 are similar to the previous two simulations, except with 30 ACH instead of 6. The simulations will reveal to what degree a higher ventilation will counter the evaporation in the event of a catastrophic failure. With ventilation at 30 ACH, the steady state concentrations reached by the two evaporation rates (48 g/s and 18 g/s) in a mixed room would be 2.8% and 1.1%. This relates to equivalence ratios of 0.43 and 0.17, respectively. For 6 ACH, the ratios were 1.9 and 0.8, in comparison. 30 ACH was therefore assumed to control the catastrophic failure scenario for both evaporation rates. Local clouds of flammable volumes were expected, especially for scenario 700007, which models the higher evaporation rate.

The grid was not similar to that of scenarios 700001 and 700012. In 700007 and 700008, the grid cells were 20 cm long in the X and Y directions. In the Z direction, the length was 5 cm for 1 m closest to the evaporation, before spreading out with a maximum factor of 1.1. The difference in grid is not assumed to have affected the results relative to the other scenarios.

The equivalent stoichiometric cloud volumes (Q9) developed in the two scenarios are presented with time in Figure8.5. In scenario 700007, the steady state concentration is close to the LFL, and local clouds of flammable volume will exist in multiple locations in

the FSHS. These clouds are highly dependent on the air flows in the FSHS. The varying amount of flammable volume is assumed a result of the ventilation not having stabilised. For scenario 700007, the flammable clouds remained close to the ground. An illustration of the concentration distribution is presented in Figure 8.6. Also for scenario 700008, the ethanol concentrations remain close to the ground. In 700007 20 m^3 of Q9 volume developed. From Figure 8.6, the flammable volumes seem to average at an equivalence ratio of around $\phi = 0.7$. In a room of 110 m^3, 20 m^3 of equivalent stoichiometric cloud volume will manage to cause an explosion, but the pressures should not be of any concern.

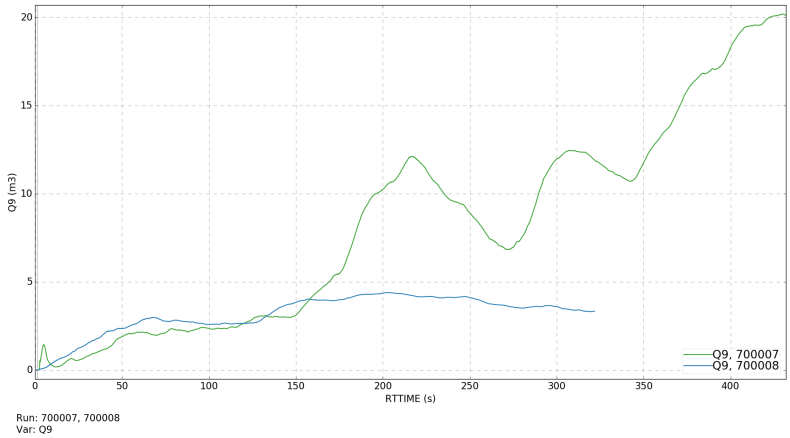

Figure 8.5: The equivalent stoichiometric cloud volume (Q9) volume over time in scenarios 700007 (green) and 700008 (blue).

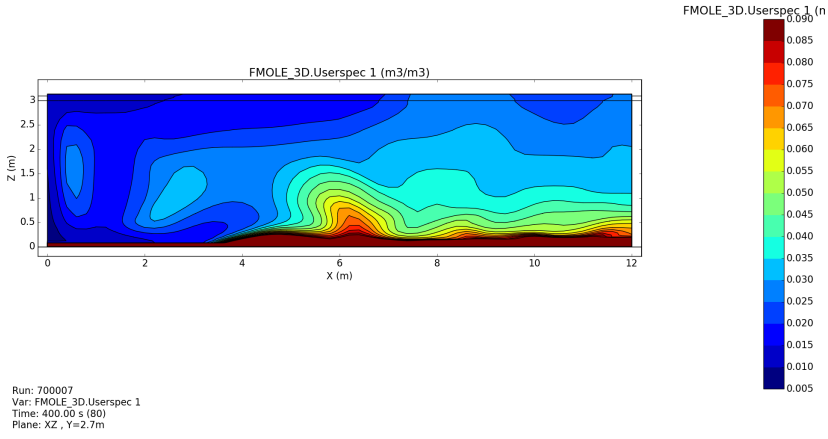

Figure 8.6: The ethanol concentration levels in scenario 700007 after 400 s.

From the scenarios, the higher ventilation was demonstrated to control the ethanol evaporation in the event of a catastrophic failure. In case higher pressures are developed from the explosions in scenarios 700013 and 700014, the ability to increase the ventilation should be considered in order to fully control the situation following a catastrophic tank failure. The simulations further demonstrate that the air inlet and outlet should be placed at different heights to avoid local concentrations by the ground.

Scenarios 700009, 700013 and 700014

Scenarios 700009, 700013 and 700014 all model explosions following a catastrophic failure. 700009 concerns the ignition of a 20 m^3 stoichiometric flammable cloud ($\phi = 1.0$). The cloud is placed close to the floor as illustrated in Figure 8.7. Scenarios 700013 and 700014 model the ignition of the flammable clouds from scenarios 700001 and 700012. 700012 is the more realistic of the two, and can reach a steady-state concentration in the FSHS correlating to $\phi = 0.8$. 700001 can reach $\phi = 1.9$, but the most powerful explosion is observed at $\phi = 1.2$, as demonstrated by the validation results in Appendix B. Therefore, 700013 models the ignition of a well-mixed atmosphere where the equivalence ratio equals 1.2. This represents a theoretical and highly unlikely worst-case scenario. The results will assert whether the bulkhead and hull can be at danger from explosions in the room. The grid is similar for all three scenarios, with the cell length equal to 20 cm in all directions.

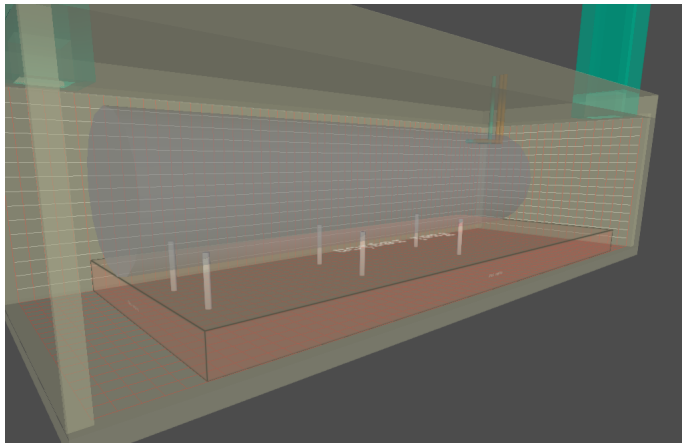

Figure 8.7: The setup for scenario 700009. The semi-transparent box below the storage tank represents the fuel region.

The explosion over-pressures for the three scenarios are presented in Figure 8.8. From the figure, the assumption that a flammable volume of 20 m^3 is of little concern is confirmed, as it will generate only minor over-pressures (12 kPa). The theoretical worst-case scenario (700013) will generate an over-pressure up to 1.8 barg, remaining above 1 barg for less

than 1 s. The bulkheads and the hull are assumed able to handle this pressure, especially due to the short duration. 700014 was more realistic and the explosion modelled should not pose any risk to the surrounding structures, due to the low over-pressure. It must be said, that the over-pressure is to a large degree dependent on the size of the ventilation ducts. If they were designed smaller, the pressure in the room would reach higher levels. If they were closed, the pressure from a well mixed $\phi = 1.2$ explosion would reach 8.5 barg, which probably is more than the bulkheads would manage.

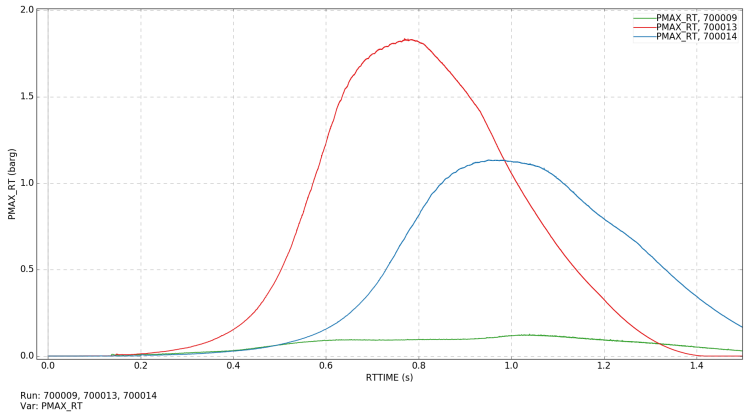

Figure 8.8: The maximum pressures over time of scenarios 700009 (green), 700013 (red) and 700014 (blue).

For the explosions in 700013 and 700014 to occur, multiple failures would have to coincide. The refrigeration system, warm seawater, the catastrophic failure and ignition at the most critical time. The probability of a catastrophic failure causing an explosion is therefore unlikely to the degree that several fatalities would be acceptable. The fact that even this scenario would be contained, highlights the safety of the system and demonstrates further that 6 ACH is sufficient ventilation for a situation as described in the FSHS.

8.1.3 Conclusion

The frequent leaks were demonstrated to be safely handled even if the main safety measure (refrigeration) failed. That left the only potentially hazardous situations to develop from the catastrophic failure of the tank. This would also only be a cause for concern if the refrigeration had failed, in addition to the the room being warm due to hot seawater. The worst-case events were demonstrated to pose limited risk to the structures of the room. Explosions could produce lethal over-pressures, but the time required to generate large enough explosive atmospheres in the room would allow for plenty of time to evacuate the area, which in the first place should be avoided during operation.

Given that the refrigeration system is 90% reliable and if the seawater is warm enough to heat the room so that the ventilation cannot handle the evaporation (water temperature 20 °C) 10% of the year, and also assuming a 10% probability of ignition, the explosion frequency can be estimated to 2e-8 occurrences per year. This is a frequency well below any tolerance criteria and would give a negligible risk contribution even if a major accident would result. The results indicate that a ventilation level of 6 ACH is sufficient for ethanol storage areas, when coupled with other safety measures, as refrigeration.

8.2 Simulations of hydrogen releases inside the FCHS

8.2.1 Procedure

The proposed safety philosophy to limit risk from hydrogen leaks in the FCHS were the following:

1. Maintain ventilation of 30 ACH

2. By mechanical valves automatically isolate any part of the system in which large pressure differences develop. By this measure, the amount of hydrogen available to leak from any single part of the system can be limited.

Due to the high levels of ventilation in the FCHS, ethanol leaks were not considered potentially hazardous and hydrogen leaks presented the highest risk. The steps in demonstrating the safety of the FCHS are outlined below.

1. The unit holding the largest amounts of hydrogen is the reformer. As described in Chapter 6, only 9.4 g of hydrogen can potentially leak from the reformer unit. A leak of that size would quickly mix with the surrounding air to concentrations below the LFL of hydrogen (4.0%). To demonstrate that the reformer unit could not potentially represent a hazard, a scenario (600001) modelling an explosion of 9.4 g of hydrogen stoichiometrically mixed with air was set up. The explosion yielded low over-pressures.

2. The potential inclusion of a buffer tank in the design was also discussed in Chapter 6. Although initially expected to be unnecessary, such a tank may provide the system with increased stability. If included, the tank would replace the reformer as the largest single container of hydrogen (116 g). A scenario (600002) modelling an explosion of 116 g hydrogen mixed stoichiometrically with air was initiated to observe whether a this event would generate over-pressures of concern. The explosion yielded close to lethal pressures, local to the source of ignition.

3. To demonstrate that the setting for the explosion of simulation 600002 was unrealistic and to observe the behaviour of a hydrogen leak in the FCHS, two scenarios, 600003 and 600004, were set up to respectively model 1% and 10% leaks from the buffer tank connection. The leaks did not manage to generate flammable volumes except for the area just outside the leak.

4. Hydrogen leaks from the different pipes of smaller size will happen frequently in the FCHS, about every 5 years according to the frequencies derived in Chapter 7. As the larger leaks are handled safely by a margin, the smaller leaks are assumed not to represent any potential hazard. The room is of simple shape, and small amounts of hydrogen will be removed by ventilation.

Table 8.2: An overview of the simulations performed in the fuel cell holding space.

Fuel cell holding space					
Scenario number	Description	Release [g]	Duration [s]	T [K]	Ventilation [ACH]
600001	Hydrogen mixed stoichiometrically with air and ignited	9.4	2.0	298	0
600002	Hydrogen mixed stoichiometrically with air and ignited	116	2.0	298	0
600003	1% Hydrogen/steam leak from buffer tank	116	100	298	30
600004	10% Hydrogen/steam leak from buffer tank	116	100	298	30

8.2.2 Simulation results

Scenario 600001

According to the estimates in Chapter 6, only 9.4 g of hydrogen can potentially leak from the FCHS design. The purpose of scenario 600001 was to observe whether that amount of hydrogen could, if stoichiometrically and ideally blended with air, produce hazardous pressure levels if ignited. The fuel region illustrated in Figure 8.9 represents the volume containing the mix of hydrogen and air. The flammable volume ($\phi = 1.0$) was 0.39 m^3 when mixed with air at 298 K and 1 bar. The nearby fuel cell panels and the closest FCHS-wall were fitted with panels measuring pressure. The grid in the FCHS was uniform, measuring 10 cm in all cell directions.

An illustration of the pressure levels at 30 ms after ignition is given in Figure 8.10, at the time when the highest pressure levels were reached. The maximum pressure registered was 5.2 kPa. Pressures above 4.0 kPa were only present for 6 ms before scattering. The highest pressure levels were local to small volumes close to the ignition location. Low-pressure shock waves seemed to bounce between the modules for some time, but after 130 ms, the maximum pressure remained lower than 1.0 kPa. These pressures are too low to cause any concern.

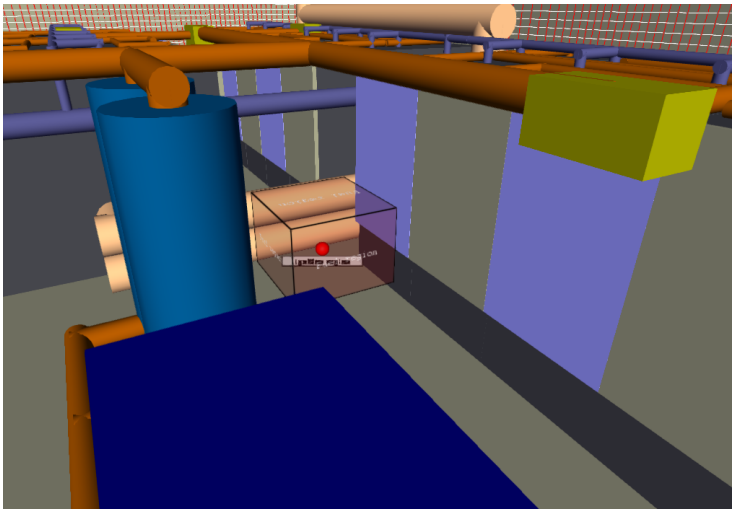

Figure 8.9: The fuel region in scenario 600001.

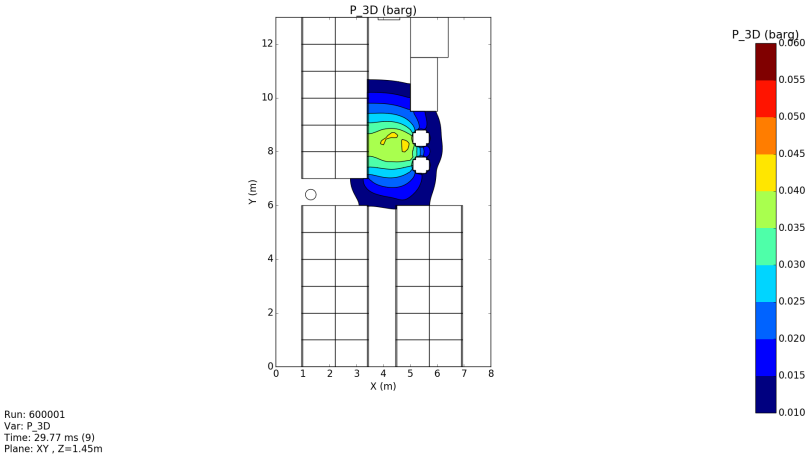

Figure 8.10: Local pressure levels at height 1.45 m in the FCHS 30 ms after ignition in scenario 600001.

The amount of hydrogen available in the reformer was concluded to be small and of no concern. The levels of over-pressure produced by a scenario in which all the available hydrogen in the reformer ignited in a stoichiometric mixture with air are unable to cause harm to people or structures present. In addition, such a scenario is highly unlikely, as a leak would quickly mix with air and only 55% of the hydrogen that can potentially leak will manage to do so, as the pressure difference will even out, as discussed earlier in Chapter 6.

Scenario 600002

Scenario 600002 concerned an eventual buffer tank placed close to the reformer units. The scenario set up was similar to simulation 600001, except for a larger fuel region, as a result of the larger amount of hydrogen which could potentially leak. The size of the fuel region was 4.80 m^3.

The explosion in this scenario was more powerful than in 600001, and the highest pressure levels were reached at 80 ms after ignition. In this case, the maximum pressure registered was 35 kPa, close to the human fatality limit. In contrast to scenario 600001, the pressure reached across the FCHS and the highest levels of over-pressures were experienced in the confined areas between the modules, as demonstrated by Figure 8.11. The pressures experienced by the closest fuel cell modules and FCHS walls are presented in Figure 8.12. The two panels face opposite directions, and so the pressure registered by the fuel cell module is defined by FLACS as negative, but as in the negative direction of the two. The pressures generated by the explosion are too low to cause damage to the surrounding structures. The pressures are also lower than the human fatality limit of 40 kPa.

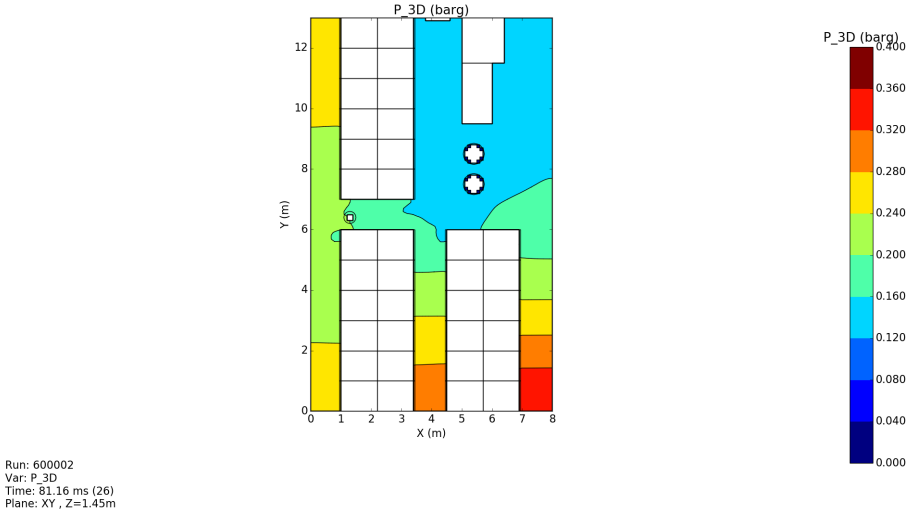

Figure 8.11: Local pressure levels at height 1.45 m in the FCHS 81 ms after ignition during simulation 600002.

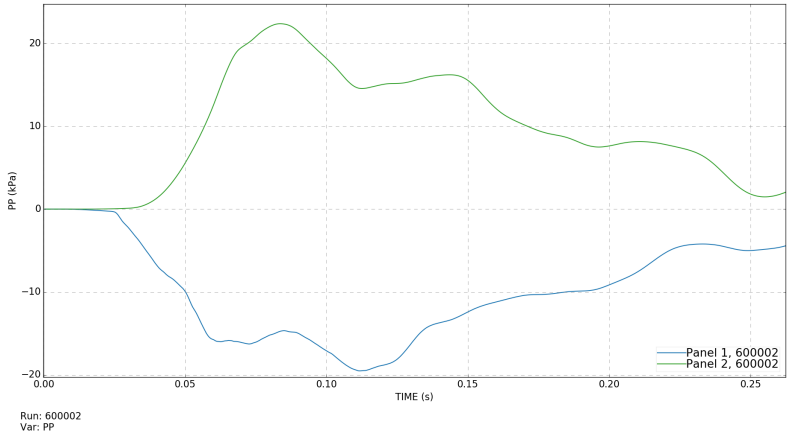

Figure 8.12: Maximum pressures experienced by the fuel cell modules (blue) and FCHS walls (green) closest to the explosion.

The over-pressures of the explosion in scenario 600002 came close to lethal levels. In reality, only 55% of the hydrogen would manage to leak and stoichiometric mixtures would only exist in small volumes and for short periods of time. A leak and following ignition would therefore not be able to generate as high pressures. The situation was concluded to be safe.

Scenarios 600003 and 600004

To assert that the situation in Scenario 600002 is safe and to demonstrate the behaviour of a hydrogen leak, scenarios 600003 and 600004 were set up to respectively model a 1% and a 10% leak from the buffer tank connection. The tank contained 2.8 m^3 of hydrogen (2/3) and steam (1/3) at 850 K and 2.2 bar. Scenario 600003 considered a hole diameter of 1 cm and scenario 600004 a hole diameter of 3.2 cm. The grid was in the FCHS part closest to the leak set to 0.2 m in the X and Y directions, and 0.1 m in the Z direction. The leak initiated after 10 s, to allow the fans to establish air flows in the area. An illustration of the leak is given in Figure 8.13.

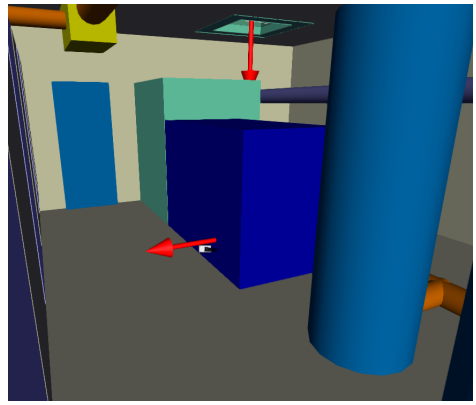

Figure 8.13: The setup for simulation 600003 and 600004. The arrow represents the location of the hydrogen-steam leak. The arrow in the back represents the air coming from the fan units.

Flammable volumes did not develop following the leak from simulation 600003. Figure 8.14 presents the concentration levels close to the leak. The maximum gas concentrations close to the leak remained below 1%. Figure 8.15 presents the gas concentration levels in the same area but for scenario 600004. The concentrations following the leak were higher in the latter scenario, but remained mostly below 3% and below the LFL of hydrogen.

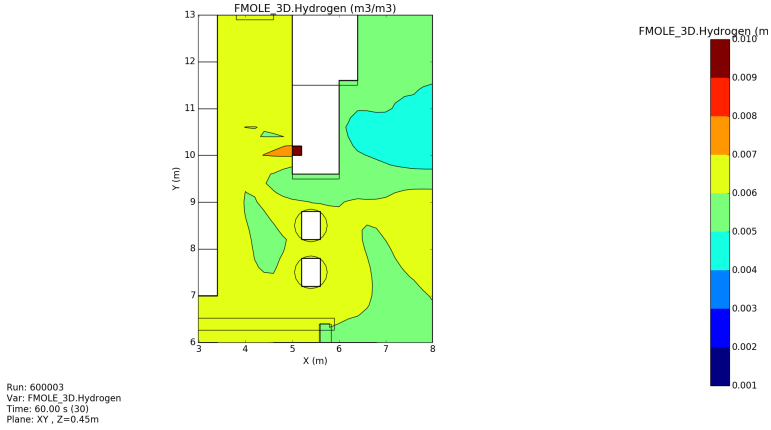

Figure 8.14: The concentration levels local to the leak in simulation 600003. Given at height 0.45 m and at 50 s after the leak initiated.

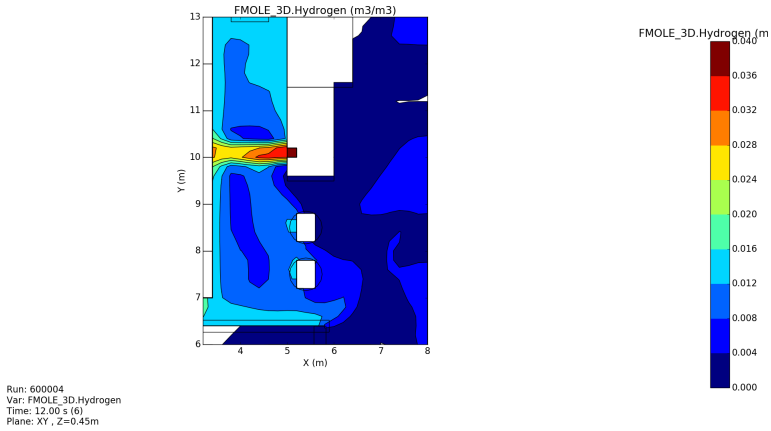

Figure 8.15: The concentration levels local to the leak in simulation 600004. Given at height 0.45 m and at 2 s after the leak initiated.

For hydrogen explosions to pose a major risk, concentrations of 4% are not sufficient. Flames propagate downwards at closer to 8%. At concentrations below 8%, the ignition would cause a fire that quickly would rise towards the roof, but it would not be able to propagate downwards, remaining local. In scenarios 600003 and 600004, all of the hydrogen in the buffer tank was assumed to leak, while in reality only 55% would manage to do so and the gas concentration levels would be even lower. The potential leaks from the buffer tank were concluded not to pose any risk.

8.2.3 Conclusion

Leaks happen frequently in the FCHS, but none of the leaks seem potentially hazardous. Leaks from the large units are also rare, as presented in Table 8.3 below. The buffer tank is assumed a cylinder shape with a diameter of 1.2 m. The probability of ignition is included for the different leaks. The leak frequencies and the ignition probabilities form the basis for the estimated explosion frequencies. The frequencies are very low, and the scenarios in this section demonstrated that failures in which hydrogen leaks and even ignites will not be able to damage surrounding structures. People could be hurt by direct jet flames, but the area is restricted during operation and the room is assumed empty of personnel. From the ignition probabilities below, it also becomes evident that most leaks would mix with the surrounding air without igniting. The room was concluded to be safe from potential hazards.

Table 8.3: Leak frequencies and ignition probabilities for the largest containers of hydrogen in the FCHS.

Unit	Release size [%]	D [mm]	Leak frequency [y^{-1}]	Ignition probability [%]	Explosion frequency [%]
Reformers	0.01	6	2.36e-5	0.1	2.36e-8
	0.1	19	1.96e-5	1.1	2.16e-7
	1	60	1.36e-5	8.2	1.12e-6
	10	190	7.80e-6	28.4	2.22e-6
	100	600	4.18e-6	93.8	3.92e-6
Buffer tank	0.01	12	1.18e-6	0.5	5.90e-9
	0.1	38	9.98e-7	3.7	3.69e-8
	1	120	6.80e-7	17.6	1.20e-6
	10	380	3.90e-7	58.3	2.27e-7
	100	1200	2.09e-7	100	2.09e-7

8.3 Simulations of ethanol spills at the car deck

8.3.1 Procedure

The proposed safety philosophy to limit risk from ethanol spills on the car deck during bunkering were the following:

1. Open atmosphere. Wind and temperature at nighttime will usually prevent gas concentrations from reaching LFL.
2. Two people monitoring the bunkering procedure. One from on-board the ferry and one by the truck.
3. Incline on the car deck, leading eventual spills to the sides and reduces surface area.

The only scenario considered potentially hazardous on the car deck was a spill caused by the rupture of the bunkering hose. A scenario (800001) was set up to demonstrate the limited consequences from this event.

Table 8.4: An overview of the simulations performed.

Car deck Simulation number	Description	Release [g]	Duration [s]	T [K]	Wind [m/s]
800001	80 m^3 ethanol area leak	80/s	900	298	0.5

8.3.2 Simulation results

Scenario 800001

Scenario 800001 is inspired by the discussion in Chapter 6. As was done for the spill scenarios in the FSHS, spills during bunkering were modelled using an area leak from the deck rather than the FLACS pool evaporation model. In 800001, the temperature was set to 25 °C, in order to relate to the empirical evaporation rates of maximum 1 g/m^2s and 0.37 g/m^2s as the average for the first 15 minutes. In this case, the highest rate was used for a 80 m^2 spill (0.080 kg/s). 25 °C can also be considered a maximum temperature at nights along the Norwegian coast.

In the scenario, the leak was initiated after 10 s to allow the wind conditions (0.5 m/s) some time to stabilise. The area was modelled as a square 80 m^2 leak and was placed close to the roof section of the ferry. The scenario is illustrated in Figure 8.16. The grid cells were 0.40 m long in both the X and Y directions. In the Z direction, the grid measured 5.0 cm in length for the first 1.0 m, before stretching out with a maximum factor of 1.1. Monitor points measuring gas concentration were placed as indicated in Figure 8.16.

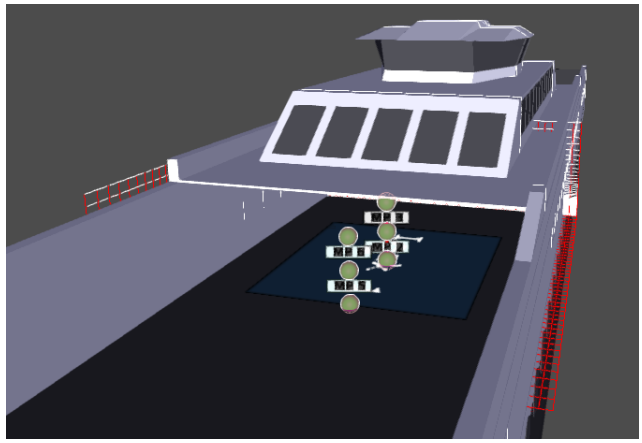

Figure 8.16: An illustration of scenario 800001. The highlighted spheres are monitor points and the square on the deck represents the leak area.

The simulation finished without any problems. The evaporation seemed to reach a steady state with regard to flammable gas volume after 400 s. The equivalent stoichiometric cloud size (Q9) is presented over time in Figure 8.17. The maximum Q9 volume was reached after 140 s. It remained below 15 m^3, distributed across the 80 m^2.

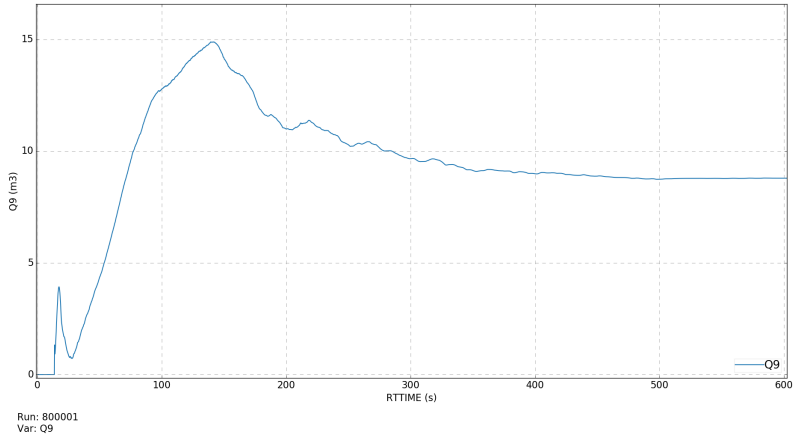

Figure 8.17: The equivalent stoichiometric cloud volume (Q9) volume over time in simulation 800001.

The evaporation rate simulated is the maximum empirically observed at 25 °C, according to Lyulin et al. (Lyulin et al. 2015). As mentioned earlier, the rate would in practise quickly drop to lower levels. The time of 10 s before the leak is stopped is a conservative estimate, as two trained employees are monitoring the situation, assumed able to instantly stop the

process if noticing unusual behaviour. The conditions must also be especially warm and calm for a spill to generate flammable clouds. A single day with 25 °C at nighttime is unlikely along the Norwegian coast for a given year. In addition, the wind must be especially calm, also unusual for the Norwegian coast, and the spill must spread out in a thin layer. The situation simulated was therefore considered an unlikely worst-case scenario.

8.3.3 Conclusion

By conservatively assuming 1 out of 100 days in which the conditions are optimal and a 10% chance that the personnel require 10 s to stop the pump, the estimated annual frequency of a spill causing smaller flammable clouds is 1e-7. This is inside acceptable area for frequencies by a margin. The flammable volumes are not large enough to be of concern either. The bunkering situation was not considered to be potentially hazardous.

Chapter 9

Risk evaluation

The results from the scenarios simulated in Chapter 8 indicate that the risk related to ethanol as fuel on the conceptual ferry can be kept very low.

In the FSHS, the main safety measures of keeping the room cool combined with moderate ventilation would effectively prevent any explosion risk when room and fuel temperature is kept below the flashpoint of ethanol, even if ventilation should fail.If active refrigeration would fail, only low-likelihood scenarios with catastrophic rupture of the tank flooding the FSHS would be of concern, and then also only in the rare situations where the sea holds temperatures well above the ethanol flashpoint. A coarse estimate of the scenario frequency for a significant explosion is of the order 1e-8 per year. Even if this should happen, it is far from sure that the incident will lead to severe consequences with loss of life among crew or passengers. The estimated incident frequency (combination of catastrophic tank rupture, failure of room temperature control, exceptionally warm weather, and ignition of explosive cloud) is about 10^{-4} times lower than proposed tolerance criteria for loss of individual lives. The potential for loss of lives given such an event is further likely limited. Thus, the risk contribution from fuel related incidents in the FSHS is estimated to be insignificant, and several orders of magnitude lower than the risk acceptance criteria discussed for crew and passengers.

In the FCHS, the amount of hydrogen available to leak would be much too low to lead to powerful explosions that would be a concern for the integrity of the walls, even if the entire buffer tank would leak. For most leak scenarios, leak rates will be low and gas would get diluted to non-flammable concentration in the FCHS. Only large or catastrophic leaks from a buffer tank would have potential to generate explosive clouds that could give some pressure build-up inside the FCHS, still the energy would be much too low to threaten the integrity of the FCHS. The event frequency for such incidents is also very low, around 1e-7. Whether local explosions inside the SOFC fuel cells may be possible is unclear, but available energy is very low and no significant damage would result. No risk contribution to people outside the FCHS is therefore assumed.

Spills at the car deck during bunkering, would have a potential to generate flammable atmospheres on very warm and calm days. Any wind or movement of air, which would normally be generated at very warm days, should however be enough to prevent generation of significant flammable clouds. Spill during bunkering should further be discovered quickly and stopped by the people overseeing the bunkering operation. If a flammable cloud would form above the deck, there could be a flash-fire risk to people, but no potential for explosion pressures. Event frequency was estimated to 1e-7 at most. As the bunkering situation takes place at port at night with only essential people present, no risk to passengers and very limited risk to crew should be assumed.

If placed in a risk matrix as described in Chapter 4 on methodology, all the potentially hazardous events related to the fuel systems would belong to the green zone both related to expected crew fatality rates and passenger safety. The proposed ethanol based fuel system, including the sorption-enhanced system for hydrogen generation, should not pose any risk to passengers travelling with the ferry, and the IMO targets of annual fatality rates of 1e-5 or lower should be possible to meet. For members of the crew, the safety measures related to fuel systems are concluded to prevent potential hazardous situations to a degree that should make it possible to satisfy the IMO targets of annual fatality rates of 1e-4 or lower.

Chapter 10

Discussion on alternative fuels and safety

Results have been obtained from a safety evaluation of a concept ethanol-based double-ended ferry. In this chapter, the results for ethanol are discussed relative to presumed results for some of the other fuels discussed in Chapter 3.3. The fuels discussed are hydrogen, ammonia and LNG, and the discussion centres on the aspects of operation studied in the present work, namely fuel storage, fuel application and bunkering.

10.1 Hydrogen

10.1.1 Fuel storage

Hydrogen is in pure form generally stored either pressurised as gas, cryogenically as liquid or in solid metal hydrides (Abe et al. 2019). All of these forms of storage require specialised storage tanks. In theory, hydrogen maintains a high gravimetric energy density, but in practise, this benefit of hydrogen will disappear once stored in tanks. The hydrogen storage and tank connections represent the primary safety challenge with large amounts of hydrogen that can leak at significant leak rates. Due to the high propensity for hydrogen to leak, the wide flammability range, the low ignition energy and the high reactivity, a main focus on a hydrogen vessel is to prevent any possibility for large, uncontrolled releases or significant accumulation of hydrogen gas that can lead to explosions with severe consequences.

10.1.2 Fuel application

Downstream of the tank system, the maximum potential hydrogen flows and leak rates will be much lower, and with proper safety systems (double containment/piping, ventilation, detection and shut-down systems) the hydrogen explosion risk can be controlled. In many cases explosions can still take place, but energy can be limited and consequences kept very local.

In a hydrogen system, fuel cells would often be utilised as in this thesis, however the low temperature operation of the PEMFCs is a more practical choice if the available hydrogen is sufficiently pure. In this thesis, the SOFCs were chosen due to the synergies from an integrated reformer and SOFC system, both operating at high temperatures, plus that the SOFCs can handle the impurities in the reformer product stream. From the reformer units, the heating requirements would be lower compared to the increased efficiency promised by the SOFCs. For a low-temperature hydrogen system, the higher power density and lower cost of the PEMFC seems to be more appealing. According to the EMSA study on use of fuel cells in shipping, the PEMFCs are given a higher safety rating than the SOFCs due to the low-temperature operation (Tronstad et al. 2017).

10.1.3 Bunkering

The bunkering procedure for hydrogen is dependent on the method of storage. Liquefied hydrogen can be delivered as for LNG, using cryogenic fuel trucks. For metal hydrides and gas storage, hydrogen is delivered compressed, usually from storage bottles or dedicated refuelling stations. Solutions with delivery from LH2 trucks vaporising LH2 into compressed gas also exist.

Safety related to releases of compressed gas refuelling may be the least challenging of the alternatives, as gas will quickly seek upwards when losing momentum after a release. Large releases which are not immediately stopped could still be a concern. Safety concepts implemented at car refuelling stations may be applied. For LH2-releases, the flammable gas cloud may remain denser than air and there may be a need for larger safety zones to ensure safe bunkering (Hansen 2020*a*).

10.2 Ammonia

10.2.1 Fuel storage

Ammonia differs from the other fuels discussed in this thesis in its toxicity. While explosions are seen as the most serious event for systems based on hydrogen, ethanol or LNG, ammonia becomes highly toxic and fatal long before flammable levels are reached. As mentioned earlier, people are incapacitated at concentrations around 0.1%. Short exposure can be fatal at 0.5%, while clouds first become flammable at around 15% (TFI 2010). The high LFL concentration and the very high minimum ignition energy make it unlikely for explosions to happen. If explosions were to happen, the low reactivity/burning velocity and low heat of combustion would seldom represent a serious hazard, neither to people nor to structures. Toxic exposure to people would thus be the major concern when handling ammonia.

Ammonia is stored as a liquid, either cooled or pressurised, or a combination of these. Ammonia has a boiling point at about -33.4 °C, and local cooling systems are more straightforward than with hydrogen or LNG, which are both cryogenic gases. Ammonia can therefore avoid boil-off challenges. The choice of storage method is important with regard to safety. Pressurised storage will generate a flashing spray ammonia when leaks occur, generating ammonia droplets which evaporate when mixed in air. As these evaporate in the air, the temperature of the surrounding air will drop towards -70 °C and cause the gas mixture to become denser than ambient air and remain close to the ground rather than lift towards the roof as would be seen for gaseous ammonia evaporating from refrigerated storage pool spill. If ventilated to a gas mast on a vessel, the ammonia released from compressed storage may fall onto deck in low winds, while the ammonia evaporating from a pool would rise. The process is described in a review by Griffiths et al. published in 1982 (Griffiths & Kaiser 1982). According to Olav R Hansen, the same behaviour can be observed with leaks of liquefied hydrogen (Hansen 2020*a*,*b*). Both release rates and evaporation rates will be much lower from a refrigerate storage pool spill. The cooled ammonia storage should therefore be a highly favourable option with regard to safety.

10.2.2 Fuel application

Presently, the ICE is the most straightforward way of utilising ammonia as a fuel. Compared to the fuel cells in the system of the present thesis, ICE units will have a higher energy density and require less space. As mentioned in Chapter 3.3, ammonia fuelled to ICEs is often mixed with a secondary fuel to ensure combustion. Hydrogen is one of the standard alternatives as secondary fuel. Such a solution would require additional hydrogen storage or handling, increasing the risk associated with the system. Ammonia slip is a common aspect of ICE application, in addition to NO_x gases forming part of the exhaust stream (Brown 2018*b*). This stream will have to be treated before released to the atmosphere. As also discussed earlier, SCR is a means for converting NO_x and ammonia into nitrogen and water. A variety of catalysts are used for the process, although Cu and Mn are frequently used in the active materials and TiO_2 is a popular support (Damma et al.

2019). While the SCR systems are efficient, they require specially trained personnel and regular service (Melhus et al. 2017).

A coming alternative to the ICE, is application of a direct ammonia SOFC. Such fuel cells are currently being developed and have not yet been applied for maritime applications. In Norway, the Viking Energy vessel of Eidesvik Offshore is intended to be retrofitted with a 2 MW ammonia fuel cells system. The system is aimed operative in 2024 (Stensvold & Jensen 2020, Brown 2020*b*). Direct ammonia high-temperature SOFCs can allow for a similar power density to that of hydrogen fuel cells and would not require the SCR treatment, although technology is not yet commercially mature (Lan & Tao 2014, Zhao et al. 2019, Brown 2018*a*).

10.2.3 Bunkering

Bunkering of ammonia would be similar to the ethanol bunkering process. The fuel truck would require more specialised storage equipment and hose, as ammonia either requires pressurised or cooled storage. A rupture during bunkering of ammonia would be a larger hazard than with ethanol, given the fuel's toxic properties, this in particular applies for pressurised storage for which significant safety zones may be required (Hansen 2020*a*).

10.3 Liquefied natural gas

10.3.1 Fuel storage

As with liquefied hydrogen, LNG requires specialised cryogenic storage tanks. Even though the tanks are well insulated, some heat will leak into the tank and generate boil-off gas, as discussed in Chapter 3.3. For double-ended ferries, the LNG can more reliably be expected to be consumed before boil-off gas becomes an issue.

A main safety challenge with LNG is naturally to prevent major leaks from the fuel storage tank and fuel systems. Accidents including LNG will generally have a higher explosive potential than similar situations with ethanol. LNG leaks will instantly evaporate and produce flammable clouds without the ventilation able to contain the process. The storage tank is normally double walled to prevent uncontrolled leaks, and all tank connections are contained inside a well ventilated tank connection space (TCS). As LNG is much less reactive than hydrogen (however more likely to form flammable clouds than ethanol spills), this TCS concept would normally ensure a sufficient level of safety related to fuel storage and connections.

10.3.2 Fuel application

LNG is a more conventional fuel and has been used in ferries since MF Glutra entered into operation in 2000. LNG is based on carbon, and so CO_2 is emitted from the combustion process. Although LNG emits less CO_2, NO_x or particulates than other petrol fuels, methane slip still represents a challenge. Methane is considered a more potent greenhouse gas than CO_2. In a life-cycle comparison of LNG with other fuels, Bengtsson et al. concluded in 2011 the methane slip to negate the positive effect of lower CO_2 emissions compared to distillate fuels (Bengtsson et al. 2011). LNG has seen increased application in later years, much due to agreement among the members of the IMO to substantially reduce the sulphur emissions from the sector. The acceptable limit for sulphur content changed in 2020 from 3.5% to 0.5% by mass globally, and to 0.1% in dedicated emission control areas (ECAs) (IMO 1973). LNG is by many considered as a transition fuel and will in the longer term not be sufficient to satisfy the emission ambitions of the sector.

The flow rates and gas quantities downstream of the TCS are limited and can be handled safely. Natural gas is usually applied to gas turbines and as discussed in Chapter 3.1, ICE units provide clouds with an ignition source. Some potential for incidents exist, e.g. exhaust pipe explosions due to misfiring of ICEs, but consequences can generally be kept local.

10.3.3 Bunkering

Spills during bunkering of LNG can cause much greater flammable gas clouds than with ethanol, and a certain safety zone will be required. LNG is typically bunkered at a lower

rate than ethanol, at 40 m^3/h. Any significant leak should quickly be noticed by the employees monitoring the process and gas flow stopped.

10.4 Ethanol

Safety should be easier to ensure with ethanol as a fuel than with the other fuels discussed in this chapter. The sorption-enhanced reforming method offers an efficient method of converting ethanol to hydrogen while keeping the amount of hydrogen available low. Ethanol itself evaporates slowly enough for risk to be mitigated by standard safety measures. LNG, hydrogen and ammonia leaks can instantly pose a risk to people by evaporation of flammable or toxic gases, while ethanol will require more time to evaporate, enabling people to evacuate the area if a spill is noticed. The simple storage of ethanol is another advantage over the other fuels. As revealed in Chapter 3.3, the price of bioethanol is high compared to the other fuels discussed, however it may be currently competitive to green ammonia and hydrogen. Electrolysis costs are predicted to fall in the coming years and to remain competitive with these renewable fuels, the ethanol prices should likewise decrease.

Chapter 11

Conclusion

This thesis discussed the potential for using ethanol as a maritime fuel and evaluated the safety aspects of a local ethanol sorption-enhanced reforming system. A double-ended ferry was conceptualised and its power systems were described in detail. The thesis was structured as a standard risk assessment. Consequences from loss of containment (release, dispersion and explosion) were quantified using FLACS, a state of the art CFD code specialised for gas explosion and dispersion studies.

The storage, consumption and bunkering of the fuel were considered in the risk assessment. No scenario evaluated was considered to represent a major risk to either crew or passengers. The slow evaporation rate of ethanol and the low volumes of hydrogen available are highlighted as important factors in reaching this result. In effect, the system risk can be mitigated by standard safety measures.

Sorption-enhanced reforming of ethanol is a novel technology and seems not to have been visualised locally on-board a vessel prior to this thesis. The method can produce hydrogen close to the theoretical yield and the coupling with SOFCs proposed in this thesis is a solution of future potential. The method allows for efficient and low-pressure conversion of ethanol to hydrogen, while limiting the amount of hydrogen that can potentially leak.

An ethanol based system would today need to go through an alternative design process and document safety through risk and consequence modelling as presented in this thesis. Work on rules for ethanol and methanol application as fuels is ongoing, and this work is briefly discussed in this thesis. Once rules are developed, the approval process will be simplified. Some of the solutions proposed in this thesis deviate from the proposed rules and would in any case have to be documented by an alternative design process and risk assessment.

As part of this thesis, ethanol has been defined as a species and to some degree validated for application in FLACS. As the popularity of bioethanol increases, so will the demand for risk assessments concerning the use of ethanol. The configuration of ethanol is a pre-

requisite for the ability to quantify consequences using FLACS. At the present, no other CFD code seem to have defined ethanol as species for explosion purposes.

In the present work, only the safety of the concept ferry was assessed. The economic viability of the sorption-enhanced ethanol system remains to be examined. Ethanol has potential as a safe and efficient carrier of hydrogen, but currently the price of bioethanol seems to acts as a deterrent. An study on the economic viability would be another important part of a complete feasibility evaluation of the concept.

Bibliography

Aarskog, F. G., Hansen, O. R., Strømgren, T. & Ulleberg, Ø. (2020), 'Concept risk assessment of a hydrogen driven high speed passenger ferry', *International Journal of Hydrogen Energy* **45**(2), 1359–1372.

Abe, J. O., Popoola, A. P. I., Ajenifuja, E. & Popoola, O. M. (2019), 'Hydrogen energy, economy and storage: Review and recommendation', *International Journal of Hydrogen Energy* **44**(29), 15072–15086.

Alonso, C. G., Furtado, A. C., Cantão, M. P., dos Santos, O. A. A. & Fernandes-Machado, N. R. C. (2009), 'Reactions over Cu/Nb2o5 catalysts promoted with Pd and Ru during hydrogen production from ethanol', *International Journal of Hydrogen Energy* **34**(8), 3333–3341.

Andersen, I. (2015), 'Ni av de ti mest miljøvennlige skipene i verden er norske', *Teknisk Ukeblad* . Available at `https://www.tu.no/artikler/ni-av-de-ti-mest-miljovennlige-skipene-i-verden-er-norske/223184` [Accessed 21/08/2020].

Arntzen, B. J. (1998), *Modelling of turbulence and combustion for simulation of gas explosions in complex geometries, Thesis for Dr. Ing. Deg.*, Norwegian University of Science and Technology, Division of Applied Mechanics, Thermodynamics and Fluid Dynamics, Trondheim, Norway.

Assael, M. J., Sykioti, E. A., Huber, M. L. & Perkins, R. A. (2014), 'Reference correlation of the thermal conductivity of ethanol from the triple point to 600 K and up to 245 MPa', *Journal of Physical and Chemical Reference Data* **42**(4), 043101.

Assum, T. (1998), Døds- og personskaderisiko i persontransport – foreløpige beregninger, Technical Report 1089/1998, Norwegian Centre for Transport Research, Oslo, Norway.

Astbury, G. R. & Hawksworth, S. J. (2007), 'Spontaneous ignition of hydrogen leaks: A review of postulated mechanisms', *International Journal of Hydrogen Energy* **32**(13), 2178–2185.

Baglione, M. L. (2007), Development of system analysis methodologies and tools for modeling and optimizing vehicle system efficiency. Thesis for Degree of PhD.), Technical report, University of Michigan, Ann Arbor, MI, USA.

Bahar, H., Abdelilah, Y., Briens, F., Daszkiewicz, K., Feuvre, P. L., Kamitatara, H., Rinke, T., Jiménez, G. R. & Cheng, C. (2019), Renewables 2019, Technical Report ISBN 978-92-64-36998-6, International Energy Agency, Paris, France.

Bailly, C. & Juvé, D. (2000), 'Numerical solution of acoustic propagation problems using Linearized Euler Equations', *AIAA Journal* **38**(1), 131–135.

Barrett, S. (2008), 'METHAPU prototypes methanol SOFC for ships', *Fuel Cells Bulletin* **2008**(5), 4–5.

Bellini, E. (2020), 'Green hydrogen economy assessment for US, Europe', *PV Magazine* . Available at `https://www.pv-magazine.com/2020/08/04/green-hydrogen-economy-assessment-for-us-europe/` [Accessed 21/08/2020].

Benedetti, J. A. & Benedetti, R. P. (2003), Understanding fire protection for flammable liquids, Technical report, National Fire Protection Association, Quincy, MA, USA.

Bengtsson, S., Andersson, K. & Fridell, E. (2011), 'A comparative life cycle assessment of marine fuels: Liquefied natural gas and three other fossil fuels', *Journal of Engineering for the Maritime Environment* **225**(2), 97–110.

Birol, F., Morgan, T., Cozzi, L., Emoto, H., Argiri, M., Rech, O., Malyshev, T., Bennaceur, K., Centurelli, R., Chen, M.-X., Dowling, P., Lyons, L., Magne, B., Mullin, C., Öcal, U., Olejarnik, P., Roques, F., Sassi, O. & Sims, R. (2008), World Energy Outlook 2008, Technical Report ISBN 978-92-64-04560-6, International Energy Agency, Paris, France.

Blaalid, G. E. (2010), 'M/F Moldefjord', *Skipsrevyen* . Available at `https://www.skipsrevyen.no/batomtaler/m-f-moldefjord/` [Accessed 21/07/2020].

Blackman, A. & Gahan, L. (2013), *Aylward and Findlay's SI Chemical Data*, John Wiley & Sons Australia Ltd, Hoboken, NJ, USA.

Blikom, L. P. (2012), 'Status and way forward for LNG as a maritime fuel', *Australian Journal of Maritime & Ocean Affairs* **4**(3), 99–102.

Bloom Energy (2019), Energy Server 5 Product Datasheet, Technical Report 1011392, Bloom Energy, San Jose, CA, USA.

BQ (2015), 'Exploding lead acid batteries', *Business Queensland. Mines safety bulletin* (150). Available at `https://www.taxpayer.net/energy-natural-resources/federal-subsidies-for-corn-ethanol-and-other-corn-based-biofuels/` [Accessed 21/08/2020].

Bragin, M. V. & Molkov, V. V. (2011), 'Physics of spontaneous ignition of high-pressure hydrogen release and transition to jet fire', *International Journal of Hydrogen Energy* **36**(3), 2589–2596.

Brooks, M. R. & Crowl, D. A. (2007), 'Flammability envelopes for methanol, ethanol, acetonitrile and toluene', *Journal of Loss Prevention in the Process Industries* **20**(2), 144–150.

Brown, T. (2018*a*), 'Ammonia for Fuel Cells: A literature review', *Ammonia Energy Association* . Available at https://www.ammoniaenergy.org/articles/ammonia-for-fuel-cells-a-literature-review/ [Accessed 24/08/2020].

Brown, T. (2018*b*), 'Ammonia for power: A literature review', *Ammonia Energy Association* . Available at https://www.ammoniaenergy.org/articles/ammonia-for-power-a-literature-review/ [Accessed 17/08/2020].

Brown, T. (2019*a*), 'The cost of hydrogen: Platts launches hydrogen price assessment', *Ammonia Energy Association* . Available at https://www.ammoniaenergy.org/articles/the-cost-of-hydrogen-platts-launches-hydrogen-price-assessment/ [Accessed 27/06/2020].

Brown, T. (2019*b*), 'Gigawatt-scale electrolyzer manufacturing and deployment', *Ammonia Energy Association* . Available at https://www.ammoniaenergy.org/articles/gigawatt-scale-electrolyzer-manufacturing-and-deployment/ [Accessed 03/08/2020].

Brown, T. (2020*a*), 'Industry report sees multi-billion ton market for green ammonia', *Ammonia Energy Association* . Available at https://www.ammoniaenergy.org/articles/industry-report-sees-multi-billion-ton-market-for-green-ammonia/ [Accessed 03/08/2020].

Brown, T. (2020*b*), 'Viking Energy to be retrofit for ammonia fuel in 2024', *Ammonia Energy Association* . Available at https://www.ammoniaenergy.org/articles/viking-energy-to-be-retrofit-for-ammonia-fuel-in-2024/ [Accessed 17/08/2020].

Brunborg, I. (2019), 'Hellesylt Hydrogen Hub får 37,6 millioner fra Enova', *E24* . Available at http://min.e24.no/hellesylt-hydrogen-hub-far-37-6-millioner-fra-enova/a/Qo2RzR [Accessed 31/07/2020].

Brzezinska, D. (2018), 'Experimental evaluation of hydrogen explosion hazards in industrial battery rooms', *SFPE Europe* (9). Available at https://www.sfpe.org/page/Issue9Feature4/Experimental-Evaluation-of-Hydrogen-Explosion-Hazards-in-Industrial-Ba.html [Accessed 21/07/2020].

BU (2017), 'What causes Li-ion to die?', *Battery University: Learn About Batteries* (BU-808b). Available at https://batteryuniversity.com/index.php/learn/article/bu_808b_what_causes_li_ion_to_die [Accessed 14/08/2020].

Buschman, C. H. (1980), Richtlinien statische elektrizität, Technical report, Berufsgenossenschaften, Bonn, Germany.

Caton, J. A. (2017), 'Maximum efficiencies for internal combustion engines: Thermodynamic limitations', *International Journal of Engine Research* **19**(10), 1005–1023.

Cerdá-Moreno, C., Costa-Serra, J. F. D. & Chica, A. (2019), 'Co and La supported on Zn-hydrotalcite-derived material as efficient catalyst for ethanol steam reforming', *International Journal of Hydrogen Energy* **44**(25), 12685–12692.

CFDO (2020*a*), 'Favre averaged Navier-Stokes equations', *CFD-Online Wiki* . Available at https://www.cfd-online.com/Wiki/Favre_averaged_Navier-Stokes_equations [Accessed 11/08/2020].

CFDO (2020*b*), 'K-epsilon models', *CFD-Online Wiki* . Available at https://www.cfd-online.com/Wiki/K-epsilon_models [Accessed 11/08/2020].

CFDO (2020*c*), 'Navier-Stokes equations', *CFD-Online Wiki* . Available at https://www.cfd-online.com/Wiki/Navier-Stokes_equations [Accessed 10/08/2020].

Chase, M. W. (1998), 'NIST-JANAF themochemical tables, Fourth edition', *Journal of Physical and Chemical Reference Data* **Monograph 9**, 1–1951.

Chevron (2010), Safety data sheet distillate marine gas oil (DMA), Technical Report 01-2119484664-27-0052, Chevron Ltd., London, England, UK.

Chilcott, R. P. (2006), Compendium of chemical hazards: Diesel, Technical report, Health Protection Agency, UK, London, England, UK.

Chiu, C.-H. (2008), 'History of the development of LNG technology', *AIChE Annual Conference* .

Chong, C. T. & Hochgreb, S. (2011), 'Measurements of laminar flame speeds of liquid fuels: Jet-A1, diesel, palm methyl esters and blends using particle imaging velocimetry (PIV)', *Proceedings of the Combustion Institute* **33**(1), 979–986.

Chun, K. W. & Davison, R. R. (1972), 'Thermodynamic properties of binary mixtures of triethylamine with methyl and ethyl alcohol', *Journal of Chemical & Engineering Data* **17**, 307–310.

Colonna, G. R., ed. (2010), *Fire Protection Guide to Hazardous Materials. 14th edition*, National Fire Protection Association, Quincy, MA, USA.

Contreras, J. L., Salmones, J., Colín-Luna, J. A., Nuño, L., Quintana, B., Córdova, I., Zeifert, B., Tapia, C. & Fuentes, G. A. (2014), 'Catalysts for H2 production using the ethanol steam reforming (a review)', *International Journal of Hydrogen Energy* **39**(33), 18835–18853.

Coronado, C. J. R., Carvalho, J. A., Andrade, J. C., Cortez, E. V., Carvalho, F. S., Santos, J. C. & Mendiburu, A. Z. (2012), 'Flammability limits: A review with emphasis on ethanol for aeronautical applications and description of the experimental procedure', *Journal of Hazardous Materials* **241-242**, 32–54.

Cottrell, W. D. (2011), 'Comparison of ferry boat and highway bridge energy use', *Energies* **4**, 239–253.

CSB (2010), Investigation report. Catastrophic rupture of heat exchanger (Seven fatalities), Technical Report 2010-08-I-WA, US Chemical Safety and Hazard Investigation Board, Washington, DC, USA.

Cui, G., Li, Z., Yang, C., Zhou, Z. & Li, J. (2016), 'Experimental study of minimum ignition energy of methane–air mixtures at low temperatures and elevated pressures', *Energy Fuels* **30**(8), 6738–6744.

da Silva, A. L. M., den Breejen, J. P., Mattos, L. V., Bitter, J. H., de Jong, K. P. & Noronha, F. B. (2009), 'Cobalt particle size effects on catalytic performance for ethanol steam reforming – Smaller is better', *Journal of Catalysis* **318**, 67–74.

Dahoe, A. E. (2005), 'Laminar burning velocities of hydrogen–air mixtures from closed vessel gas explosions', *Journal of Loss Prevention in the Process Industries* **18**, 152–166.

Damma, D., Ettireddy, P. R., Reddy, B. M. & Smirniotis, P. G. (2019), 'A review of low temperature NH3-SCR for removal of NOx', *Catalysts* **9**(4), 349.

Date, A. W. (2011), *Analytic Combustion*, Cambridge University Press, Cambridge, England, UK.

DNV GL (2020), Current price development oil and gas, Technical report, DNV GL, Oslo, Norway. Available at `https://www.dnvgl.com/maritime/lng/current-price-development-oil-and-gas.html` [Accessed 08/06/2020].

Donati, G. & Paludetto, R. (1997), 'Scale up of chemical reactors', *Catalysis Today* **34**(17), 483–533.

Dong, C., ZHOU, Q., ZHANG, X., ZHAO, Q., XU, T. & HUI, S. (2010), 'Experimental study on the laminar flame speed of hydrogen/ natural gas/air mixtures', *Frontiers of Chemical Engineering in China* **4**, 417–422.

Donnez, P. (2007), *ESSENTIALS OF RESERVOIR ENGINEERING. VOL. 1*, Editions Technip, Paris, France.

Dorofeev, S. B., Sidorov, V. P., Efimenko, A. A., Kochurko, A. S., Kuznetsov, M. S., Chaivanov, B. B., Matsukov, D. I., Pereverzev, A. K. & Avenyan, V. A. (1995), 'Fireballs from deflagration and detonation of heterogeneous fuel-rich clouds', *Fire Safety Journal* **25**(4), 323–336.

Dou, B., Zhang, H., Cui, G., Wang, Z., Jiang, B., Wang, K., Chen, H. & Xu, Y. (2018), 'Hydrogen production by sorption-enhanced chemical looping steam reforming of ethanol in an alternating fixed-bed reactor: Sorbent to catalyst ratio dependencies', *Energy Conversion and Management* **155**, 243–252.

EB (2020), 'Natural gas', Online database. Encyclopædia Britannica. Available at `https://www.britannica.com/science/natural-gas/Composition-and-properties-of-natural-gas` [Accessed 21/08/2020].

EC (2019*a*), The European Green Deal, Technical Report 52019DC0640, EU European Comission, Brussels, Belgium.

EC (2019*b*), Going climate-neutral by 2050. a strategic long-term vision for a prosperous, modern, competitive and climate-neutral EU economy, Technical Report ISBN 978-92-76-02037-0, EU European Comission, Brussels, Belgium.

ECHA (2020*a*), 'Ethanol', Online database. European Chemicals Agency. Available at `https://echa.europa.eu/registration-dossier/-/registered-dossier/16105/1` [Accessed 03/08/2020].

ECHA (2020*b*), 'Methanol', Online database. European Chemicals Agency. Available at `https://echa.europa.eu/registration-dossier/-/registered-dossier/15569/1` [Accessed 03/08/2020].

EI (2020), Sepuran® N2, membrane technology for efficient on-site nitrogen generation, Technical report, Evonik Industries, Schorfling, Austria.

EIA (2016), 'Biofuels production database', Online database. US Energy Information Administration. Available at `https://www.eia.gov/international/data/world/biofuels/biofuels-production` [Accessed 12/05/2020].

Einang, P. M. & Haavik, K. M. (2000), The Norwegian LNG Ferry, Technical Report A-095 NGV, SINTEF, Trondheim, Norway.

Ellis, J. & Tanneberger, K. (2015), Study on the use of ethyl and methyl alcohol as alternative fuels in shipping, Technical Report 20151204.5, Lloyd's Register; SSPA Sweden, Goteborg, Sweden.

Essaki, K., Muramatsu, T. & Kato, M. (2008), 'Effect of equilibrium-shift in the case of using lithium silicate pellets in ethanol steam reforming', *International Journal of Hydrogen Energy* **33**(22), 6612–6618.

ET (2008), Gases - velocity of sound, Technical report, Engineering ToolBox, Online. Available at: `https://www.engineeringtoolbox.com/speed-sound-gases-d_1160.html` [Accessed 18/07/2020].

ET (2018), Hydrogen - Density and Specific Weight, Technical report, Engineering ToolBox, Online. Available at: https://www.engineeringtoolbox.com/hydrogen-H2-density-specific-weight-temperature-pressure-d_2044.html [Accessed 21/08/2020].

Etienne, X., Trujillo-Barrera, A. & Wiggins, S. (2016), 'Price and volatility transmissions between natural gas, fertilizer, and corn markets', *Agricultural Finance Review* **76**(1), 151–171.

Eurostat (2018), Accidents at work statistics. eurostat statistics explained, Technical report, EU European Comission. Eurostat, Luxembourg. Available at: https://ec.europa.eu/eurostat/statistics-explained/index.php/Accidents_at_work_statistics [Accessed 11/7/20].

EVD (2020), 'Useable battery capacity of full electric vehicles', Online database. Electric Vehicle Database. Available at https://ev-database.org/cheatsheet/useable-battery-capacity-electric-car [Accessed 21/07/2020].

Faanes, A. & Skogestad, S. (2003), 'Buffer tank design for acceptable control performance', *Industrial & Engineering Chemistry Research* **42**(10), 2198–2208.

FAO (2019), World fertilizer trends and outlook to 2022, Technical Report ISBN 978-92-5-131894-2, UN Food and Agriculture Organization, Rome, Italy.

Faramawy, S., Zaki, T. & Sakra, A. A.-E. (2016), 'Natural gas origin, composition, and processing: A review', *Journal of Natural Gas Science and Engineering* **34**, 34–54.

Fermoso, J., He, L. & Chen, D. (2018), 'Sorption enhanced steam reforming (SESR): A direct route towards efficient hydrogen production from biomass-derived compounds', *Journal of Chemical Technology and Biotechnology* **87**(10), 1367–1374.

Fjeldheim, N. (2012), Safety data sheet natural gas, refrigerated with high methane content, Technical report, Gasnor, Avaldsnes, Norway.

Forsman, B. & Algell, J. (2013), Pilot study on the use of LNG as a fuel for a high speed passenger ship from the port of spain ferry terminal in trinidad and tobago, Technical Report RE20136645-01-00-A, SSPA, Gotheborg, Sweden.

Fossan, I. & Sæbø, A. O. (2016), Process leak for offshore installations frequency assessment model - PLOFAM(2), Technical Report 107566/R1, Statoil; Lloyd's Register; DNV GL; SAFETEC; Lilleaker Consulting, Stavanger, Norway.

Fu, D., Lu, J. F., Bao, T. Z. & Li, Y. G. (2000), 'Investigation of surface tension and interfacial tension in surfactant solutions by SAFT', *Industrial & Engineering Chemistry Research* **39**, 320–327.

Gexcon (2019), FLACS v10.9 User Manual, Technical report, Gexcon AS, Bergen, Norway.

Gill, S. S., Chatha, G. S., Tsolakis, A., Golunski, S. E. & York, A. P. E. (2012), 'Assessing the effects of partially decarbonising a diesel engine by co-fuelling with dissociated ammonia', *International Journal of Hydrogen Energy* **37**(7), 6074–6083.

Giuliano, A. D. & Gallucci, K. (2018), 'Sorption enhanced steam methane reforming based on nickel and calcium looping: A review', *Chemical Engineering and Processing - Process Intensification* **130**, 240–252.

GP (2016), Safety data sheet - diesel fuel, Technical report, Global Partners LP, Waltham, MA, USA.

GPP (2020*a*), 'Diesel prices, liter, 08-jun-2020', Online database. GlobalPetrolPrices.com. Available at `https://www.globalpetrolprices.com/diesel_prices/` [Accessed 15/06/2020].

GPP (2020*b*), 'Ethanol prices, liter, 22-jun-2020', Online database. GlobalPetrolPrices.com. Available at `https://www.globalpetrolprices.com/ethanol_prices/` [Accessed 27/06/2020].

Griffiths, R. F. & Kaiser, G. D. (1982), 'Production of dense gas mixtures from ammonia releases - A review', *Journal of Hazardous Materials* **6**, 197–212.

Gulder, O. L. (1982), 'Laminar burning velocities of methanol, ethanol and isooctane-air mixtures', *Nineteenth symposium (international) on combustion* **19**(1), 275–281.

Gül, T., Abergel, T., Bunsen, T., Gorner, M., Leduc, P., Pal, S., Paoli, L., Raghavan, S., Tattini, J., Teter, J., Wachche, S., Widell, P.-A., Ambrose, H., Dunn, J. & Slattery, M. (2020), Global EV Outlook, Technical report, International Energy Agency, Paris, France.

Gül, T., Turk, D., Bennett, S. & Remme, U. (2019), The future of hydrogen, Technical report, International Energy Agency, Paris, France.

Han, X., Wang, Y., Zhang, Y., Yu, Y. & He, H. (2017), 'Hydrogen production from oxidative steam reforming of ethanol over Ir catalysts supported on Ce–La solid solution', *International Journal of Hydrogen Energy* **42**(16), 11177–11186.

Hansen, O. R. (2018), GKP7H2 high speed passenger ferry concept risk assessment. MoZEES project, Technical Report 106575/R1, Lloyd's Register, Oslo, Norway.

Hansen, O. R. (2020*a*), Hydrogen and Ammonia Infrastructure, Technical Report PRJ11100256122r1/R0, Lloyd's Register, Bergen, Norway.

Hansen, O. R. (2020*b*), 'Liquid hydrogen releases show dense gas behavior', *International Journal of Hydrogen Energy* **45**(2), 1343–1358.

Hansen, O. R., Gavelli, F., Davis, S. G. & Middha, P. (2013), 'Equivalent cloud methods used for explosion risk and consequence studies', *Journal of Loss Prevention in the Process Industries* **26**, 511–527.

Hansen, O. R. & Johnson, D. M. (2020), 'Improved far-field blast predictions from fast deflagrations, DDTs and detonations of vapour clouds using FLACS CFD', *Journal of Loss Prevention in the Process Industries* **35**, 293–306.

Haryanto, A., Fernando, S., Murali, N. & Adhikari, S. (2005), 'Current status of hydrogen production techniques by steam reforming of ethanol: A review', *Energy and Fuels* **19**(5), 2098–2106.

Hayakawa, A., Goto, T., Mimoto, R., Arakawa, Y., Kudo, T. & Kobayashi, H. (2015), 'Laminar burning velocity and Markstein length of ammonia/air premixed flames at various pressures', *Fuel* **159**, 98–106.

Haynes, W. M. (1973), 'Viscosity of saturated liquid methane', *Physica* **70**, 410–412.

Haynes, W. M., ed. (2015), *CRC Handbook of Chemistry and Physics. 95th Edition*, CRC Press LLC, Boca Raton, FL, USA.

HC (2020), Path to hydrogen competitiveness: A cost perspective, Technical report, Hydrogen Council, Brussels, Belgium.

He, L., Berntsen, H. & Chen, D. (2010), 'Approaching sustainable H2 production: Sorption enhanced steam reforming of ethanol', *Journal of Physical Chemistry A* **114**(11), 3834–3844.

Hisken, H. (2018), *Investigation of instability and turbulence effects on gas explosions: Experiments and modelling, Thesis for Degree of PhD.*, University of Bergen, Bergen, Norway.

Hossain, N., Zaini, J. & Mahlia, T. M. I. (2019), 'Life cycle assessment, energy balance and sensitivity analysis of bioethanol production from microalgae in a tropical country', *Renewable and Sustainable Energy Reviews* **115**(109371).

HSDB (2020*a*), 'Ethanol', Online database. Hazardous Substances Data Bank. Available at `https://pubchem.ncbi.nlm.nih.gov/source/hsdb/82` [Accessed 25/08/2020].

HSDB (2020*b*), 'Methane', Online database. Hazardous Substances Data Bank. Available at `https://pubchem.ncbi.nlm.nih.gov/source/hsdb/167` [Accessed 25/08/2020].

HSE (2017), Failure rate and event data for use within risk assessments (06/11/17), Technical Report PCAG chp_6K Version 14, Health and Safety Executive CEMHD5, London, England, UK.

Huang, Y., Xie, L., Lu, C.-B., An, G.-J., Xiong, C.-H. & Zhu, Y.-Z. (2015), 'Experimental study on minimum ignition energy of diesel-air cloud', *Chinese Journal of High Pressure Physics* **29**(2), 149–154.

IEA (2019), Marine bunkers product demand, 2015-2024, Technical report, International Energy Agency, Paris, France. Available at https://www.iea.org/data-and-statistics/charts/marine-bunkers-product-demand-2015-2024 [Accessed 18/07/2020].

ILO (2017), ICSC Ethanol (anhydrous), Technical Report 0044, UN WHO International Labour Organisation, Geneve, Switzerland.

IMO (1973), International convention for the prevention of pollution from ships (MARPOL), Technical report, International Maritime Organisation, London, UK.

IMO (1974), International convention for the safety of life at sea, Technical report, International Maritime Organisation, London, UK.

IMO (2015), International code of safety for ship using gases or other low-flashpoint fuels, Technical Report MSC.391(95), International Maritime Organisation, London, UK.

IMO (2018*a*), Adoption of the initial IMO strategy on reduction of GHG emissions from ships and existing imo activity related to reducing GHG emissions in the shipping sector, Technical Report MEPC.304(72), International Maritime Organisation, London, UK.

IMO (2018*b*), Revised guidelines for formal safety assessment (FSA) for use in the IMO rule-making process, Technical Report MSC-MEPC.2/Circ.12, International Maritime Organisation, London, England, UK.

IMO (2019), 'Sub-committee on Carriage of Cargoes and Containers, 6th session (CCC 6) 9-13 September 2019', *International Maritime Organisation: Meeting Summaries* . Available at http://www.imo.org/en/MediaCentre/MeetingSummaries/CCC/Pages/CCC-6th-session.aspx [Accessed 30/06/2020].

IOM (2014), *Gulf War and Health, Volume 9. Long-Term Effects of Blast Exposures*, Institute of Medicine; Board on the Health of Select Populations; Committee on Gulf War and Health, Washington, DC, USA.

Iruretagoyena, D., Hellgardt, K. & Chadwick, D. (2018), 'Towards autothermal hydrogen production by sorption-enhanced water gas shift and methanol reforming: A thermodynamic analysis', *International Journal of Hydrogen Energy* **43**(9), 4211–4222.

ISO (2018), ISO 31000:2018 Risk management — Guidelines, Technical report, International Organization for Standardization. TC 262, Geneva, Switzerland.

Jafari, M. J., Mohammadfam, I. & Zarei, E. (2014), 'Analysis and simulation of severe accidents in a steam methane reforming plant', *International Journal of Occupational Hygiene* **6**(3), 120–130.

Janardhanan, V. M., Heuveline, V. & Deutschmann, O. (2007), 'Performance analysis of a SOFC under direct internal reforming conditions', *Chemical Engineering Journal* **172**, 296–307.

Jiang, Q., Chen, Z., Tong, J., Yang, M., Jiang, Z. & Li, C. (2017), 'Direct thermolysis of CO2 into CO and O2', *Chemical Communications* **53**(6), 1188–1191.

Johnsen, K., Ryu, J. H., Grace, J. R. & Lim, C. J. (2006), 'Sorption-enhanced steam reforming of methane in a fluidized bed reactor with dolomite as CO2-acceptor', *Chemical Engineering Science* **61**(4), 1195–1202.

Josdal, A. (2019), Evalueringsrapport, Brann i MF Ytterøyningen, Technical report, Kvinnherad brann- og redning, Vest brann- og redningsregion and Bergen brannvesen, Bergen, Norway.

Kaviraj, A., Bhunia, F. & Saha, N. C. (2004), 'Toxicity of methanol to fish, crustacean, oligochaete worm, and aquatic ecosystem', *International Journal of Toxicology* **23**(1), 55–63.

Kilner, J. A., Skinner, S. J., Irvine, S. J. C. & Edwards, P. P., eds (2012), *Functional Materials for Sustainable Energy Applications*, Woodhead Publishing Series in Energy, Woodhead Publishing Limited, Sawston, England, UK.

Klingner, M. (2005), FELICITAS fuel-cell powertrains and clustering in heavy-duty transports, Technical report, Fraunhofer Institut Verkehrs und Infrastruktursysteme, Dresden, Germany.

Knottenbelt, C. (2002), 'Mossgas "gas-to-liquid" diesel fuels—an environmentally friendly option', *Catalysis Today* **71**(3-4), 437–445.

Knudsen, Ø., Stokmo, T. & Spangelo, J. Ø. (2017), Rapport til Mongstad Eiendomsselskap AS. "anlegg for lagring og levering av MGO, metanol, glykoler m.v.", Technical Report Gexcon-16-F100024-RA-1. R3., Gexcon, Bergen, Norway.

Konnov, A. A., Meuwissen, R. J. & de Goey, L. P. H. (2011), 'The temperature dependence of the laminar burning velocity of ethanol flames', *Proceedings of the combustion institute* **33**(1), 1011–1019.

Kretschmer, C. B. & Wiebe, R. (1949), 'Liquid-vapor equilibrium of ethanol-toluene solutions', *Journal of the American Chemical Society* **71**, 1793–1797.

Kristiansen, A., Pappas, J. & Henriksen, H. (2017), Guidelines for quantitative risk analysis of facilities handling hazardous substances, Technical Report 106535/R1, Lloyd's Register, Oslo, Norway.

Kumar, S., Kwon, H.-T., Choi, K.-H., Cho, J. H., Lim, W. & Moon, I. (2016), 'Current status and future projections of LNG demand and supplies: A global prospective', *Energy Policy* **39**(7), 4097–4104.

LaChance, J., Houf, W., Middleton, B. & Fluer, L. (2008), Analyses to support development of risk-informed separation distances for hydrogen codes and standards, Technical Report SAND2009-0874, Sandia National Laboratories, Albuquerque, NM, USA.

Lan, R. & Tao, S. (2014), 'Ammonia as a suitable fuel for fuel cells', *Frontiers in Energy Research* **2**, 35.

Lanz, A., Heffel, J. & Messer, C. (2001), Hydrogen fuel cell engines. Module 6: Fuel cell engine safety, Technical report, College of the Desert, Palm Desert, CA, USA.

Lapuerta, M., Garcia-Contreras, R., Campos-Fernandez, J. & Dorado, M. P. (2010), 'Stability, lubricity, viscosity, and cold-flow properties of alcohol-diesel blends', *Energy & Fuels* **24**(8), 4497–4502.

Launder, B. E. & Spalding, D. B. (1974), 'The numerical computation of turbulent flows', *Computer Methods in Applied Mechanics and Engineering* **3**, 269–289.

Law, C. K., Makino, A. & Lu, T. F. (2006), 'On the off-stoichiometric peaking of adiabatic flame temperature', *Combustion and flame* **145**(4), 808–819.

Le, L. & Phillips, J. (2015), 'LNG: An emerging transport fuel', *Energy News* **33**(4), 15–17.

Levi, P., Vass, T., Mandova, H. & Gouy, A. (2019), Chemicals, Technical report, International Energy Agency, Paris, France.

Levichev, S. A. (1964), 'Oberflächenspannung, Dichte und Exzessvolumina in binären und ternären Lösungen', *Fiziko-chimiceskie Svojstva Rastvorov* **80**, 219–226.

Li, Q., Cheng, Y. & Huang, Z. (2015), 'Comparative assessment of the explosion characteristics of alcohol-air mixtures', *Journal of Loss Prevention in the Process Industries* **37**, 91–100.

Liao, S. Y., Cheng, Q., Jiang, D. M. & Gao, J. (2005), 'Experimental study of flammability limits of natural gas–air mixture', *Journal of Hazardous Materials* **119**(1-3), 81–84.

Linstrom, P. J. & Mallard, W. G., eds (2020), *NIST Chemistry WebBook, NIST Standard Reference Database Number 69*, National Institute of Standards and Technology, Gaithersburg, MD, USA. Available at `https://doi.org/10.18434/T4D303` [Accessed 17/06/2020].

Liu, X. & Zhang, Q. (2014), 'Influence of initial pressure and temperature on flammability limits of hydrogen-air', *International Journal of Hydrogen Energy* **39**(12), 6774–6782.

LR (2018), Shipright - design and construction. additional design procedures. risk based designs (RBD), Technical report, Lloyd's Register, London, England, UK.

LR (2020), Rules and Regulations for the Classification of Ships, Technical report, Lloyd's Register, London, England, UK.

Luo, M., Yi, Y., Wang, S., Wang, Z., Du, M., Pan, J. & Wang, Q. (2018), 'Review of hydrogen production using chemical-looping technology', *Renewable and Sustainable Energy Reviews* **81**(2), 3186–3214.

Lyulin, Y. V., Feoktistov, D. V., Afanas'ev, I. A., Chachilo, E. S., Kabov, O. A. & Kuznetsov, G. V. (2015), 'Measuring the rate of local evaporation from the liquid surface under the action of gas flow', *Technical Physics Letters* **41**(7), 665–667.

Mamedov, A. A. & Shikhaliev, Y. A. (1972), 'Untersuchung der viskosität von binären ethylbenzen-ethanol- und ethylbenzen-propanol-mischungen in der abhängigkeit von temperatur und konzentration', *Izv. Vyssh. Uchebn. Zaved. Neft Gaz* pp. 63–66.

Martinez, I. (2020), 'Fuel properties', *Combustion* . Available at `http://webserver.dmt.upm.es/~isidoro/` [Accessed 07/06/2020].

Mattos, L. V., Jacobs, G., Davis, B. H. & Noronha, F. B. (2012), 'Production of hydrogen from ethanol: Review of reaction mechanism and catalyst deactivation', *Chemical Reviews* **112**(7), 4094–4123.

Medina, E. & Roberts, R. R. (2013), Methanol safe handling manual, Technical report, METHANOL INSTITUTE, Alexandria, VA, USA.

Melhus, Ø., Bjørn, Haukebø, Reitan, D. R. & Sørheim, H. (2017), Ammoniakkutslipp fra scr-anlegg om bord i fartØy, Technical Report P0401-04 Report V4, Ecoxy, Trondheim, Norway.

Memon, M. Z., Zhao, X., Sikarwar, V. S., Vuppaladadiyam, A. K., Milne, S. J., Brown, A. P., Li, J. & Zhao, M. (2017), 'Alkali metal CO2 sorbents and the resulting metal carbonates: Potential for process intensification of sorption-enhanced steam reforming', *Environmental Science & Technology* **51**(1), 12–27.

Menendez, R. B., Graschinsky, C. & Amadeo, N. E. (2018), 'Sorption-enhanced ethanol steam reforming process in a fixed-bed reactor', *Industrial & Engineering Chemistry Research* **57**(34), 11547–11553.

Meyer, J., Mastin, J. & Pinilla, C. S. (2014), 'Sustainable hydrogen production from biogas using sorption-enhanced reforming', *Energy Procedia* **63**, 6800–6814.

Meyertons, K. (2020), 'Viewpoint: IMO 2020 to have delayed price effect', *Argus blog* . Available at `https://www.argusmedia.com/en/news/2044862-viewpoint-imo-2020-to-have-delayed-price-effect` [Accessed 21/08/2020].

MI (2019), Ammonia market - Growth, trends, and forecast (2020 - 2025), Technical report, Mordor Intelligence, Hyderabad, India.

MI (2020), 'Commodities', Online database. Markets Insider. Available at https://markets.businessinsider.com/commodities [Accessed 21/08/2020].

Middha, P. (2010), *Development, use, and validation of the CFD tool FLACS for hydrogen safety studies*, University of Bergen, Bergen, Norway.

Miret, C., Chazara, P., Montastruc, L., Negny, S. & Domenech, S. (2016), 'Design of bioethanol green supply chain: Comparison between first and second generation biomass concerning economic, environmental and social criteria', *Computers and Chemical Engineering* **85**, 16–35.

Mishchenko, K. P. & Subbotina, V. V. (1967), 'Dampfdruck von ethanol bei temperaturen von 4 bis 46°', *Russian Journal of Applied Chemistry A* **40**, 1156–1159.

Mitu, M. & Brandes, E. (2017), 'Influence of pressure, temperature and vessel volume on explosion characteristics of ethanol/air mixtures in closed spherical vessels', *Fuel* **203**, 460–468.

Morales, G. F., Ehrhart, B. D. & Muna, A. B. (2008), HyRAM V2.0 User Guide, Technical Report SAND2019-8940, Sandia National Laboratories, Albuquerque, NM, USA.

Munuera, L. (2020), Energy storage, Technical report, International Energy Agency, Paris, France.

Muratov, G. N. (1980), 'Oberflächespannung von Benzol und Ethanol', *Russian Journal of Physical Chemistry A* **54**, 2088–2089.

NBV (2018), 'Global LNG fleet set for record year', *Offshore Energy. Navingo BV* . Available at https://www.offshore-energy.biz/global-lng-fleet-set-for-record-year/ [Accessed 30/07/2020].

NIST TRC (1997), Selected values of properties of chemical compounds, Technical report, US Department of Commerce. NIST Thermodynamics Research Center, Boulder, CO, USA.

Njøsen, F. H. (23/01/2020), 'Får 77 Enova-millioner til karbonfangst', *Finansavisen* . Available at https://finansavisen.no/nyheter/industri/2020/07/10/7546491/far-77-enova-millioner-til-karbonfangst [Accessed 19/08/2020].

NYSERDA (2005), Hydrogen fact sheet hydrogen production - steam methane reforming (SMR), Technical report, New York State Energy Research and Development Authority, Albany, NY, USA.

Ogo, S. & Sekine, Y. (2020), 'Recent progress in ethanol steam reforming using non-noble transition metal catalysts: A review', *Fuel Processing Technology* **199**, 106238.

Ogo, S., Shimizu, T., Nakazawa, Y., Mukawa, K., Mukai, D. & Sekine, Y. (2015), 'Steam reforming of ethanol over K promoted Co catalyst', *Applied Catalysis A: General* **495**, 30–38.

OGP (2010), Risk assessment data directory, Technical Report 434, International Association of Oil & Gas Producers, London, England, UK.

O'Neil, M. J., ed. (2013), *The Merck Index - An Encyclopedia of Chemicals, Drugs, and Biologicals. Cambridge*, Royal Society of Chemistry, London, England, UK.

Ono, R., Nifuku, M., Fujiwara, S., Horiguchi, S. & Oda, T. (2007), 'Minimum ignition energy of hydrogen-air mixture: Effects of humidity and spark duration', *Journal of Electrostatics* **65**(2), 87–93.

OSHA (2012), Internal combustion engines as ignition sources. Fact sheet., Technical Report DSG FS-3589-10, US Occupational Safety and Health Administration, Washington, D.C., USA.

Ozkan, G., Şahbudak, B. & Ozkan, G. (2019), 'Effect of molar ratio of water/ethanol on hydrogen selectivity in catalytic production of hydrogen using steam reforming of ethanol', *International Journal of Hydrogen Energy* **44**(20), 9823–9829.

Panton, R. L. (2013), *Incompressible Flow, 4th Edition*, John Wiley & Sons, Hoboken, NJ, USA.

Pawelec, G. (2020), Hydrogen, part of Riviera's Marine Fuels Webinar Week. Hydrogen Europe. Brussels, Belgium.

PDA (2020), Bi-monthly bio-ethanol reference price, crop year 2019-2020, Technical report, Philippines Department of Agriculture. Sugar Regulatory Administration, Quezon City, Philippines.

PEI (2010), 'Gas turbines breaking the 60% efficiency barrier', *Power Engineering International* . Available at `https://web.archive.org/web/20130930233542/http://www.cospp.com/articles/print/volume-11/issue-3/features/gas-turbines-breaking.html` [Accessed 21/07/2020].

Plasmans, J., Donnat, L., de Carvalho, E., Debelle, T., Marechal, B. & Baillou, F. (2013), 'Challenges with the use of CFD for major accident dispersion modelling', *Process Safety Progress* **32**(2), 207–211.

Pratt, J. W. & Klebanoff, L. E. (2016), Feasibility of the SF-BREEZE: A zero-emission, hydrogen fuel cell, high-speed passenger ferry, Technical Report SAND2016-9719, Sandia National Laboratories, Albuquerque, N.M., USA.

Raheem, A., Prinsen, P., Vuppaladadiyam, A. K., Zhao, M. & Luque, R. (2018), 'A review on sustainable microalgae based biofuel and bioenergy production: Recent developments', *Journal of Cleaner Production* **181**, 42–59.

Rastogi, M. & Shrivastava, S. (2017), 'Recent advances in second generation bioethanol production: An insight to pretreatment, saccharification and fermentation processes', *Renewable and Sustainable Energy Reviews* **80**, 330–340.

Rawadieh, S. & Gomes, V. G. (2009), 'Steam reforming for hydrogen generation with in situ adsorptive separation', *International Journal of Hydrogen Energy* **34**(1), 343–355.

Reif, K. (2017), *Diesel Engine Management*, Springer Vieweg, Berlin, Germany.

Reigstad, G. A., Coussy, P., Straus, J., Bordin, C., Jaehnert, S., Størset, S. & Ruff, B. (2019), Hydrogen for Europe, Technical Report 502002187, IFPEN and SINTEF, Trondheim, Norway.

RFA (2020), 'Annual fuel ethanol production database', Online database. Renewable Fuels Association. Available at https://ethanolrfa.org/statistics/annual-ethanol-production/ [Accessed 12/05/2020].

Ritchie, H. & Roser, M. (2014), 'Energy', *Our World in Data* . Available at https://ourworldindata.org/energy [Accessed 07/06/2020].

RIVM (2009), Reference Manual Bevi Risk Assessments, Technical report, National Institute of Public Health and the Environment. RIVM Centre for External Safety, Bilthoven, Netherlands.

Rodriguez-Gomez, A. & Caballero, A. (2015), 'Bimetallic Ni-Co/SBA-15 catalysts for reforming of ethanol: How cobalt modifies the nickel metal phase and product distribution', *Molecular Catalysis* **449**, 122–130.

SA (2017), Safety Data Sheet for Ethyl alcohol, pure. Product Number: E7023, Version 4.12 (Revision Date 07/09/2015), Technical Report ISBN 603-002-00-5, Sigma-Aldrich, Saint-Louis MO, USA. Available at http://www.sigmaaldrich.com/safety-center.html [Accessed 04/06/2020].

Sampson, J. (2020), '$5bn green hydrogen-based ammonia facility to be constructed in Saudi Arabia', *H2View* . Available at https://www.h2-view.com/story/plans-unveiled-for-5bn-green-hydrogen-based-ammonia-production-facility-in-saudi-arabia/ [Accessed 31/07/2020].

Sanches, O. J. & Cardona, C. A. (2007), 'Trends in biotechnological production of fuel ethanol from different feedstocks', *Bioresource Technology* **99**, 5270–5295.

S&B (2020), 'Rotterdam bunker prices', Online database. Ship& Bunker. Available at: https://shipandbunker.com/prices/emea/nwe/nl-rtm-rotterdam#MGO [Accessed 18/07/2020].

Scatchard, G. & Raymond, C. L. (1938), 'Chloroform-ethanol mixtures at 35, 45 and 55°', *Journal of the American Chemical Society* **60**, 1278–1287.

Scatchard, G. & Satkiewicz, F. G. (1964), 'The system ethanol-cyclohexane from 5 to 65°', *Journal of the American Chemical Society* **86**, 130–133.

Sengodan, S., Lan, R., Humphreys, J., Du, D., Xu, W., Wang, H. & Tao, S. (2018), 'Advances in reforming and partial oxidation of hydrocarbons for hydrogen production and fuel cell applications', *Renewable and Sustainable Energy Reviews* **81**(1), 761–780.

Sharma, Y. C., Kumar, A., Prasad, R. & Upadhyay, S. N. (2015), 'Ethanol steam reforming for hydrogen production: Latest and effective catalyst modification strategies to minimize carbonaceous deactivation', *Renewable and Sustainable Energy Reviews* **74**, 89–103.

Shell (2016*a*), Shell LNG outlook 2016, Technical report, Royal Dutch Shell, Haag, The Netherlands.

Shell (2016*b*), Shell LNG outlook 2017, Technical report, Royal Dutch Shell, Haag, The Netherlands.

Shell (2016*c*), Shell LNG outlook 2018, Technical report, Royal Dutch Shell, Haag, The Netherlands.

Shell (2016*d*), Shell LNG outlook 2019, Technical report, Royal Dutch Shell, Haag, The Netherlands.

Shell (2016*e*), Shell LNG outlook 2020, Technical report, Royal Dutch Shell, Haag, The Netherlands.

Sigales, B. (1975), 'How to design reflux drums', *Chemical Engineering Journal* **82**(5), 157–160.

Skarsgård, M. L. (11/05/2020), 'Hydrogenproduksjon til Mongstad', *Finansavisen* . Available at `https://finansavisen.no/nyheter/shipping/2020/05/11/7526423/mongstad-valgt-til-planlagt-hydrogenproduksjon` [Accessed 21/08/2020].

Smeets, M. A. M., Bulsing, P. J., van Rooden, S., Steinmann, R., de Ru, J. A., Ogink, N. W. M., van Thriel, C. & Dalton, P. H. (2007), 'Odor and irritation thresholds for ammonia: A comparison between static and dynamic olfactometry', *Chemical Senses* **32**(1), 11–20.

Smith, R. L. (2001), 'Predicting evaporation rates and times for spills of chemical mixtures', *Annals of Occupational Hygiene* **45**(6), 437–445.

Soave, G. (1972), 'Equilibrium constants from a modified Redlich-Kwong equation of state', *Chemical Engineering Science* **27**(6), 1197–1203.

SSB (2020), 'Trafikkulykker med personskade', Online database. Statistics Norway. Available at `https://www.ssb.no/transport-og-reiseliv/statistikker/vtu/aar` [Accessed 14/07/2020].

Stensvold, T. (2015*a*), 'Denne fergen er revolusjonerende. Men passasjerene merker det knapt', *Teknisk Ukeblad* . Available at https://www.tu.no/artikler/denne-fergen-er-revolusjonerende-men-passasjerene-merker-det-knapt/222522 [Accessed 30/07/2020].

Stensvold, T. (2015*b*), 'Maritim bransje vil ikke skrote LNG-ferger', *Teknisk Ukeblad* . Available at https://www.tu.no/artikler/maritim-bransje-vil-ikke-skrote-lng-ferger/276313 [Accessed 21/08/2020].

Stensvold, T. (2018*a*), 'Kaster ut seks LNG-motorer – inn med batterier og elektromotor', *Teknisk Ukeblad* . Available at https://www.tu.no/artikler/kaster-ut-seks-lng-motorer-inn-med-batterier-og-elektromotor/451484 [Accessed 21/08/2020].

Stensvold, T. (2018*b*), 'Norled bygger verdens første hydrogen-ferge', *Teknisk Ukeblad* . Available at https://www.tu.no/artikler/norled-bygger-verdens-forste-hydrogen-ferge/452526 [Accessed 26/06/2020].

Stensvold, T. (2019*a*), 'Norled skal bygge hydrogenferge nummer to', *Teknisk Ukeblad* . Available at https://www.tu.no/artikler/norled-skal-bygge-hydrogenferge-nummer-to/465145 [Accessed 30/07/2020].

Stensvold, T. (2019*b*), 'Ulstein sier de kan levere hydrogendrevet skip i 2022', *Teknisk Ukeblad* . Available at https://www.tu.no/artikler/ulstein-sier-de-kan-levere-hydrogendrevet-skip-i-2022/479540 [Accessed 27/06/2020].

Stensvold, T. (2019*c*), 'Yara skal produsere hydrogen med solenergi', *Teknisk Ukeblad* . Available at https://www.tu.no/artikler/yara-skal-produsere-hydrogen-med-solenergi/460657 [Accessed 30/07/2020].

Stensvold, T. (2020), 'Drivstoffet alle har ventet på kan gi nullutslipp på flere tusen skip', *Teknisk Ukeblad* . Available at https://www.tu.no/artikler/drivstoffet-alle-har-ventet-pa-kan-gi-nullutslipp-pa-flere-tusen-skip/483692 [Accessed 30/07/2020].

Stensvold, T. & Jensen, A. B. (2020), 'Eidesvik skal få verdens første utslippsfrie offshorefartøy: Bruker ammoniakk', *Teknisk Ukeblad* . Available at https://www.tu.no/artikler/verdens-forste-eidesvik-bygger-om-viking-energy-til-ammoniakk-drift/483392 [Accessed 26/06/2020].

Stepanov, K. L., Stanchits, L. K. & Stankevich, Y. A. (2011), 'Modeling of explosion thermal radiation', *Journal of Engineering Physics and Thermophysics* **84**(1), 179–206.

Stephens, M. & Olson, J. D. (1984), 'Measurement of excess heat capacities by differential scanning calorimetry', *Thermochimica Acta* **76**, 79–85.

Stocker, A. (2018), Investigation of renewable fuels for a Scottish ferry service. thesis for degree of msc., Technical report, University of Strathclyde, Glasgow, Scottland, UK.

Stultz, S. C. & Kitto, J. B. (2002), *Computational Methods for Fluid Dynamics*, Springer Verlag, Berlin, Germany.

Stultz, S. C. & Kitto, J. B. (2015), *STEAM / its generation and use*, Babcock & Wilcox, Akron, OH, USA.

Taibi, E., Miranda, R., Vanhoudt, W., Winkel, T., Lanoix, J.-C. & Barth, F. (2018), Hydrogen from renewable power, Technical Report ISBN 978-92-9260-077-8, International Renewable Energy Agency, Abu Dhabi, UAE.

Takaishi, T., Numata, A., Nakano, R. & Sakagutchi, K. (2008), Approach to high efficiency diesel and gas engines, Technical Report Technical Review Vol. 45 No. 1, Mitsubishi Heavy Industries, Ltd., Tokyo, Japan.

Tang, M., Xu, L. & Fan, M. (2015), 'Progress in oxygen carrier development of methane-based chemical-looping reforming: A review', *Applied Energy* **151**, 143–156.

Tarzimanov, A. A. & Mashirov, V. E. (1970), 'Experimentelle bestimunng der wärmeleitfähigkeit von n-alkan-, alkol- und säuredämpfen', *Teplofiz. Svoistva Vesh. Mater* **2**, 183–193.

Taylor, M. P., Eley, K. L., Martin, S., Tuffin, M. I., Burton, S. G. & Cowan, D. A. (2009), 'Thermophilic ethanologenesis: Future prospects for second-generation bioethanol production', *Trends in Biotechnology* **27**(7), 398–405.

Tchouvelev, A. V. (2006), Risk assessment studies of hydrogen and hydrocarbon fuels, fuelling stations: Description and review, Technical report, IEA HIA Task 19, Mississauga, ON, Canada.

TCS (2015), 'Federal subsidies for corn ethanol and other corn-based biofuels', *Taxpayers for Common Sense Energy & Natural Resources* . Available at `https://www.taxpayer.net/energy-natural-resources/federal-subsidies-for-corn-ethanol-and-other-corn-based-biofuels/` [Accessed 21/08/2020].

Teter, J. (2020), Tracking transport 2020, Technical report, International Energy Agency, Paris, France.

TFI (2010), Health effects of ammonia, Technical report, The Fertilizer Institute, Washington, DC, USA.

Thomas, C. E. (2012), 'Fuel cell and battery electric vehicles compared', *International Journal of Hydrogen Energy* **34**(15), 6005–6020.

Tietze, V. & Stolten, D. (2015), 'Comparison of hydrogen and methane storage by means of a thermodynamic analysis', *International Journal of Hydrogen Energy* **40**(35), 11530–11537.

Tomasgard, A., Blekkan, E. A., Karstad, P. I., Møller-Holst, S., Størset, S., Ulleberg, Ø., Berstad, D., Dawson, J., Løvås, T., Nekså, P., Sundseth, K., Burheim, O. S., Espegren, K. A., Meyer, J., Pollet, B. G. & Thomassen, M. (2019), Hydrogen i fremtidens lavkarbonsamfunn, Technical Report ISBN 978-82-93198-31-4, NTNU, SINTEF, IFE, The Research Council of Norway, CenSES and MoZEES, Trondheim, Norway.

Tomasgard, J. A. (2020), 'El-boom i ferge-Norge: Over 60 nye el-ferger er under bygging', *Teknisk Ukeblad* . Available at `https://www.tu.no/artikler/el-boom-i-ferge-norge-over-60-nye-el-ferger-er-under-bygging/490695` [Accessed 30/07/2020].

Tronstad, T., Åstrand, H. H., Haugom, G. P. & Langfeldt, L. (2017), Study on the use of fuel cells in shipping, Technical report, DNV GL, Oslo, Norway.

TU (2000), 'Når små uhell blir fatale', *Teknisk Ukeblad* . Available at `https://www.tu.no/artikler/nar-sma-uhell-blir-fatale/269861` [Accessed 21/08/2020].

Vaidy, P. D. & Rodrigues, A. E. (2006), 'Insight into steam reforming of ethanol to produce hydrogen for fuel cells', *Chemical Engineering Journal* **117**(1), 39–49.

van der Waals, J. D. (1873), *On the Continuity of the Gas and Liquid State, Thesis for Degree of PhD.*, University of Leiden, Leiden, Netherlands.

Vegvesenet (2020), 'Vegvesenets ferjedatabank', Online database. Norwegian Public Roads Administration. Available at `https://www.vegvesen.no/fag/trafikk/ferje/ferjedatabanken` [Accessed 14/07/2020].

Venetsanos, A. G., Papanikolaou, E., Delichatsios, M., Garcia, J., Hansen, O. R., Heitsch, M., Huser, A., Jahn, W., Jordan, T., Lacome, J.-M., Ledin, H. S., Makarov, D., Middha, P., Studer, E., Tchouvelev, A. V., Teodorczyk, A., Verbecke, F. & der Voort, M. M. V. (2009), 'An inter-comparison exercise on the capabilities of CFD models to predict the short and long term distribution and mixing of hydrogen in a garage', *International Journal of Hydrogen Energy* **34**(14), 5912–5923.

Verbruggen, J. (2018), Powering a representative ROPAX ferry in 2050 with minimal greenhouse gas emissions. thesis for degree of msc., Technical report, Delft University of Technology and C-Job, Delft, The Netherlands.

Vinogradov, V. I., Sergeev, E. N. & Krestov, G. A. (1982), 'Lösungsthermodynamik des argons in binären wasserfreien ethanol-isopropanol-mischungen', *Chemistry and Chemical Technology* **25**, 1539–1541.

Wang, Q., Sun, J. & Chu, G. (2005), 'Lithium ion battery fire and explosion', *Fire Safety Science* **8**, 375–382.

Wang, W., Herreros, J. M., Tsolakis, A. & York, A. P. E. (2013), 'Ammonia as hydrogen carrier for transportation; investigation of the ammonia exhaust gas fuel reforming', *International Journal of Hydrogen Energy* **38**(23), 9907–9917.

WBA (2019), Global bioenergy statistics 2019, Technical report, World Bioenergy Association, Stockholm, Sweden.

Weast, R. C., ed. (1972), *CRC Handbook of Chemistry and Physics. 53rd Edition*, CRC Press LLC, Boca Raton, FL, USA.

Whall, C., Cooper, D., Archer, K., Twigger, L., Thurston, N., Ockwell, D., McIntyre, A. & Ritchie, A. (2002), Quantification of emissions from ships associated with ship movements between ports in the european community, Technical report, Entec UK Ltd., Northwich, England, UK.

Williams, T., Al-Mejlad, F., Al-Naimi, F., Freens, P., Taha, B., Sarkova, V. & Senina, O. (2015), Life cycle assessment of LNG, Technical report, International Gas Union, Programme Committee D Study Group 4, Barcelona, Spain.

Zabetakis, M. G. (1965), Flammability characteristics of combustible gases and vapors, Technical Report Bulletin 627, US Bureu of Mines, Washington, DC, USA.

Zakurenov, V. M., Konyakhin, V. P. & Nozdrev, V. F. (1982), 'The viscosities of ethanol-cyclohexane mixtures', *Russian Journal of Physical Chemistry A* **25**, 1539–1541.

Zanchet, D., Santos, J. B. O., Damyanova, S., Gallo, J. M. R. & Bueno, J. M. C. (2015), 'Toward understanding metal-catalyzed ethanol reforming', *ACS Catalysis* **6**(5), 3841–3863.

Zervos, A. & Adib, R. (2019), Renewables 2019: Global status report, Technical Report ISBN 978-3-9818911-7-1, REN21, Paris, France.

Zhao, Y., Setzler, B. P., Wang, J., Nash, J., Wang, T., Xu, B. & Yan, Y. (2019), 'An efficient direct ammonia fuel cell for affordable carbon-neutral transportation', *Joule* **3**(10), 2472–2484.

Zuckerwar, A. J., ed. (2002), *Handbook of the Speed of Sound in Real Gases*, Academic Press, Cambridge, MA, USA.

Appendix A

Definition of ethanol as a species in FLACS

Ethanol being defined as a fuel in FLACS was a prerequisite for performing simulations. However, the standard fuels available consisted mostly of hydrocarbons without oxygen content, in addition to hydrogen, chlorine and a few other gases. To use ethanol in simulations, a significant number of properties of the substance must be derived and defined manually by the user. These required properties, along with the values inserted and their reference, are listed in Table A.1 below. The same table lists for which simulation scenarios the different properties are required. According to Gexcon, new gas species should not be defined and used without proper testing and validation, especially for combustion simulations (Gexcon 2019). An alternative could be to use an already defined component, for example heptane or octane, to estimate the behaviour of ethanol. On the basis of the number and type of simulations planned in this thesis, it was considered necessary to define ethanol properly.

To validate the ethanol configured in FLACS for explosion, a simple simulation with a closed box containing ethanol and air was set up. As the mixture was ignited, the resulting pressure was compared to the theoretical energy released from the combustion, along with empirical values. This benchmark is discussed further in Appendix B.
Octane was used for comparison during the configuration, due to the similar flash points for the two species (Octane at 286 K and ethanol at 287 K)(Colonna 2010, SA 2017). The predefined values of octane in FLACS are presented in a separate table (Table A.3) for comparison. For the pressure and temperature dependency of the laminar burning velocity for ethanol, the values are assumed similar to those of octane. The reason for this is the similar behaviour regarding burning velocity among many hydrocarbons, as observed by Michael G. Zabetakis, along with little published information on the laminar burning velocity of ethanol (Zabetakis 1965). As a consequence, FLACS uses similar values for most hydrocarbons, except methane, propane and a few more. The ability to use the same value as that of octane is therefore regarded as a reasonable assumption. In a 1982 arti-

cle, Omer L. Gulder provided the burning velocity dependence on initial temperature and initial pressure, while the burning velocity dependence on pressure and flame radius are similar to other hydrocarbons.

The critical temperature and pressure for ethanol was found in Logsdon's *Kirk-Othmer Encyclopedia of Chemical Technology*. The references for the rest of the parameters are presented in the following subchapters.

For many of the parameters presented in the following paragraphs, the underlying data has been gathered from databases like the NIST Webbook or the Dortmund Data Bank. These data sets include data points from several different references and as a consequence, the data points are not evenly distributed across the range. This can cause problems, as higher densities in some areas of the data range will bias a regressional curve to be relatively more influenced by the denser areas. This bias will in turn affect the parameters, which become more accurate for the denser areas. Under-sampling, or removing random points from the dense areas of the data sets, could prove a solution to this problem. In the end, no action was made to solve the problem. As the following paragraphs show, the fitted curves matched well with the complete data set, and the issue was considered unproblematic for this thesis.

Table A.1: The properties necessary to define ethanol in FLACS, for different application areas.

Property	Dispersion	Combustion	Pool evaporation
Fuel molar mass	x	x	x
Stoichiometric molar ratio O_2/fuel mass		x	x
Moles of C in 1 mol of fuel		x	x
Moles of H_2 in 1 mol of fuel		x	x
Moles of S in 1 mol of fuel		x	x
Moles of O_2 in 1 mol of fuel		x	x
Laminar burning velocity dependence on flame radius		x	
Laminar burning velocity dependence on pressure		x	
Laminar burning velocity dependence on initial temperature		x	
Laminar burning velocity dependence on initial pressure		x	
Liquid density			x
First enthalpy constant for gas phase	x	x	x
Second enthalpy constant for gas phase	x	x	x
Third enthalpy constant for gas phase	x	x	x
First enthalpy constant for liquid phase			x
Second enthalpy constant for liquid phase			x
Third enthalpy constant for liquid phase			x
First surface tension constant			x
Second surface tension constant			x
First vapour pressure constant			x
Second vapour pressure constant			x
Third vapour pressure constant			x
First gas viscosity constant			x
Second gas viscosity constant			x
First liquid viscosity constant			x
Second liquid viscosity constant			x
First gas thermal conductivity constant			x
Second gas thermal conductivity constant			x
First liquid thermal conductivity constant			x
Second liquid thermal conductivity constant			x
Critical temperature			x
Critical pressure			x

Table A.2: The values inserted to define ethanol in FLACS.

Property	Unit	Ethanol value
Fuel molar mass	kg/kmol	4.60684000e+01
Stoichiometric molar ratio O_2/fuel mass	-	3.00000000e+00
Moles of C in 1 mol of fuel	-	2.00000000e+00
Moles of H_2 in 1 mol of fuel	-	3.00000000e+00
Moles of S in 1 mol of fuel	-	0.00000000e+00
Moles of O_2 in 1 mol of fuel	-	5.00000000e-01
Laminar burning velocity dependence on flame radius	-	2.50000000e+00
Laminar burning velocity dependence on pressure	-	2.70000000e-01
Laminar burning velocity dependence on initial temperature	-	1.75000000e+00
Laminar burning velocity dependence on initial pressure	-	-1.70000000e-01
Liquid density	kg/m^3	7.89000000e+02
First enthalpy constant for gas phase	J/(kg K	1.39150000e+03
Second enthalpy constant for gas phase	J/(kg K^2)	1.39170000e+00
Third enthalpy constant for gas phase	J/kg	5.65965604+06
First enthalpy constant for liquid phase	J/(kg K)	-1.44020000e+02
Second enthalpy constant for liquid phase	J/(kg K^2)	8.94570000e+00
Third enthalpy constant for liquid phase	J/kg	6.51866738e+06
First surface tension constant	N/m	4.69770489e-02
Second surface tension constant	N/(m K)	-8.43475027e-05
First vapour pressure constant	N/m^2	2.19500000e+01
Second vapour pressure constant	N/(m^2 K)	2.85094000e+03
Third vapour pressure constant	K	-7.84000000e+01
First gas viscosity constant	N/(m^2 s)	1.05443000e-03
Second gas viscosity constant	N s/m^{2}s	-2.00000000e-06
First liquid viscosity constant	K	7.00000000e+02
Second liquid viscosity constant	K	1.31660000e+02
First gas thermal conductivity constant	(J/S)/(m K)	-2.88477922e-02
Second gas thermal conductivity constant	(J/S)/(m K^2)	1.36907043e-04
First liquid thermal conductivity constant	(J/S)/(m K)	2.15090909e-01
Second liquid thermal conductivity constant	(J/S)/(m K^2)	-1.69454545e-04
Critical temperature	K	5.14000000e+02
Critical pressure	N/m^2	6.30000000e+06

Table A.3: The pre-defined values of octane in FLACS.

Property	Unit	Octane value
Fuel molar mass	kg/kmol	1.14232700e+02
Stoichiometric molar ratio O_2/fuel mass	-	1.25000000e+01
Moles of C in 1 mol of fuel	-	8.00000000e+00
Moles of H_2 in 1 mol of fuel	-	9.00000000e+00
Moles of S in 1 mol of fuel	-	0.00000000e+00
Moles of O_2 in 1 mol of fuel	-	0.00000000e-00
Laminar burning velocity dependence on flame radius	-	2.50000000e+00
Laminar burning velocity dependence on pressure	-	2.70000000e-01
Laminar burning velocity dependence on initial temperature	-	1.58700000e+00
Laminar burning velocity dependence on initial pressure	-	-2.71000000e-01
Liquid density	kg/m^3	7.03000000e+02
First enthalpy constant for gas phase	J/(kg K	1.09000000e+03
Second enthalpy constant for gas phase	J/(kg K^2)	2.59000000e+00
Third enthalpy constant for gas phase	J/kg	2.26000000e+06
First enthalpy constant for liquid phase	J/(kg K)	3.78000000e+03
Second enthalpy constant for liquid phase	J/(kg K^2)	0.0000000e+00
Third enthalpy constant for liquid phase	J/kg	3.37000000e+06
First surface tension constant	N/m	4.07000000e-02
Second surface tension constant	N/(m K)	-7.29000000e-05
First vapour pressure constant	N/m^2	2.08353700e+01
Second vapour pressure constant	N/(m^2 K)	3.12029000e+03
Third vapour pressure constant	K	-6.36300000e+01
First gas viscosity constant	N/(m^2 s)	7.10400000e-07
Second gas viscosity constant	N s/m^{2}s	2.52500000e-08
First liquid viscosity constant	K	4.73700000e+02
Second liquid viscosity constant	K	9.70313000e+01
First gas thermal conductivity constant	(J/S)/(m K)	-8.29800000e-03
Second gas thermal conductivity constant	(J/S)/(m K^2)	8.69000000e-05
First liquid thermal conductivity constant	(J/S)/(m K)	1.50000000e-01
Second liquid thermal conductivity constant	(J/S)/(m K^2)	0.00000000e+00
Critical temperature	K	5.68700000e+02
Critical pressure	N/m^2	2.49000000e+06

A.1 Values and assumptions of FLACS

A.1.1 Enthalpy

The enthalpy calculations were in FLACS based on the following formula, Equation A.1, and its derivative, Equation A.2. A, B and C in the equations correspond respectively to the first, second and third enthalpy constants from the tables in the previous section. These equations were used with differing values of the constants for the species in liquid and gaseous form.

$$H = (A + B \cdot T/2) \cdot T - C \tag{A.1}$$

$$Cp = A + B \cdot T \tag{A.2}$$

The linear approach to estimating the heat capacity of the species is not exact. Substances with more degrees of freedom than the basic two-atomic gases display a more complex relationship between heat capacity and pressure than that assumed of ideal gases. According to the Equipartition theorem, each degree of freedom contributes equally to the substance's heat capacity. More degrees of freedom are activated with increasing temperature. For example, vibrational modes are often first activated at high temperatures (T ¿ 2000 K). As these are activated, the heat capacity will increase in a non-linear fashion. By the linear model, the temperature range for which the model is accurate must be calibrated to fit the temperatures of the desired scenarios.

For ethanol, the enthalpy gas constants were based on a linear approach to the heat capacity in the temperature range of 273-2250 K. The final constants are displayed in Table A.2. The mean values of the linearised values and the empirical values were equal, at 2804 J/(kg K), and the double standard deviation between the two data sets was calculated to be 700 J/(kg K). The relationship between the linear fit used in FLACS and the empirical values for gaseous ethanol is illustrated in Figure A.1. The estimate for the gaseous heat capacity is not exact, but for rapid heating purposes, the average value is assumed of most importance.

For the liquid ethanol constants, the heat capacity values used for the estimates were derived from data points in the temperature range 266-318 K. Studies with temperatures up to 351 K, the boiling point, could not be found. These constants would be used to build simulations where leaks create pools that evaporate and generate explosive atmospheres. These pools should not reach temperatures far above room temperature, and so 318 K was considered to function well as an upper limit. The values also provided a good fit for a linear approach, with the double standard deviation between the linear fit and the empirical data set calculated to 7.99 J/(kg K). The relationship between the linear approach and the empirical values for liquid ethanol is illustrated in Figure A.2.

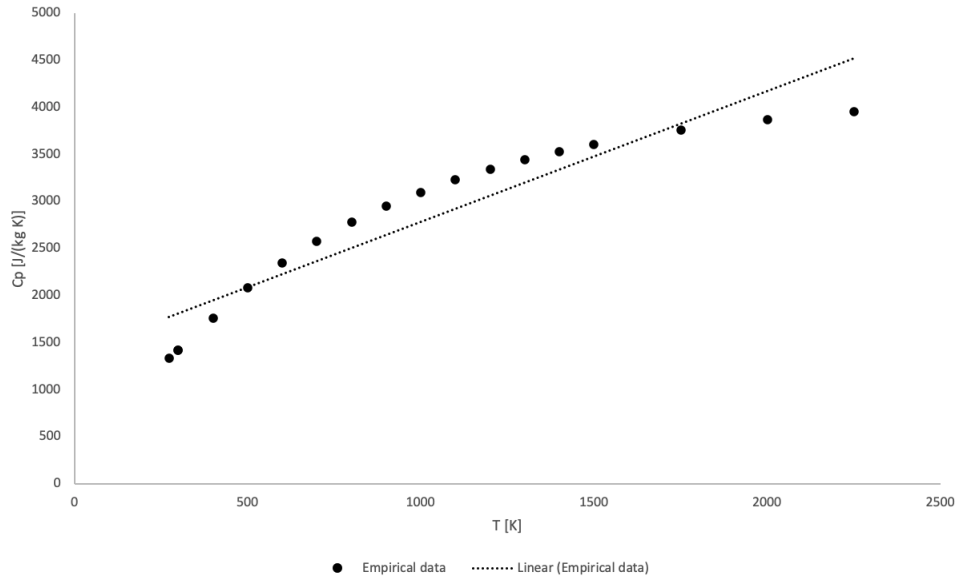

Figure A.1: The relationship between the empirical data set for the heat capacity of gaseous ethanol and the linear fit used in FLACS (NIST TRC 1997).

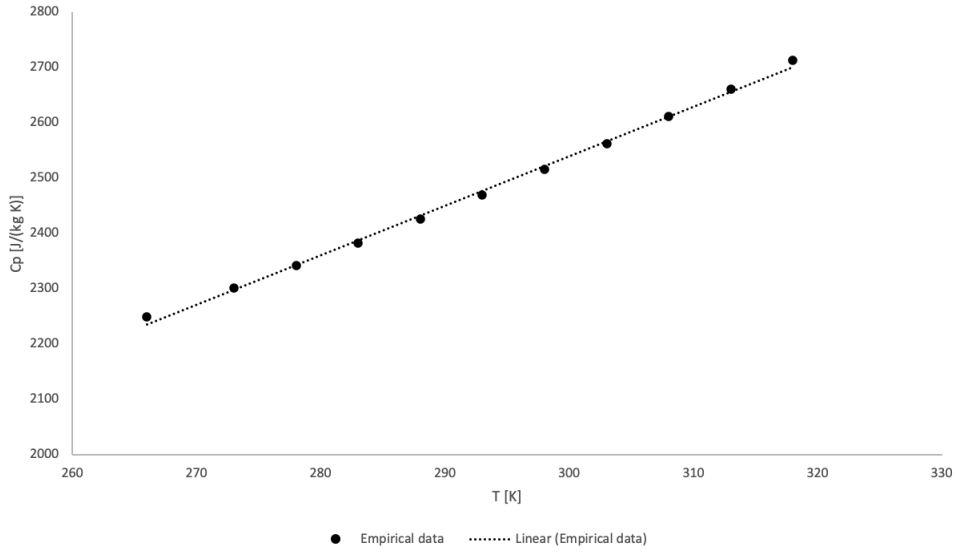

Figure A.2: The relationship between the empirical data set for the heat capacity of liquid ethanol and the linear fit used in FLACS (Stephens & Olson 1984).

A.1.2 Surface tension

The surface tension of species in FLACS is estimated by a linear approach. According to Gexcon, Equation A.3 is used for the line (Gexcon 2019). In the equation, A and B are the surface tension constants of Table A.2, while T is the temperature. The empirical values ranged from 293-351 K, producing a good foundation for the constants. The double standard deviation between the linear fit and the empirical data set was calculated to 0.0511 mN/m and the average value for both sets was 0.020 N/m. The relation between the empirical values and the linear fit is illustrated in Figure A.3.

$$\sigma = A + B \cdot T \tag{A.3}$$

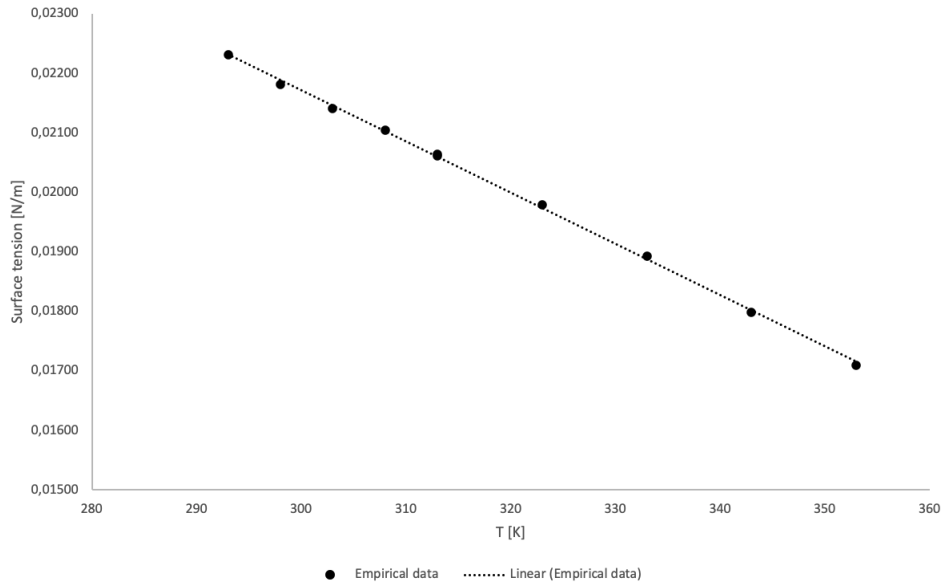

Figure A.3: The relationship between the empirical data set for the dynamic surface tension of ethanol and the linear fit used in FLACS (Levichev 1964, Muratov 1980, Fu et al. 2000).

A.1.3 Vapour pressure

The vapour pressure is perhaps the most important property for pool behaviour, where the development of an explosive atmosphere is monitored. To estimate the vapour pressure, FLACS uses the Antoine equation, Equation A.4. The constants A, B and C in the equation correspond to the vapour pressure constants of Table A.2 and T is the temperature. The Antoine equation fitted well with the empirical data, with a double standard deviation between the approach and the empirical data set of 1.11 kPa. The relationship between the empirical data and the fitted curve is illustrated in Figure A.4.

$$p_{vap} = exp\Big(A - \frac{B}{T + C}\Big) \tag{A.4}$$

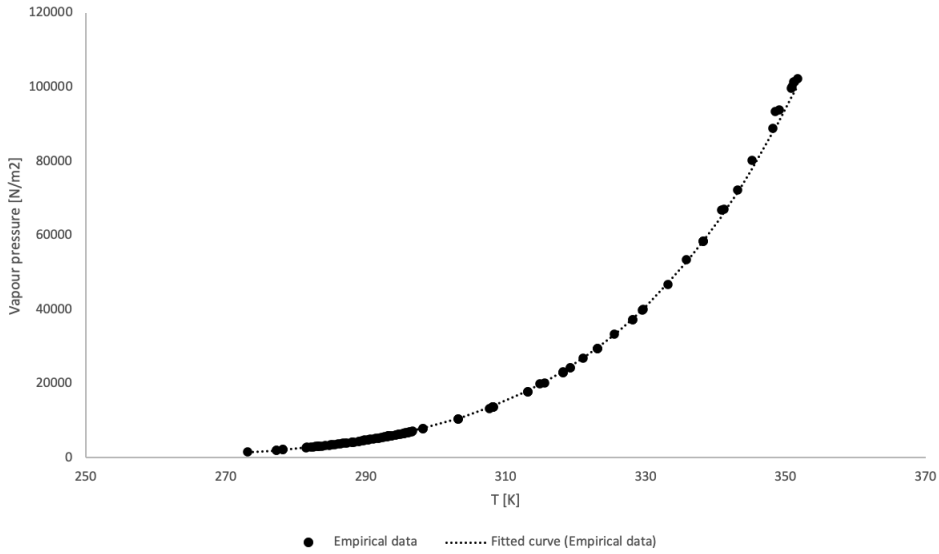

Figure A.4: The relationship between the empirical data set for the vapour pressure of ethanol and the fitted curve (Mishchenko & Subbotina 1967, Chun & Davison 1972, Scatchard & Satkiewicz 1964, Scatchard & Raymond 1938, Kretschmer & Wiebe 1949).

A.1.4 Conductivity

The gas and liquid conductivities were estimated in FLACS using a linear approach, based on Equation A.5. The constants A and B correspond to the conductivity constants of Table A.2. The empirical data for both the gas and liquid conductivities fitted well with the linear model, giving double standard deviations between the approach and the data set of 2.90 W/K for the gas conductivity and 2.73 W/K for the liquid conductivity. The average values were 39.4 W/K and 152 W/K, respectively. The relationships between the empirical data and the fitted lines are illustrated in Figure A.5 for the gas conductivity and in Figure A.6 for the liquid conductivity.

$$COND = A + B \cdot T \tag{A.5}$$

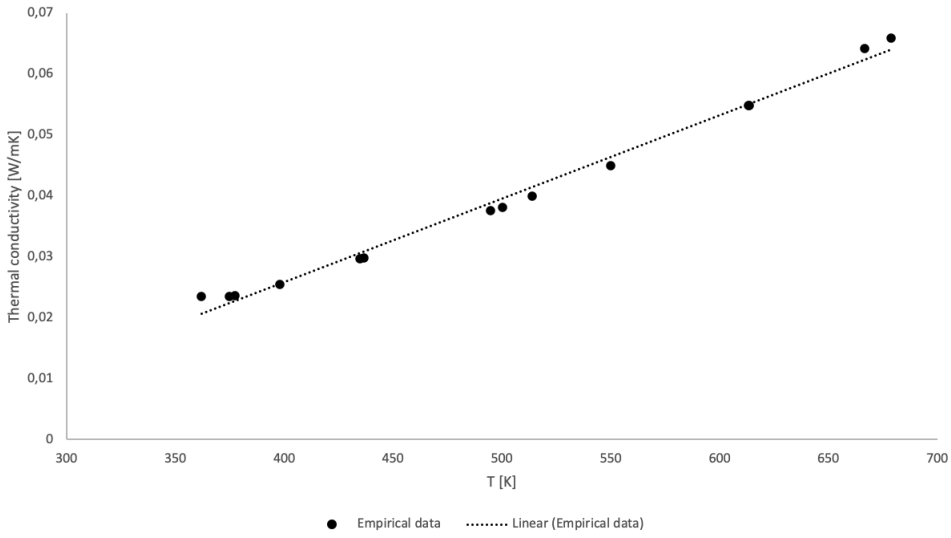

Figure A.5: The relationship between the empirical data set for the thermal conductivity of gaseous ethanol and the linear fit used in FLACS (Tarzimanov & Mashirov 1970).

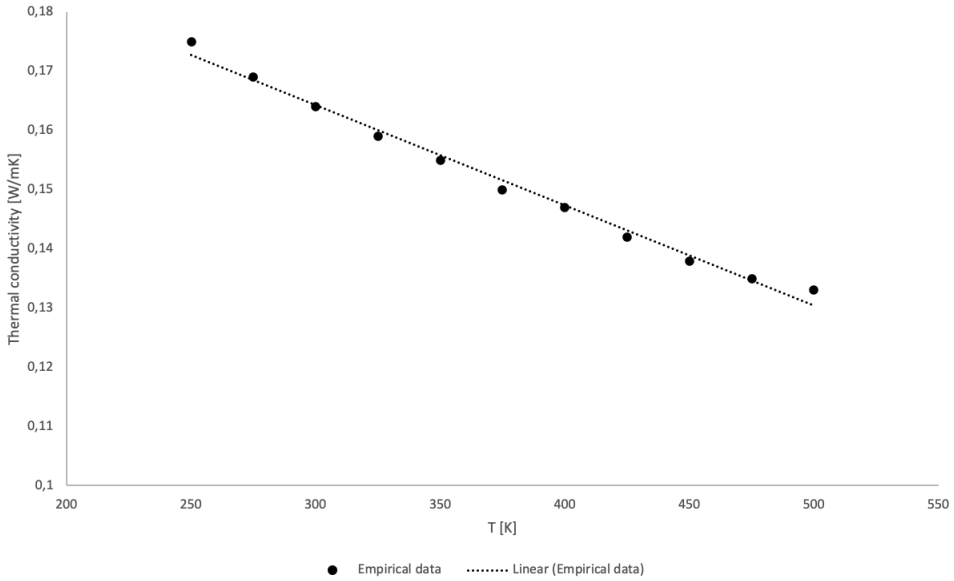

Figure A.6: The relationship between the empirical data set for the thermal conductivity of liquid ethanol and the linear fit used in FLACS (Assael et al. 2014).

A.1.5 Viscosity

The gas viscosity of ethanol was estimated in FLACS using a linear approach, see Equation A.6, with A and B corresponding to the constants in Table A.2. The liquid viscosity was on the other hand estimated using a fitted curve. The curve was based on the formula in Equation A.7, with A and B corresponding to the constants for liquid viscosity in Table A.2. The empirical data for the gas viscosity fitted well with the linear approach, as illustrated in Figure A.7, and gave a double standard deviation of 28.2 Ns/mm^2. For the liquid viscosity, the fitted curve also proved a good fit, with a double standard deviation of 84.1 Ns/mm^2. The average values were 172 Ns/mm^2 and 948 Ns/mm^2 respectively for the gas and liquid viscosities.

$$VISC_{gas} = A + B \cdot T \tag{A.6}$$

$$VISC = 10^{A \cdot (1/T - 1/B)} \tag{A.7}$$

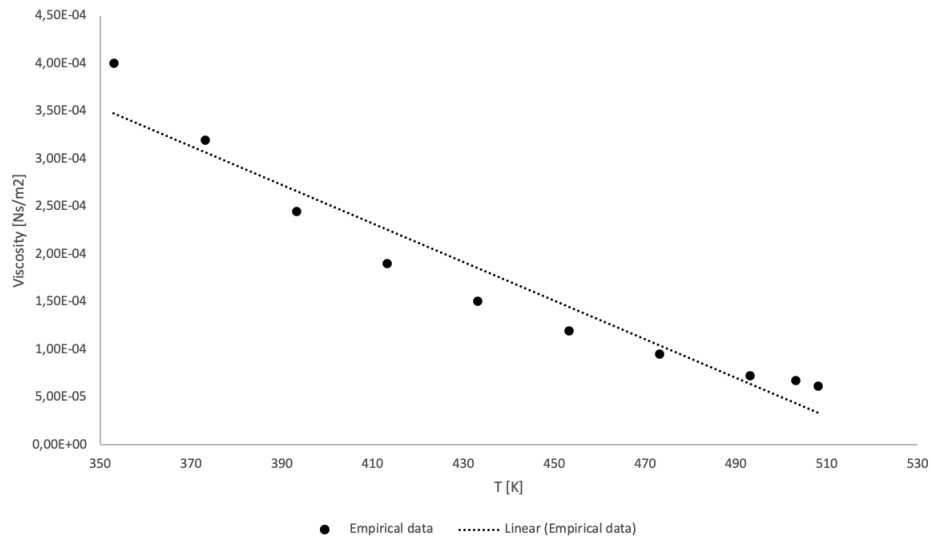

Figure A.7: The relationship between the empirical data set for the viscosity of gaseous ethanol and the linear fit used in FLACS (Vinogradov et al. 1982, Zakurenov et al. 1982, Mamedov & Shikhaliev 1972).

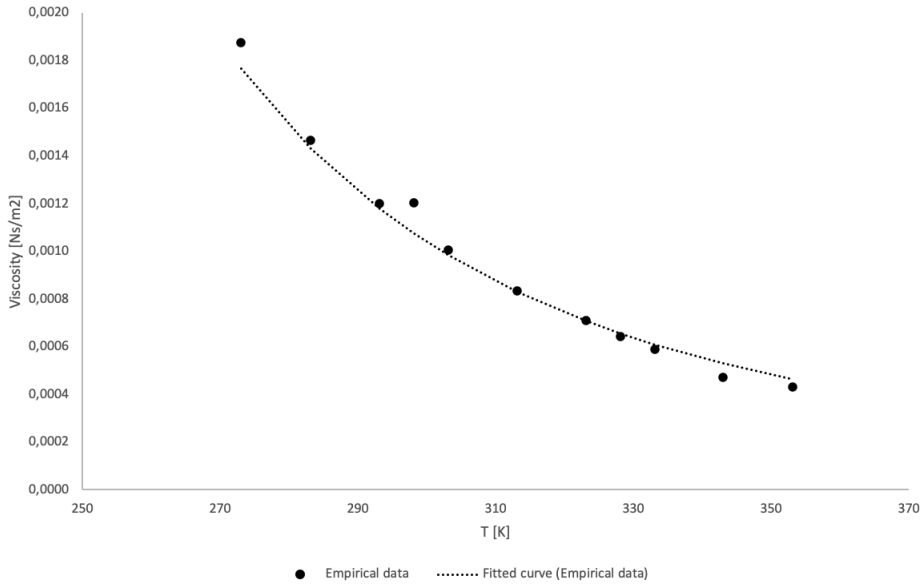

Figure A.8: The relationship between the empirical data set for the viscosity of liquid ethanol and the fitted curve (Vinogradov et al. 1982, Zakurenov et al. 1982, Mamedov & Shikhaliev 1972).

A.1.6 Summary

The assumptions of FLACS can be concluded give a good estimate of the empirical data. The fitted lines and curves matched the data sets with accuracy, with the largest deviations concerning the gaseous viscosity and the gaseous heat capacity. These had somewhat larger deviations than the other parameters, but were considered sufficiently accurate given matching average values between the fitted lines and the data sets.

Appendix B

Validation of ethanol in FLACS

B.1 FLACS explosion simulations

B.1.1 Method

Gexcon recommends in the FLACS manual a thorough validation of any self-created species to check that it corresponds to real behaviour (Gexcon 2019). The ethanol species created was therefore compared with both theory and empiric values. A box of about 54 m^3 (2.80 x 4.80 x 4.00 m) was created in FLACS, with uniform grid resolution of 0.20 m in all directions. The box is illustrated in Figure B.1. This box was filled with ethanol and air at varying equivalence ratios. The gas was ignited, and the final temperatures and the pressures were observed. The box is illustrated in Figure B.1 and the results are presented in Table B.1.

The stoichiometric ethanol concentration can be calculated using Equation B.1, where C_{O_2} is the concentration of oxygen in the atmosphere, 0.2095 for air. The stoichiometric relationship between oxygen and ethanol is 3.0, as given by the combustion reaction of Equation B.3. In this case, the value for $C_{EtOH,sto}$ becomes 6.53%. The equivalence ratio can then be calculated by using Equation B.2. The lower flammability limit of ethanol is 3.3% while the upper is at 19%, corresponding to equivalence ratios of of 0.51 and 2.91, respectively (Coronado et al. 2012, Brooks & Crowl 2007). According to Omer L. Gulder, the burning velocity of ethanol is similar at equivalence ratios of 0.80 and 1.4 (27 cm/s), with the highest burning velocity around the equivalence ratio of 1.1 (47 cm/s) (Gulder 1982). Even though the UFL of ethanol is at a ratio of 2.91, the burning velocity is low at higher values, making ignition difficult. Therefore, the simulations only included ratios from 0.45 to 2.0, although the one at 0.45 should not manage to ignite, as it was below the lower flammability limit. Temperature was measured in the middle of the container, at differing heights of 0.5, 1.5, 2.5 and 3.5 m. The highest recorded temperature was included in the table. The results are illustrated in Figure B.2 and in Figure B.3.

$$C_{EtOH,sto} = \frac{1}{1 + 3/C_{O_2}} \tag{B.1}$$

$$\phi_{EtOH} = \frac{C_{EtOH}}{C_{EtOH,sto}} \tag{B.2}$$

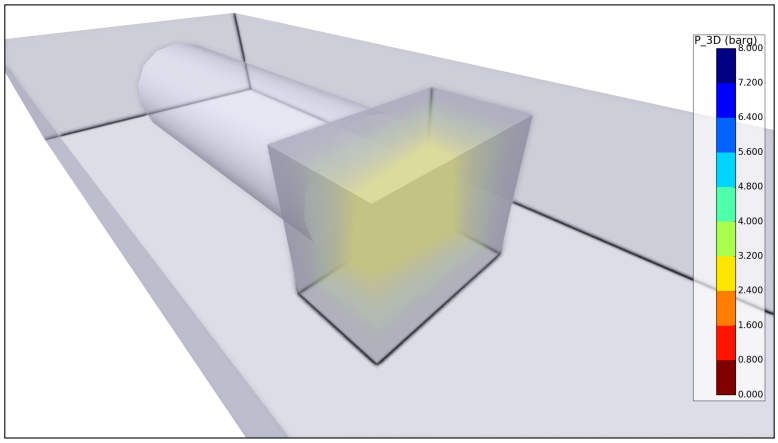

Figure B.1: The container for the combustion simulations used to validate the defined ethanol substance.

Table B.1: Final temperatures and pressures at different equivalence ratios of ethanol combustion in closed chamber.

Equivalence ratio	Final temperature [K]	Final pressure [barg]
0.45	298	0.000
0.50	2066	5.427
0.55	2065	5.824
0.60	2240	6.197
0.65	2413	6.548
0.70	2537	6.874
0.75	2622	7.173
0.80	2665	7.446
0.85	2720	7.699
0.90	2759	7.928
0.95	2783	8.130
1.00	2802	8.297
1.05	2814	8.418
1.10	2824	8.488
1.15	2831	8.519
1.20	2836	8.522
1.25	2835	8.511
1.30	2822	8.490
1.35	2800	8.464
1.40	2790	8.439
1.45	2746	8.401
1.50	2705	8.355
1.55	2661	8.306
1.60	2614	8.255
1.65	2564	8.201
1.70	2511	8.145
1.75	2455	8.088
1.80	2396	8.028
1.85	2335	7.967
1.90	2271	7.904
1.95	2205	7.840
2.00	2137	7.775

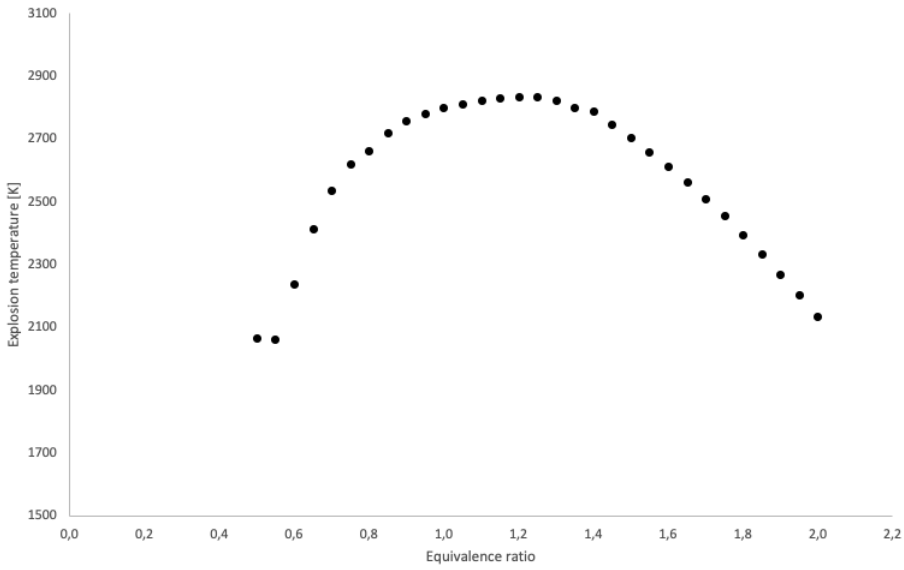

Figure B.2: The final temperatures of the simulations for validating the ethanol implementation.

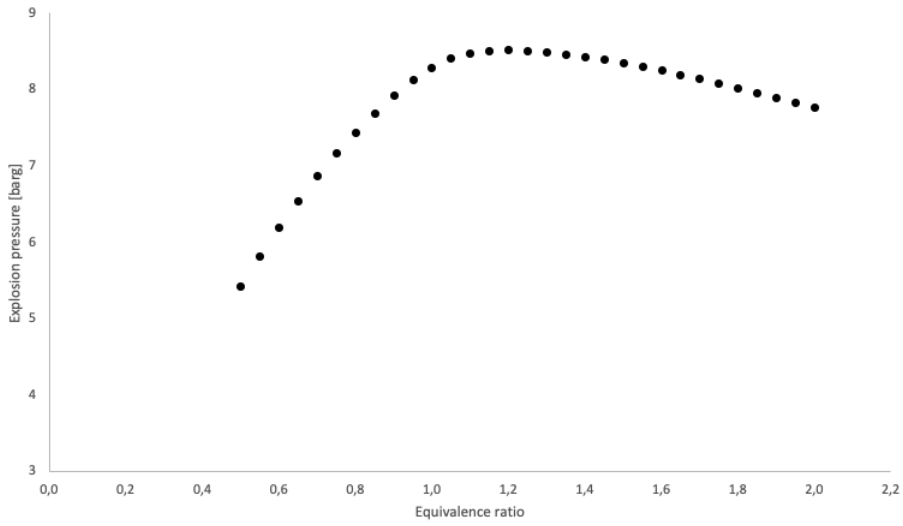

Figure B.3: The final pressures of the simulations for validating the ethanol implementation.

B.1.2 Results and discussion

The simulations finished, largely without problems. For the simulation with equivalence ratio of 0.45, the ignition failed, as it should., With the input provided FLACS has managed to calculate the upper and lower flammability limits with good precision, to 2.91 and 0.50, respectively. The scenario with equivalence ratio of 0.50 barely managed to ignite, but still managed to generate temperatures similar to the case with equivalence ratio of 0.55. It is unclear why this happened, potentially due to interpolation of burning velocities provided. The temperature curves from the four monitor points are illustrated in Figure B.4. Initially it can be seen that the upper three points see a short transient peak in temperature before falling, until temperature increased towards the maximum after a few seconds. The reason is that the lean flame has too low a reactivity to burn against gravity, so the flameball goes upwards to the ceiling before slowly burning back down. As can be seen in Figure B.4, the highest reported temperatures were in the upper part of the room, the upper monitor reported a significantly higher temperature than the other three. This produced an artificially high reported temperature for the graph of Figure B.2, as only the largest temperature was used. This phenomenon was only seen for the low reactivity cases near LFL or UFL.

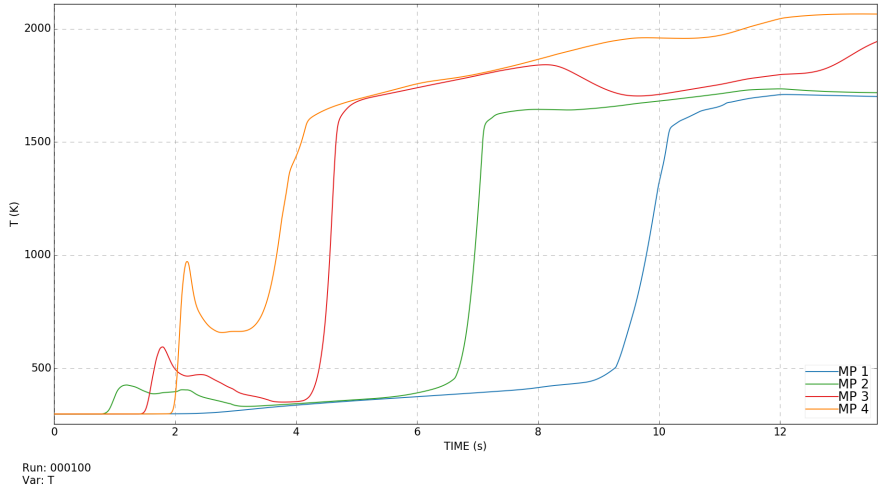

Figure B.4: The temperature curves of the simulation with equivalence ratio of 0.50.

Both the graphs of Figure B.2 and Figure B.3 indicated the equivalence ratio of 1.20 to return the highest values for temperature and pressure, respectively. Empirical studies also indicate the built up pressures to be highest at an equivalence ratio of 1.20 (Mitu & Brandes 2017). The shift of the maximum pressure towards higher equivalence ratios than 1.0 is characteristic for many hydrocarbons and is caused by product dissociation at higher temperatures. Such dissociation happens to a larger degree on the lean side, and so the peak occurs on the rich side (Law et al. 2006). FLACS accounts for dissociation of this kind, and the dissociations of CO_2 and H_2O are especially relevant for ethanol (Arntzen

1998).

Another observation to be made, was the mild decline in pressure with increasing equivalence ratios above the peak. The decline does not follow the decline of the temperature curve of Figure B.2. This is explained by the fact that pressure adjusts with the speed of sound, while the temperature is more governed by the flame front, moving at the burning velocity of ethanol, which is much slower, at less than 1 m/s (Konnov et al. 2011, Gulder 1982). Therefore, local temperatures arise, with highest temperatures near the ceiling, while the pressure stays constant throughout the container, illustrated in Figure B.5 and also in Figure B.4.

The pressure is to a greater degree dependent on the average temperature in the container. The mild reduction in the pressure with concentration can be predicted by examining the combustion reaction, given in Equation B.3. The energy released through the reaction may either be decreased by removing ethanol or by removing oxygen. From the peak of the curve in Figure B.3, one could observe the following. On the lean side, ethanol is removed with a ratio of 1 mol removed corresponds to 1 mol of ethanol less to react. On the rich side, oxygen is removed as air. So, as 1 mol of ethanol replaces 1 mol of air, only 0.07 mol less ethanol will manage react. Therefore, the pressure reduction on the rich side should be milder. This effect was also observed in empirical studies (Gulder 1982).

$$C_2H_5OH(g) + 3O_2 \longrightarrow 3H_2O(g) + 2CO_2(g) \quad \Delta H^{\circ}_{r298} = -1240kJ/mol \tag{B.3}$$

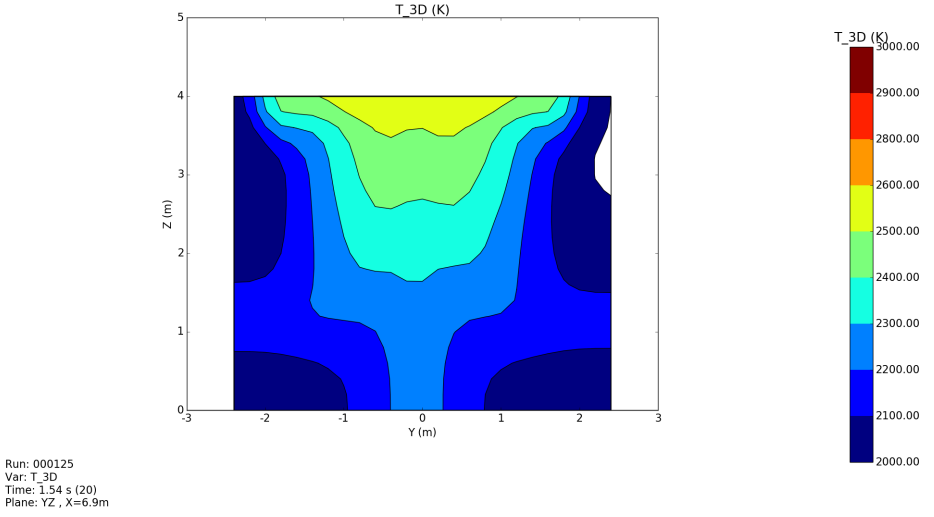

Figure B.5: A cross-section of the box with temperature reported 1.5 s after ignition. Local temperature variations can be observed. Illustration is from the simulation with equivalence ratio of 1.75.

The maximum pressures reported in literature was an explosion pressure of 8 barg, and a corresponding average temperature would be just below 2500 K, if assuming a constant number of mol (Mitu & Brandes 2017). There existed other studies reporting lower explosion pressures for ethanol, at 5-6 barg (Li et al. 2015).

The effect of thermal radiation and heat loss to the surrounding vessel were not included in the FLACS simulations. Some studies indicate that around 30% of the energy released during an explosion is converted to thermal radiation (Stepanov et al. 2011, Dorofeev et al. 1995). For many practical purposes, ignoring thermal radiation will have a smaller impact on the blast pressure, the most important measure of FLACS in risk analyses. On the other hand, in small containers which have a higher surface area to volume relation, the radiation loss to the small scale test vessel may prove substantial. As large-scale explosion tests are expensive to study, empirical experiments struggle to reach reliable conclusions when reproducing the explosions in small containers. Ultimately, there was reason to believe that the result, 8 barg as the explosion pressure, was realistic.

B.2 Theoretical calculations

To verify the results from FLACS, a theoretical model for the ethanol explosion was set up. For simplicity, the model only regarded the stoichiometric reaction, namely the run with equivalence ratio equal to 1. The model, set up in Microsoft Excel, simulated the reaction based on the following assumptions. Temperature intervals of 25 K were assumed to be accurate. Within the temperature intervals, the heat capacities and concentrations of the species remained constant. As heat capacities change only gradually with temperature, the assumption should prove sufficiently accurate. Conservation of energy was assumed, an assumption replicated by FLACS in the software's simulations. By this assumption, the explosion energy could be assumed to take place instantly, releasing the theoretical energy and converting all of the ethanol and oxygen to carbon dioxide and water. The final pressure and temperature were then calculated by matching the required energy to heat the species in the container to the energy released from the explosion. The energy released was calculated using the lower heating value of 1291.2 kJ/mol for ethanol (Haynes 1973).

B.2.1 Dissociation of the products

The species considered in the model are mentioned in Table B.4. At the onset of the Excel simulation, only nitrogen along with the products of the combustion reaction, namely water and carbon dioxide, coexisted in the container. Hydrogen, carbon monoxide and oxygen were included as products of other reactions taking place in the container. At more than 2000 K, the reaction products would dissociate at significant rates, following the reactions of Equation B.4 and Equation B.5, according to Bjørn J. Arntzen (Arntzen 1998, Jiang et al. 2017). The NO_x formation reactions between nitrogen and oxygen would normally be significant as well, yet as all the oxygen reacted stoichiometrically with all the ethanol, the lack of an oxygen partial pressure justified the exclusion of these reactions.

$$2H_2O \rightleftharpoons 2H_2 + O_2 \tag{B.4}$$

$$2CO_2 \rightleftharpoons 2CO + O_2 \tag{B.5}$$

The pressure equilibrium constants for the dissociation reactions were calculated using the relationship between Gibbs free energies and equilibrium concentrations, given in Equation B.7. From the equilibrium constants, the pressure equilibrium constants could simply be calculated by Equation B.6, with c_{p1} defined as the concentration of product 1 and c_r defined as the reactant concentration. The Gibbs free energies were calculated using Equation B.8, where S represents the system entropy and U represents the system internal energy. As the container represented an isolated environment, the system internal energy was equal to the system enthalpy, as the system exerted no pressure-volume work. The internal energy is defined by Equation B.9, while the entropy is defined by Equation B.10. T° is the temperature at standard conditions. Correspondingly, $\Delta_f H_i^\circ$ and ΔS_i° are the enthalpy and entropy at standard conditions, respectively. The standard enthalpies and standard entropies used in the calculations are given in Table B.2.

$$K_p(T) = K_c \cdot P = \frac{c_{p1} c_{p2} P^2}{c_r P} \tag{B.6}$$

$$K_c(T) = e^{\frac{-\Delta_r G(T)}{RT}} \tag{B.7}$$

$$\Delta_r G(T) = \Delta_r U(T) - \Delta_r S(T) \tag{B.8}$$

$$\Delta_r U(T) = \sum_{products} \Delta_f H_i^\circ + Cv_i(T - T^\circ) - \sum_{reactants} \Delta_f H_j^\circ + Cv_j(T - T^\circ) \tag{B.9}$$

$$\Delta_r S(T) = \sum_{products} \Delta S_i^\circ + Cv_i ln\frac{T}{T^\circ} - \sum_{reactants} \Delta S_i^\circ + Cv_i ln\frac{T}{T^\circ} \tag{B.10}$$

Table B.2: The standard enthalpies and entropies for the species taking part in the dissociation reactions (Blackman & Gahan 2013).

Species	$\Delta_f H_i^\circ$ [kJ/mol]	ΔS_i° [J/K·mol]
CO_2	-393.5	213.79
CO	-99.0	197.66
O_2	0.0	205.15
H_2O	-241.8	188.84
H_2	0.0	130.68

The pressure equilibrium constants calculated are given for certain temperatures in Table B.3. The resulting equilibriums demonstrate how the dissociation reactions become significant at higher temperatures.

Table B.3: Calculated K_p for the CO_2 and H_2O dissociation reactions at selected temperatures.

Temperature [K]	K_{pCO2}	K_{pH2O}
373	4.80e-69	2.88e-58
773	3.56e-26	6.69e-22
1173	1.20e-12	3.27e-10
1573	4.49e-06	1.93e-04
1973	3.28-02	5.28e-01
2173	7.97e-01	9.29e+00
2373	1.11e+01	1.01e+02
2573	1.02e+02	7.56e+02
2773	6.66e+02	4.25e+03

B.2.2 Heat capacities of the species

The heat capacities of the species were calculated using the Shomate equation of Equation B.11. The constants for the equation were specific for each species. As mentioned in Appendix A.1, the heat capacity of a species is highly dependent on its current degrees of freedom. These degrees of freedom vary with temperature, causing the constants to do likewise. To calculate the C_v, the relevant heat capacity for closed systems, the ideal gas constant, R, was subtracted from the C_p. The heat capacity at constant pressure, C_p, is accounting for the work required to expand a gas as temperature increases. This work is equal to PV, by the Ideal Gas Law similar to RT. As heat capacity is enthalpy differentiated with respect to T, the change between C_p and C_v is equal to R. The development of the C_v heat capacities with temperature is illustrated in Figure B.6.

$$Cp_i(T) = A_i + B_i \cdot T + C_i \cdot T^2 + D_i \cdot T^3 + E_i/T^2 \tag{B.11}$$

Table B.4: The Shomate equation constants for the species present in the container during the simulations (Chase 1998).

Species	Temperatures [K]	A	B	C	D	E
CO_2	298-1200	24.99735	55.18696	-33.69137	7.948387	-0.136638
	1200-6000	58.16639	2.720074	-0.492289	0.038844	-6.447293
CO	298-1300	25.56759	6.096130	4.054656	-2.671301	0.131021
	1300-6000	35.15070	1.300095	-0.205921	0.013550	-3.282780
O_2	100-700	31.32234	-20.23531	57.86644	-36.50624	-0.007374
	700-2000	30.03235	8.772972	-3.988133	0.788313	-0.741599
	2000-6000	20.91111	10.72071	-2.020498	0.146449	9.245722
N_2	100-500	28.98641	1.853978	-9.647459	16.63537	0.000117
	500-2000	19.50583	19.88705	-8.598535	1.369784	0.527601
	2000-6000	35.51872	1.128728	-0.196103	0.014662	-4.553760
H_2O	500-1700	30.09200	6.832514	6.793435	-2.534480	0.082139
	1700-6000	41.96426	8.622053	-1.499780	0.098119	-11.15764
H_2	298-1000	33.066178	-11.363417	11.432816	-2.772874	-0.158558
	1000-2500	18.563083	12.257357	-2.859786	0.268238	1.977990
	2500-6000	43.413560	-4.293079	1.272428	-0.096876	-20.533862

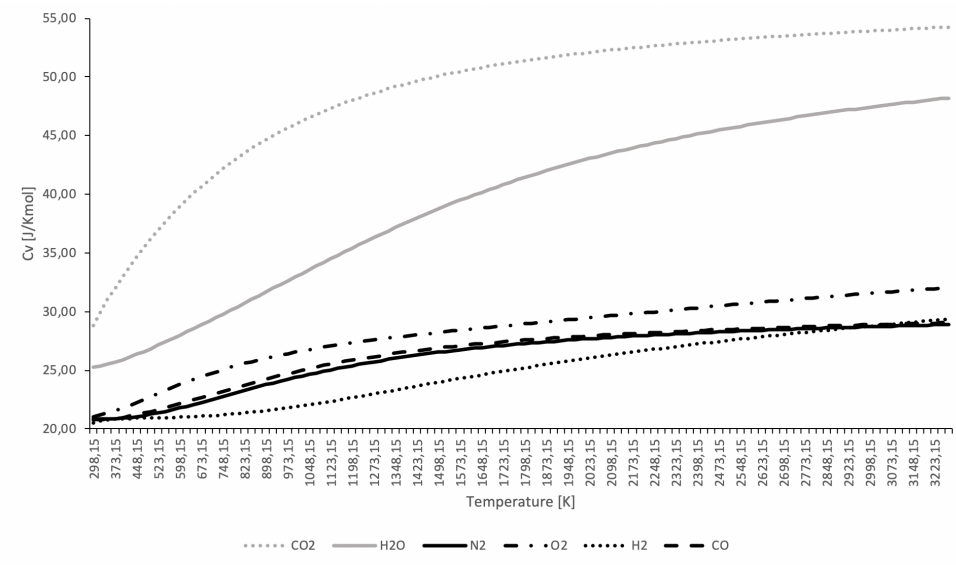

Figure B.6: The development of the C_v heat capacities for the species of the container with temperature.

B.2.3 Results and discussion

For the Microsoft Excel model, a total of 3.444 MJ of energy was released. This amount of energy was matched with a final container pressure of 7.99 barg and a corresponding average temperature of 2548 K. In the theoretical case of a 30% loss of energy to the environment due to radiation, the values would be 6.55 barg and 2098 K, respectively. The result was close to that obtained from the FLACS simulations, which reached a maximum pressure of 8.297. In Figure B.6, the inaccuracy of the linear fit used in FLACS becomes apparent. The heat capacities are not linear with temperature, and this simplification probably influenced the mismatch between the theoretical study and the simulation. Even though FLACS does not account for the capacities, the result was useful and gave a good indication of the explosion characteristics of ethanol. Hydrocarbons with similar amounts of combustion energies from stoichiometric mixtures and their maximum pressures are given in Table B.5. The self-defined ethanol species produces a pressure of the same scale as those of the established species. The ethanol was concluded to be sufficiently validated for use in the explosion scenarios of this thesis.

Table B.5: The explosion pressures of other hydrocarbons with similar energy releases from stoichiometric mixtures, obtained from FLACS simulations. The lower heating values for the hydrocarbons was obtained from the *CRC Handbook of Chemistry and Physics* (Haynes 2015, Weast 1972).

Species	Released energy $\phi = 1.0$ [MJ/m^3]	Simulation max pressure [barg]
Ethanol (self-defined)	3.42	8.297
Hexane	3.65	8.386
Heptane	3.66	8.409

B.3 Validation of ethanol pool evaporation

The ethanol species was in addition validated with regard to pool evaporation, in a simple fashion. In the simulation, ethanol was spilled onto the floor of a room measuring 1 m in all dimensions. A fan was included to provide ample mixing. The grid was defined with cubic control volumes with sides of 5 cm. The box was simulated with a small hole for pressure equalisation and as an isolated, pressure-tight chamber. To validate the pool functionality, the partial pressure of ethanol was to be observed. As the liquid ethanol filled the area of the box, the ethanol pressure should increase from zero towards the theoretical vapour pressure of about 6.0 kPa at 293 K. The pressure should increase at a high rate from the start and then slow down, as the ethanol vapour pressure of the room reaches higher values.

The partial pressure of ethanol did not approach the theoretical vapour pressure of ethanol. The pool simulations of ethanol failed each time after reaching around 40 s. The unknown error message ”Negative h_gp i pool boiling” appeared and the simulations failed. The error was assumed to be a weakness in the FLACS pool model and its handling of user-defined species, but parts of the problem could also be related to the definition of ethanol. The enthalpy of evaporation, namely the difference between ethanol liquid and gas enthalpy, was stable in the temperature region studied, which should indicate that the definition of ethanol was appropriate. The same simulations were performed with the built-in species hexane and heptane, the hydrocarbons closest to ethanol in vapour pressure. These simulations did not see the error message.

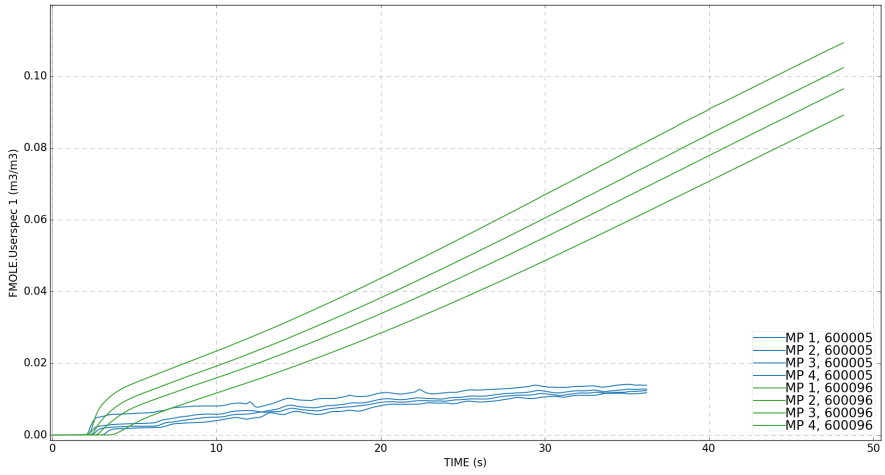

Figure B.7: The ethanol concentration by volume, reported at four different heights, for closed-box evaporation (green) and for ventilated-box evaporation.

The results did not match the expected outcome, as illustrated in Figure B.7. During the 40-50 s before failure, ethanol struggled to reach vapour pressures above 2.0 kPa when the

box had an opening. When ethanol was spilled into the closed box, however, the vapour pressure went far above the theoretical pressure. Hexane and heptane spill tests were also performed in a closed box. These were simulated for close to 200 s. The volume concentrations of hexane and heptane are illustrated below in Figure B.8.

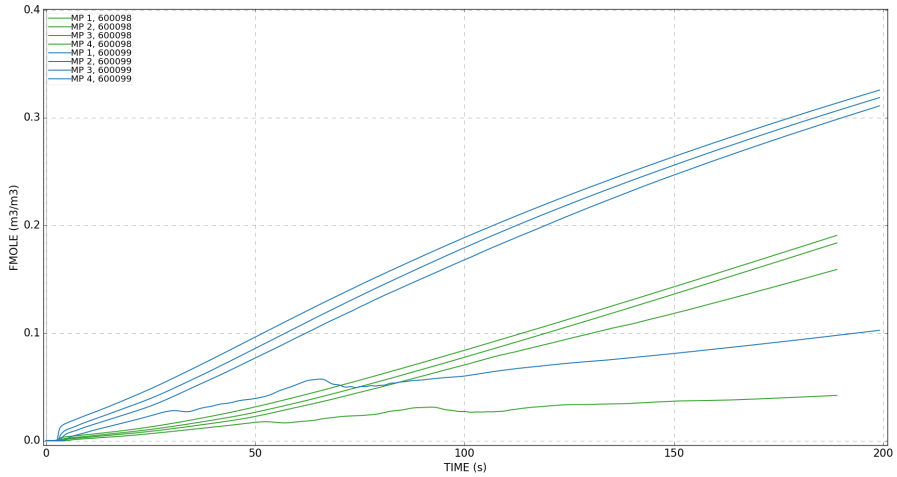

Figure B.8: The hexane (blue) and heptane (green) concentrations by volume, measured at four different heights, for closed-box evaporation.

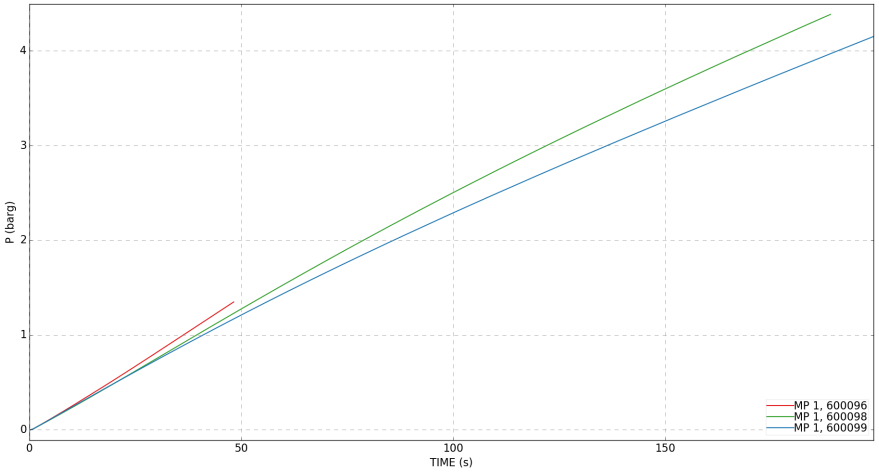

Figure B.9: The ethanol (red), hexane (green) and heptane (blue) pressures during closed-box evaporation.

As Figure B.8 shows, hexane and heptane reached concentrations well above their respective vapour pressures, at 18 kPa and 5.3 kPa at 293 K. The box was an isolated container, and so the concentrations increased to unrealistic levels with the persistent evaporation. The container pressure for the three simulations are shown in Figure B.9. This experiment indicated a weakness inherent in the FLACS software. Firstly, pool evaporation reactions seemed to only move in one direction, with condensation not taking place. This may lead to reaching higher vapour pressures than theoretically possible. The pressure in the room seemed to not have any apparent effect on the evaporation rate.

According to the FLACS manual, the pool model is mostly developed and validated for LNG and it is acknowledged that the pool model may be flawed when studying fluids with boiling points above ambient temperature. The conclusion of the validation experiment was that the pool evaporation function for ethanol should not be used further.

The FLACS support team was contacted for comments on the weaknesses discovered. They checked and concluded that the pressure build-up in the closed room had to do with a weakness in the fan model in FLACS, which seemed to generate over-pressures. The very high vapour concentrations seen in pool simulations in the same rooms seemed to be due to the fact that some parameters in the FLACS pool model were implemented using a 1 bara over-pressure (atmospheric) rather than the actual over-pressure above the pool, and together with the pressure build-up due to the fan error this gave the wrong evaporation rates from the pool models.

Due to limited time this subject could not be studied further and an alternative approach was required. One possibility could be to use experimental evaporation rates from literature. Lyulin et al. concluded that the initial evaporation rate of ethanol was 1 g/(m^2s) at 298 K (Lyulin et al. 2015). In another paper, Raymond L. Smith found that the average evaporation rate over 15 minutes at 300 K was 0.37 g/(m^2s) (Smith 2001). These two values roughly correspond and can form the basis for estimates regarding the evaporation rate. Simulations were therefore performed assuming constant evaporation rates at these levels.

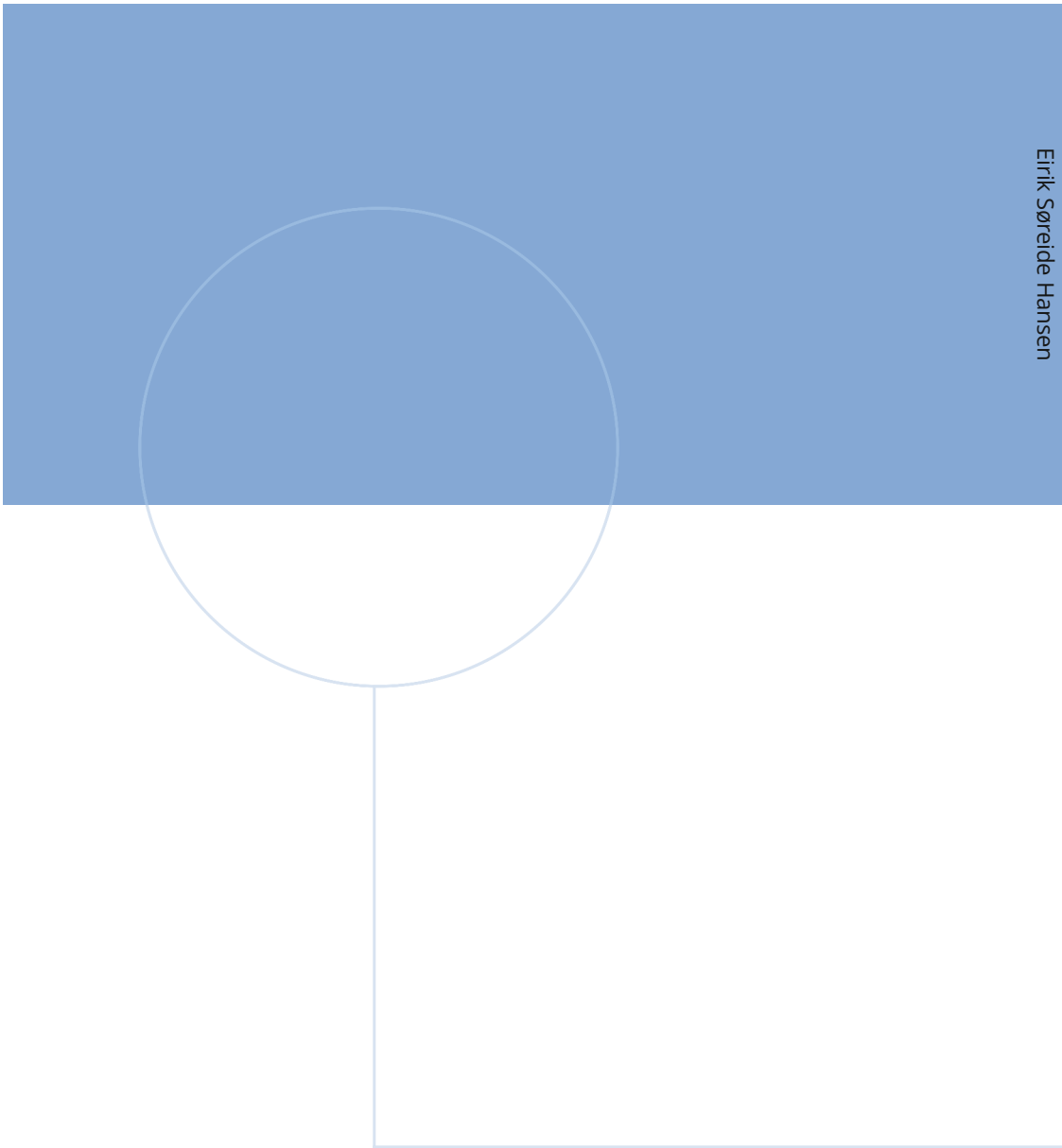

Eirik Søreide Hansen

NTNU
Norwegian University of
Science and Technology